UNIVERSITY OF PISA

School of Graduate Studies
"Scienza del Farmaco e delle Sostanze Bioattive"

(SSD Bio 10)

PhD THESIS

2009-2011

Enzymes and activation of intracellular signalling in cancer and neurodegenerative diseases

Candidate:
Sara Bendinelli

Tutor:
Prof. Claudia Martini

DIRECTOR OF THE SCHOOL

Prof. Claudia Martini

2011

INDEX

Chapter 1: Introduction

1.Glia: The Other Half of the Brain

The recent book, “Driving Mr. Albert” tells the true story of pathologist Thomas Harvey, who performed the autopsy of Albert Einstein in 1955. After finishing, Harvey irreverently took Einstein's brain home where he kept it preserved in a plastic container for the next 40 years. From time to time Harvey doled out small brain slices to scientists and pseudoscientists around the world who probed the tissue for clues to Einstein's genius. But when Harvey reached his 80’s, he placed what was left of the brain in the trunk of his Buick Skylark and embarked on a road trip across the country to return it to Einstein's granddaughter (Paterniti M, 2001).

One of the respected scientists who examined sections of the prized brain was Marian C. Diamond, of the University of California at Berkeley. She could unfortunately find nothing unusual about the number or size of the neurons in her samples. Although on closer examination of the association cortex which is responsible for higher-level cognition, she discovered a surprisingly large number of non-neuronal cells known as glia at a much greater concentration than that found in the average brain. An odd curiosity? Perhaps not. A growing body of evidence suggests that glial cells play a far more important role than historically presumed. For decades, physiologists focused on neurons as the brain's prime communicators. Glia were thought to serve only a maintenance role: bringing nutrients from blood vessels to neurons, maintaining a healthy balance of ions in the brain, and warding off pathogens that evaded the immune system. Supported by glia, neurons were free to communicate across tiny contact points called synapses and to establish a web of connections that allow us to think, remember and jump for joy.

This long-held model of brain function could change dramatically if new findings regarding glia prove to be correct. Recent advances in microscopy have shown that neurons and glia engage in a two-way dialogue from embryonic development through to old age. Glia influence the formation of synapses and help to determine which neural connections get stronger or weaker over time; such changes are essential to learning and to storing long-term memories. Most recent findings show that glia can also communicate amongst themselves, in a separate but parallel network to the neural network, influencing how well the brain performs. Neuroscientists are cautious about

assigning new prominence to glia too quickly, yet they are excited by the prospect that more than half the brain has gone largely unexplored and may contain a trove of information about how the mind works.

Ben Barres's lab has shown that brains from patients with various neurological diseases or injuries show altered glial cell phenotypes (Barres BA et al., 2008). There are many questions unanswered regarding the role of glia in the central nervous system (CNS): what is the normal function of glial cells, and what is their role in disease? Might glial cells be important drug targets? If so, this has the opportuinity to open a new avenue of drug therapies for patients suffering from brain injuries and neurological disease.

1.1.Glia in health and disease

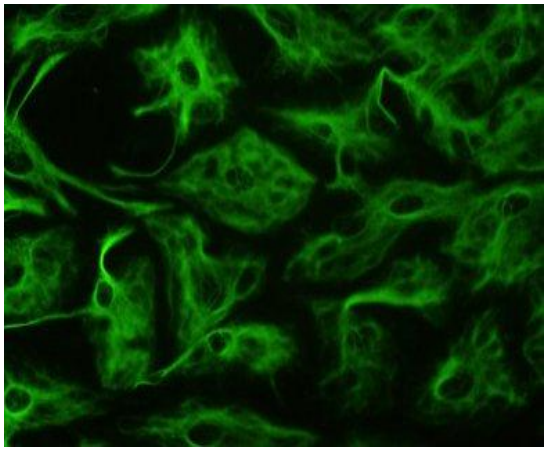

Figure 1. Astrocytes can be identified in culture because, unlike other mature glia, they express glial fibrillary acidic protein (GFAP).

Glial cells, sometimes referred to as neuroglia or simply glia, are non-neuronal cells that maintain homeostasis, form myelin, and provide support and protection for neurons in the both the CNS and parts of the nervous system such as in the autonomic nervous system (ANS) (Jessen KR and Mirsky R, 1980). In the human brain, there is roughly one glia for every neuron with a ratio of about two neurons for every glia cell in the cerebral gray matter (Azevedo FA et al., 2009).

As the Greek name implies, glia are commonly thought of as the "glue" in the nervous system; however this is not fully accurate. Currently there are four known functions of glia cells. The first is to surround neurons and provide support. Secondly,

they supply a steady stream of nutrients and oxygen to the neurons in order for the cells to maintain proper homeostasis. Thirdly, to eliminate cross-talk it is important for glia to insulate one neuron from another. The fourth and final known function of glial cells is to destroy pathogens and remove dead neurons. For over a century, it was believed that they did not play any role in neurotransmission. That idea is now discredited; they do modulate neurotransmission, although the mechanisms are not yet well understood (Gourine AV et al., 2010, Wolosker H et al., 2008).

1.1.1.Microglia

Microglia are specialized macrophages capable of phagocytosis, protecting neurons of the CNS from foreign pathogens. They are derived from hematopoietic precursors rather than ectodermal tissue and are commonly categorized as glia because of their supportive role for neurons.

They comprise approximately 15% of the total cells in the CNS and are found in all regions of the brain and spinal cord. Microglia cells are small relative to macroglial cells, with changing shapes and oblong nuclei. Notably, they are mobile and can undergo division following brain injury. In a healthy CNS, microglia processes constantly monitor all aspects of their environment including neurons, macroglia and blood vessels.

1.1.2.Macroglia

The most abundant type of macroglial cell, **astrocytes** (also called astroglia) have numerous projections that anchor neurons to their blood supply. They regulate the external chemical environment of neurons by removing excess ions, notably potassium, and recycling neurotransmitters released during synaptic transmission. The current theory suggests that astrocytes may be the predominant "building blocks" of the blood-brain barrier. Astrocytes may regulate vasoconstriction and vasodilation by producing substances such as arachidonic acid, whose metabolites are vasoactive.

Astrocytes signal to each other through calcium. The gap junctions (also known as electrical synapses) between astrocytes allow the messenger molecule inositol triphosphate (IP3) to diffuse from one astrocyte to another. IP3 activates calcium channels on cellular organelles, releasing calcium into the cytoplasm. This calcium can then stimulate the production of more IP3. The net effect is a calcium wave that propagates from cell to cell. Extracellular release of Adenosine-5'-triphosphate (ATP),

and consequent activation of purinergic receptors on other astrocytes, may also mediate calcium waves in some cases.

In general, there are two types of astrocytes; protoplasmic and fibrous. Both are similar in function but distinct in morphology and distribution. Protoplasmic astrocytes have short, thick, highly branched processes and are typically found in gray matter. Fibrous astrocytes have long, thin, less branched processes and are more commonly found in white matter.

Oligodendrocytes are cells that wrap around axons in the CNS with their cell membrane forming a specialized structure referred to as myelin. This produces a myelin sheath which provides insulation to the axon and allows electrical signals to propagate more efficiently (Baumann N and Pham-Dinh D, 2001).

Ependymal cells, also named ependymocytes, line the cavities of the CNS and compose the walls of the ventricles. These cells create and secrete cerebrospinal fluid (CSF) which is then circulated with the help of their beating cilia. They also make up the Blood-CSF barrier and are thought to act as neural stem cells (Johansson CB et al., 1996).

Radial glia cells arise from neuroepithelial cells after the onset of neurogenesis. Their ability to differeniate is more restricted than neuroepithelial cells. In the developing nervous system, radial glia function both as neuronal progenitors and as a scaffold upon which newborn neurons migrate. In the mature brain, the cerebellum and retina retain characteristic radial glial cells. In the cerebellum, these are Bergmann glia, which regulate synaptic plasticity. In the retina, the radial Müller cell is the principal glial cell, and participates in a bidirectional communication with neurons (Campbell K and Götz M, 2002).

Similar in function to oligodendrocytes, **Schwann cells** provide myelination to axons in the peripheral nervous system (PNS). They also have phagocytotic activity and clear cellular debris that allows for regrowth of PNS neurons (Jessen KR and Mirsky R, 2005).

Satellite glial cells are small cells that surround neurons in sensory, sympathetic and parasympathetic ganglia (Hanani M, 2008). These cells help regulate the external chemical environment. Like astrocytes, they are interconnected by gap junctions and respond to ATP by elevating intracellular concentration of calcium ions. They are highly sensitive to injury and inflammation, and appear to contribute to pathological states, such as chronic pain (Ohara PT et al., 2008).

Enteric glial cells are found in the intrinsic ganglia of the digestive system. They are thought to have many roles in the enteric system, some related to homeostasis and muscular digestive processes (Barsotti G et al., 2007)

1.2. Glia roles in brain diseases: astroglial cells

Over the past 25 years it has become clear that astrocytes are responsible for a wide variety of complex and essential functions in the healthy CNS, including primary roles in synaptic transmission and information processing by neural circuit functions. A growing body of evidence suggests that the loss of normal function or gain of abnormal effects in astrocytes contributes to disease progression. There are now numerous examples of how astrocytes contribute to both clinical and pathological mechanisms in neurological diseases (Barres BA 2008, De Keyser J et al., 2008, Seifert G et al., 2006, Sofroniev MV, 2000).

Because astrocytes constitute nearly half of the cells in the human brain, there is no CNS disease that does not substantially involve astrocytes. Even though astrocyte swelling is a dramatic and very harmful component of any acute neurological injury including stroke and brain trauma, we still do not understand well why astrocytes are more likely to swell than neurons and how this swelling can be lessened. Neurological diseases, including dysmyelinating diseases and epilepsy can result from mutations of astrocyte genes. Reactive gliosis (astrocytosis) also accompanies every neurological disease. Although reactive astrocytosis clearly is beneficial in that it can encapsulate infections and help seal a damaged blood-brain barrier, there are many ways in which it has been found to be harmful. Glial scarring contributes substantially to the glial cues that inhibit severed CNS axons from regenerating (Silver and Miller, 2004). Reactive astrocytes upregulate synapse-inducing genes such as thrombospondins, which have the potential to help repair the brain (Liauw et al., 2008) but may also induce unwanted synapses that can cause epilepsy or neuropathic pain (Boroujerdi et al., 2008). In addition, recent studies have found that diseased astrocytes can release a profoundly neurotoxic signal. For instance, mutant astrocytes carrying the SOD1 (G93A) allele release a toxic signal that rapidly kills wild-type motor neurons (Di Giorgio et al., 2007; Nagai et al., 2007; Lobsiger and Cleveland, 2007).

The importance of future CNS disease therapies that not only address dysfunctional neurons but also glial-cell-controlled inflammatory processes is crucial.

The involvement of glial cells has been clearly shown in CNS disorders including multiple sclerosis (MS), Alzheimer's disease (AD) (Lue LF et al., 2001), stroke (Wang X, 2005), Parkinson's disease (Hald A, 2005) (PD), Amyothropic lateral sclerosis (ALS) (Di Giorgio FP et al., 2008), gliomas, and inflammation (Sofroniew MV and Vinters HV, 2010). Development of potential drug targets and therapies would be beneficial in treating CNS diseases such as these, particularly those targeted at astrocytes which play a central role in these diseases.

1.2.1. Neuroinflammation and neurodegenerative diseases.

1.2.1.1. Neuroinflammation

Features of inflammation in many CNS diseases such for example as AD, have been studied over many years, and this topic has been reviewed extensively (Schwab C et al., 2008, Rozemuller AJ et al., 2005). There are differences in the cellular components and the ways in which inflammation is mediated in the brain (neuro-inflammation) compared with the periphery. A complex network of cells, signaling molecules and molecular mediators of inflammatory responses interact within the brain. Astrocytes undergo activation in the areas involved in the disease progress and may release a variety of signaling molecules.

A host of secreted molecules enable communication between astrocytes, microglia and neurons. Many of these have been implicated as inflammatory mediators in AD and other CNS diseases. Examples include: s100B and α1-anti-chymotrypsin (α1-ACT), which are produced by astrocytes; cytokines such as TNF-α, IL-1β and IL-6; and chemokines such as macrophage colonystimulating factor and macrophage inflammatory proteins, which can promote proliferation and trophic support of specific types of inflammatory cells. Astrocytes, microglia and neurons are all able to produce complement proteins, which may act as direct mediators of inflammation and have been detected in neuropathologic studies of various CNS diseases. Together they can produce an environmental niche that may be stressful or damaging to surrounding cells.

In various CNS diseases, it has recently been proposed as an imaging target the mitochondrial protein called Traslocator Protein (TSPO) (Chen MK and Guilarte RT, 2008). TSPO basal expression is up-regulated in a number of human pathologies, including a variety of tumors and neuropathologies, such as gliomas and neurodegenerative diseases (Huntington's and Alzheimer's diseases), as well as various forms of brain injury and inflammation (Papadopulus V and Lecanu L, 2009, Chen MK and Guilarte RT, 2008).

In this view, the evaluation of TSPO expression and distribution may represent a promising diagnostic marker in pathological conditions, prompting the development of new synthetic molecular probes specific for this protein receptor (Doorduin J et al., 2008). These compounds are generally derivatives of selected ligands that may be chemically modified in such a way to retain high receptor affinity and selectivity while permitting the visualization of the receptor protein.

Over the last decade, identification of **biomarkers** that can reliably detect the early stages of CNS diseases has been important in both the design of clinical trials and in the accurate identification of research patient populations. Markers that change with disease progression may be useful in assessing rates of disease progression and the efficacy of potential therapeutics on the pathology.

Biomarkers used to assess disease severity should be measurable, reproducible, and demonstrate changes with disease progression in longitudinal studies. The use of such markers in the trials of disease modifying therapies will help to identify the appropriate dosage, measure drug efficacy in proof-of-concept trials, and to improve safety assessments.

In recent years, research into biomarker discovery has successfully utilized genomics, proteomics, and metabolomics for the identification of several promising markers. Targets have been identified in blood, CSF and cells of individuals affected by different CNS diseases. These include proteins involved in inflammation, oxidative stress, apolipoproteins, and markers of neurodegeneration (Maes et al., 2007).

While promising, most of these markers have not yet been validated in more than one study and their ultimate usefulness awaits further studies.

Some of these biomarkers can be easily detected in blood or CSF samples, while those which are located in the membrane, the cytoplasm, or the nucleus of the target cells, require a different kind of detection. Indeed, visualization of these markers usually requires specific detection techniques such as antibody staining, in situ

hybridization, or autoradiography, unless fluorochromes are used that are detectable without further manipulation of the labeled cells.

An ideal marker should label cells efficiently and stably allowing for the specific and sensitive detection of single cells. Most markers only partially fulfill these criteria and, therefore, the choice of a certain marker depends on the experimental setup, the grade of tissue manipulation needed for marker detection, and the stability of the marker in the experimental conditions.

The use of **fluorochromes** as probes for the study of proteins has been recently considered a valid alternative to traditional methods of study and research in biology. They provide a wide range of information on the receptors to which they are related, their location and on the interaction of these receptors in viable cells. In addition, fluorescent ligands may represent a useful alternative compared to radiolabeled ligands. Indeed, fluorescent ligands have higher sensitivity and security and are more cost effective compared to radiolabeled ligands.

Recent studies employing **fluorescent compounds** capable of specifically binding cell surface receptors whose density is altered in **CNS diseases**, have highlighted the possibility of using these new ligands as probes for diagnostic imaging (Daly CJ et al., 2003, Taliani S et al., 2007). The success of these observations depends on the ability of the probe to bind the receptor specifically at low concentrations during both positron emission tomography (PET) and single photon emission tomography (SPECT). The same probes, when used in techniques such as computed tomography (CT) and magnetic resonance imaging tomography (MRT), however, require higher concentrations. Generally, to be used as a probe, the ligands must have a high affinity for the receptor. In addition it should be possible to remove the ligand in excess from the tissue under examination simply washing the sample. This may represent a limit for the studies because experiments conducted on tissues have shown that the techniques used for washing cause often an alteration of the chemical equilibrium with consequent detachment of the fluorescent ligand from the receptor. Finally, the probe must display a good resolution image even at low concentrations.

Another versatile tool for the study of receptors are irreversible ligands. (Newman AH, 1991). These agents have been invaluable in the characterization, isolation and purification of a number of receptor systems, including TSPO. This has allowed for a greater understanding of their physiological and pharmacological properties, which aid in designing better therapeutic compounds. The strategy is to

introduce on a high affinity ligand a chemical moiety that permits the covalent binding to the receptor protein.

In chapter 2 the biological characterization of two novel irreversible ligands as well as an irreversible fluorescent ligand to TSPO is described in detail.

1.2.1.2. Neurodegenerative diseases: Amyotrophic lateral sclerosis

ALS is characterized by premature death of upper and lower motor neurons starting in adulthood. The pathology of ALS is characterized by abnormal accumulation of insoluble and misfolded proteins in degenerating motor neurons. Neuronal death results in progressive paralysis, which typically is fatal 2–5 years after the onset due to respiratory failure. Ten percent of ALS cases are inherited, while the rest are considered sporadic and the cause has not been discovered yet. Twenty percent of inherited ALS cases are caused by mutations in the gene encoding for superoxide dismutase 1 (SOD1) (Rosen DR et al., 1993, Pasinelli P and Brown RH, 2006). SOD1, a ubiquitously expressed enzyme, catalytically converts reactive superoxide to oxygen and hydrogen peroxide. It is now recognized that all mutations of the SOD1 gene (both enzymatically active and inactive mutants) uniformly cause toxicity in cells not by loss but rather by gain of function where accumulation of protein in neurons and glia causes toxicity. However, the exact mechanisms and nature of toxicity is still unknown (Bruijn LI et al., 2004, Turner BJ and Talbot K, 2008). Currently, numerous mechanisms of toxicity have been proposed that could mediate pathology in mutant SOD1-mediated ALS. The most important mechanisms are thought to be excitotoxicity from glutamate, failure of protein degradation machinery, endoplasmic reticulum stress, damage to mitochondria, superoxide generation through neuroinflammation, axonal transport disruption, etc. (Rothstein JD et al., 1995, Yang Y et al., 2009, Kikuchi H et al., 2006, Liu J et al., 2004, Harraz MM, 2008, Williamson TL and Cleveland DW, 1999, Zhong Z et al 2008).

There is good evidence for all of these mechanisms to be at play, and most likely it is a combination of different events that contribute to the overall development of ALS pathology.

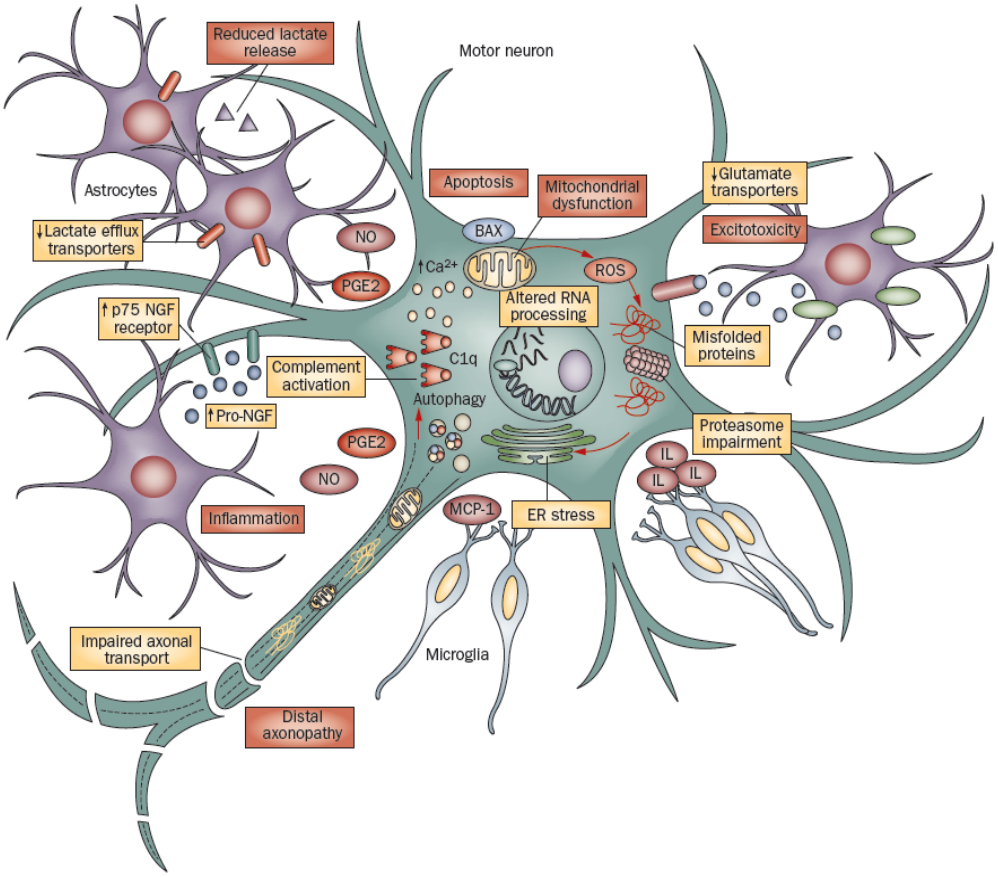

Figure 2. Molecular mechanisms of motorn neuron injury in ALS. ALS is a complex disease involving activation of several cellular pathways in motor neurons, and in dysregulated interaction with neighboring glial cells. Microglia activate an inflammatory cascade via secretion of MCP-1 and other cytochines. Astrocytes contribute to motor neuron injury through various mechanisms, including release of inflammatory ediators such as NO and PGE2; reduced expression and activity of the glutamate reuptake transporter EAAT2; reduced lactate release; and activation of pro-NGF-p75 receptor signaling. Motor neurons might also undergo transcriptional dysregulation and abnormal RNA processing which, together with overproduction of ROS, contribute to aberrant protein folding. Aberrant proteins can form aggregates, leading to proteasome impairment and ER stress, and ultimately activating autophagy and apopthotic pathways. Mitochondrial impairment and dysregulation of calcium handling are two major components of motor neuron injury that also lead to activation of the apoptotic cascade that is observed in ALS. Motor neurons can produce and secrete complement subunits that are important signals of cellular stress to neighboring cells. Abbreviations: ALS, Amyotrophic lateral sclerosis; EAAT2, excitatory amino acid transporter 2, ER, endoplasmic reticulum; IL, interleukin; MCP-1, monocyte chemoattractant protein; NGF, nerve growth factor; NO, nitric oxide; PGE2, prostaglandin E2; ROS, reactive oxygen species.

[Modified from Ferraiuolo L et al., 2011]

The discovery of SOD1 mutations led to the development of animal models that recapitulate ALS-like disease. Overproduction of mutated human SOD1 protein in these mouse models leads to a progressive neurodegenerative disease that closely resembles human pathology with a selective motor neuron death and gliosis accompanied by accumulation of misfolded proteins (Gurney ME et al.,1994.).

Originally, the selective death of motor neurons was believed to be caused by a cell autonomous mechanism. However, through genetic and chimeric mice studies there is indication that it may actually be non-cell autonomous mechanisms. These studies showed that when expression of SOD1 mutations was restricted to either motor neurons or astrocytes, but not in both simultaneously, it did not lead to the development of ALS (Lino MM et al., 2002, Pramatarova A et al., 2001, Gong YH et al., 2000.). Other labs have succeeded in producing very late onset disease in mice when mutant is expressed in only neurons (Jaarsma D et al., 2008). However, the severity and speed at which the disease progressed in the mice was much more modest when compared to mice expressing the same mutant gene ubiquitously.

Next wild-type neurons were analysed in chimeric mice containing both wildtype and mutant SOD1-expressing cells. They showed that neurons surrounded by glial cells bearing SOD1 mutation acquired an ALS phenotype (Clement AM et al., 2003). When they excised the mutant floxed SOD1 gene in either astrocytes or microglia through the use of a Cre recombinase, they saw a slowing in the disease progression and an extension in life expectancy (Yamanaka K et al., 2008, Boill´ee S et al., 2006, Wang L et al., 2009, Wang L et al., 2011). Immunohistological studies also showed glial cell involvement in ALS pathology where astrogliosis and microgliosis are considerable hallmarks of the disease (Hall ED et al., 1998, Alexianu ME et al., 2001). Among the non-neuronal cell types, a role of glial cells, and in particular of astrocytes, in ALS has been most intensively investigated.

Evidence is available suggesting two quite different potential roles for astrocytes in ALS or motor neuron disease, through either the loss of a neuroprotective function or the gain of a neurotoxic effect. Sporadic ALS is characterized by selective loss or dysfunction of astrocyte glutamate transporters in spinal cord and cerebral cortical areas that exhibit loss of lower and upper motor neurons, suggesting that increased glutamate excitotoxicity may contribute to motor neuron death and raising the possibility of different types of potential interventions (Fray AE et al., 1998, Maragakis NJ and Rothstein JD, 2006, Rattray M and Bendotti C, 2006, Rothstein JD et al., 1992).

A high-throughput screen of small molecules has identified that certain β-lactam antibiotics can stimulate the expression of glutamate transporters in astrocytes and thereby enhance glutamate uptake sufficiently enough to reduce excitotoxicity, and provide neuroprotection in animal models of stroke and ALS (Rothstein JD et al., 2005).

The β-lactam antibiotic, Ceftriaxone, began stage 3 clinical trials in May 2009 to determine efficacy in reducing excitotoxicity and neurodegeneration in ALS. Focal grafts of healthy astrocytes are reported to be neuroprotective in an animal model of ALS, suggesting that transplantation of astrocytes may be a potential therapeutic strategy (Lepore AC et al., 2008).

A second role that can be attributed to deleterious astrocytic behavior in ALS is an insufficient release of neurotrophic factors that are important in maintaining neuronal health. Glial-derived neurotrophic factor, brain derived neurotrophic factor, ciliary neurotrophic factor, and vascular endothelial growth factor are all released by astrocytes and can rescue motor neurons (Ekestern E, 2004, Dewil M et al., 2007). A loss of neurotrophins if not directly, then indirectly, might be a cause of neuronal death. In addition to neurotrophins, astrocytes may release hazardous factors. *In vitro* studies confirm that factors released by SOD1 astrocytes in culture media can induce apoptosis in motor neuron cultures. One of the identified toxic factors is neurotrophic growth factor (NGF) (Pehar M et al., 2004). Similarly, wild-type embryonic stem (ES) cell-derived motor neurons co-cultured with mutant SOD1-expressing glial fibrillary acidic protein (GFAP) positive astrocytes are induced to degenerate and die indicating non-cell autonomous degeneration mechanism (Nagai M et al., 2007, Di Giorgio FP et al., 2008, Di Giorgio FP et al., 2007, Marchetto MCN et al., 2008).

The role of astrocytes in ALS pathology has been widely recognized and appreciated. Astrocytes have become an interesting therapeutic target, and many new studies are looking at various forms of intervention.

The transcription nuclear factor erythroid 2-related factor 2 (Nrf2) regulates the expression of genes containing antioxidant response element (ARE), which are preferentially activated in astrocytes. An attempt to activate Nrf2-ARE in astrocytes has been successful in protecting neighboring neurons *in vitro*, and extends the survival in ALS mice (Vargas MR et al., 2008). Increased level of glutathione [ɣ-l-glutamyl-l-cysteinylglycine (GSH)] seems to be a major component of the protection conferred by Nrf2 activation. Glutathione is synthesized by the consecutive action of two enzymes,

glutamate-cysteine ligase (GCL) and glutathione synthetase. Nrf2 regulates both enzymes and GCL is the rate-limiting enzyme for glutathione synthesis.

Increased production and secretion of glutathione by astrocytes is known to improve the antioxidant status of co-cultured neurons and protect them from oxidative insults (Dringen et al., 2000).

In this view, the identification of activators of Nrf2-ARE pathway in astrocytes may represent a promising strategy to extend the survival of patients suffering from ALS.

Chapter 3 will describe the experiments I performed during the period I spent at the Sheffield Institute for Translational Neuroscience, SITraN, (Sheffield University, UK). There I screened two libraries of small molecules on different cell lines (as C6 rat astrocyte cell line) in order to identify activators of Nrf2-mediated transcription.

1.2.2.Glioblastoma multiforme

Glioblastoma multiforme (GBM, WHO grade IV) is the most malignant common cancer of the central nervous system and is particularly resistant to chemotherapy currently in use. The GBM represents approximately 60% of all primary malignant brain tumors, and although the techniques in neurosurgery, radiotherapy and the introduction of new cancer agents have improved, the overall survival is still low, particularly in patients with recurrent or refractory GBM.

Histologically it is characterized by the proliferation of vascular endothelial (neoangiogenesis) and large areas of necrosis with consequent alteration of the blood-brain barrier. The GBM mainly affects adults and occurs more often in the subcortical white matter of the cerebral hemispheres. The sites most commonly affected are the temporal lobe (31%), the parietal lobe (24%), the front (23%) and occipital lobes (16%) with the typical combination being fronto-temporal (Kleihues P et al., 2007). Less frequently they are localized to the cerebellum, brainstem and spinal cord. Except in very rare cases, GBM’s do not expand beyond the structures of the CNS.

Glioblastoma can develop from a diffuse astrocytoma or an anaplastic astrocytoma (secondary glioblastoma) but more frequently occurs de novo, without any evidence of previous cancer (primary glioblastoma) (Figure 3).

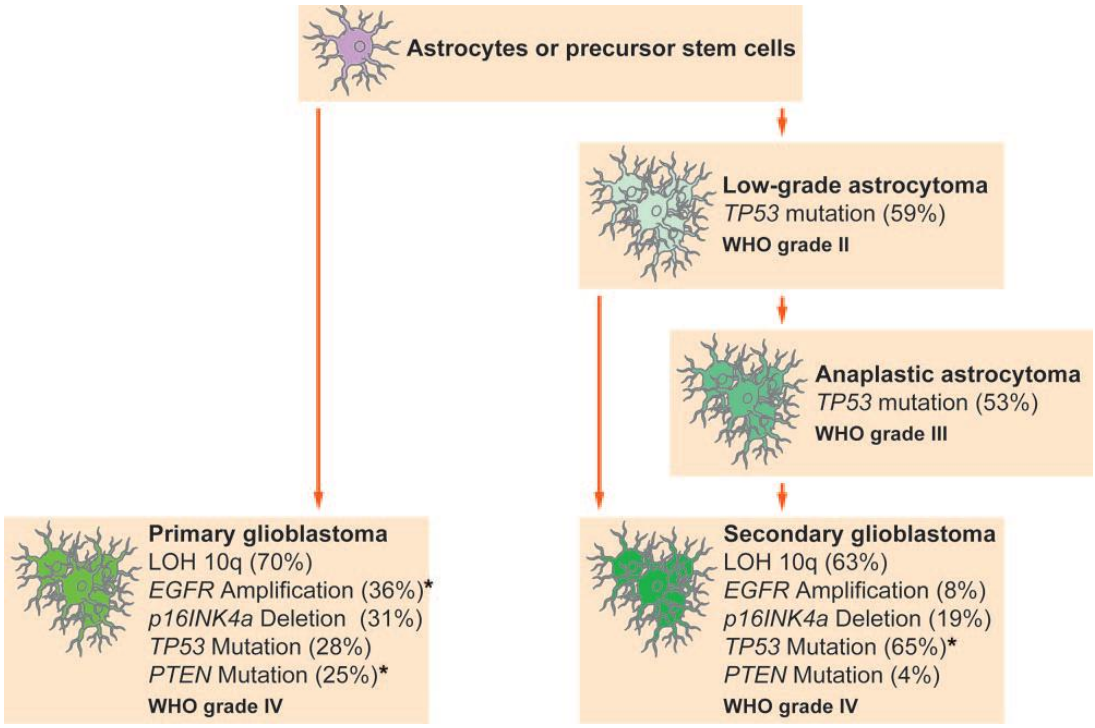

Figure 3.

The GBM cells of origin, whether potentially astrocytes, glial precursors, or stem cells, are the subject of intense investigation (Furnari FB et al., 2007). Consistent with the cancer stem cell hypothesis, there is considerable evidence that only minor populations of cells in primary gliomas are capable of forming a tumor, (Furnari FB et al., 2007, Singh SK et al., 2004). The GBM contains small numbers of cells that exhibit stem cell-like properties, called brain tumor stem-like cells (BTSC) (Charles NA et al., 2011), in that they self-renew, are multipotent and form neurospheres *in vitro* and constitutively produce the different types of cells found within the parent tumors (Nakano I and Kornblum HI, 2009). Growth properties of glioma-derived neurospheres *in vitro* were found to be significant predictors of tumor progression *in vivo* and of clinical outcome (Laks DR et al., 2009). Nevertheless, the origins of gliomas are not yet understood and could be heterogeneous.

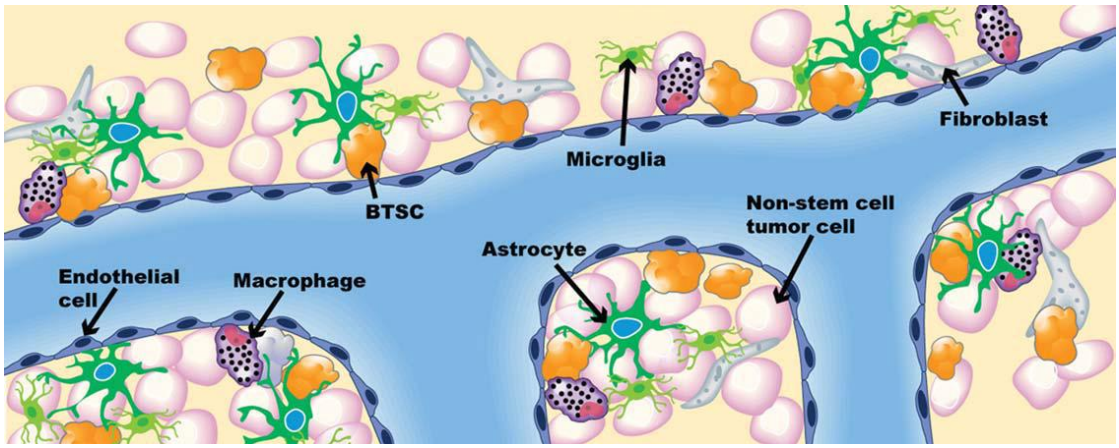

Figure 4. The glioblastoma microenvironment is composed of several stromal cell types, each of which are believed to make distinct contributions to tumor progression and invasion. These cells include but are not limited to astrocytes, macrophages, pericytes, fibroblasts, and endothelial cells.

BTSCs are refractory to conventional therapy that includes radiation therapy and chemotherapy with alkylating agents of DNA (Salmaggi A et al., 2006), also the blood-brain barrier provides extra resistance to chemotherapy because it makes difficult the distribution of drugs from the blood to the brain tissue.

Alkylating agents are the most widely used chemotherapeutic agents to treat GBM. Among the chemotherapeutic compounds used is temozolomide (TMZ), a cytotoxic alkylating agent, has shown activity in recurrent glioblastomas (Brada M et al., 1999; Conrad CA et al., 1995; Hirose Y et al., 2001; Levin VA et al., 2001).

It has delayed tumour progression and prolonged patient survival; however, many patients develop resistance to this drug, have tumour recurrence, and typically survive only 12-15 months after diagnosis.

Therefore, new approaches are essential for the treatment of these patients, especially because the occurrence of gliomas is increasing (Hess KR et al., 2004, Johannesen TB et al., 2004).

In chapters 4 and 5 the biological characterization of novel promising molecules acting on different interesting targets for glioma therapy is reported.

Chapter 2: Neuroinflammation

Translocator Protein (TSPO)

Previously named the peripheral benzodiazepine receptor (PBR), the translocator protein is an 18 kDa protein located primarily in the outer membrane of mitochondria. The earliest term, PBR, was widely accepted in the scientific community even though multiple other names have been used to identify this protein, including mitochondrial benzodiazepine receptor, mitochondrial diazepam-binding inhibitor receptor complex, isoquinoline-binding protein, pk18 and ω3 (Papadopoulos V et al., 2006). Although each name identified specific properties, none of them completely reflects the nature and function of TSPO. For this reason, the scientific community has progressively supported renaming of the protein, from PBR to TSPO, with the aim of accurately representing the subcellular roles and putative tissue-specific functions.

TSPO was first identified as a benzodiazepine-binding site outside the central nervous system (Braestrup C et al., 1977).

In addition to benzodiazepine derivatives (i.e., Ro5-4864), TSPO binds high-affinity endogenous ligands, such as protoporphyrin IX, diazepam-binding inhibitor, triakontatetraneuropeptide, phospholipase A2 and cholesterol (Ferrero P et al., 1986, Slobodyansky E et al., 1989, Snyder MJ et al., 1998, Lacapère JJ et al., 2003). It is also able to bind synthetic ligands, including isoquinolines (i.e., PK11195), imidazopyridines (i.e., Alpidem), indole derivatives (i.e., FGIN-1-27 and SSR180575), pyrrolobenzoxazepines and phenoxyphenyl acetamide derivatives (i.e., DAA1106). TSPO contains 169 amino acids that are arranged in five transmembrane segments, each of which is composed of approximately 21 amino acids in an α-helical structure (Joseph-Liauzun E et al., 1998). Potential binding sites for ligands have been described in the literature. For instance, the first cytoplasmic loop (L1) seems to be essential for the binding of PK11195, Ro5-4864 and benzodiazepines. The TSPO-binding site for carboxamide derivatives involves two loops (L1 and L3). Finally, the C-terminal region, located on the cytoplasmic side of the membrane, has been shown to be part of the binding site for cholesterol (Joseph-Liauzun E et al., 1998).

TSPO has been found in the entire animal kingdom, including insects, molluscs, amphibians, aves and mammals. Apart from its abundance in peripheral

tissues (Braestrup C et al., 1977, Verma A et al., 1989), TSPO is also present in glial cells (Syapin PJ et al., 1979, Schoemaker H, et al., 1983).

At the subcellular level, TSPO is reported to be located primarily in mitochondria, at the contact sites between the outer (OMM) and inner (IMM) mitochondrial membranes (Anholt RR et al., 1986, Antkiewicz-Michaluk L et al., 1988, Culty M et al, 1999).

The topography and organization of TSPO have been investigated by transmission electron and atomic force microscopy performed on mitochondrial preparations; these images showed that TSPO forms clusters containing four to six molecules. Notably, after hormonal treatment, the formation of 15–25 gold particle clusters, larger than the previous clusters, has been described (Papadopoulos V, et al, 1999). Furthermore, UV photoirradiation of recombinant TSPO stimulates polymer formation, probably due to the generation of reactive oxygen species, and spectroscopic analysis revealed the formation of dityrosines as covalent cross-linkers between TSPO monomers (Delavoie F et al., 2003, Papadopoulos V et al., 1999).

Many cellular functions are directly or indirectly associated with TSPO, including regulation of cholesterol transport, synthesis of steroid hormones, porphyrin transport, heme synthesis, anion transport, regulation of mitochondrial functions, immunomodulation, cell proliferation and apoptosis. In particular, TSPO is largely involved in the complicated apoptotic mechanism, forming a mitochondrial protein complex in association with the voltage-dependent anion channel (VDAC) and the adenine nucleotide transporter (ANT). These three proteins are the core components of the mitochondrial permeability transition pore (MPTP) (Maaser K et al., 2001) (see Figure 1).

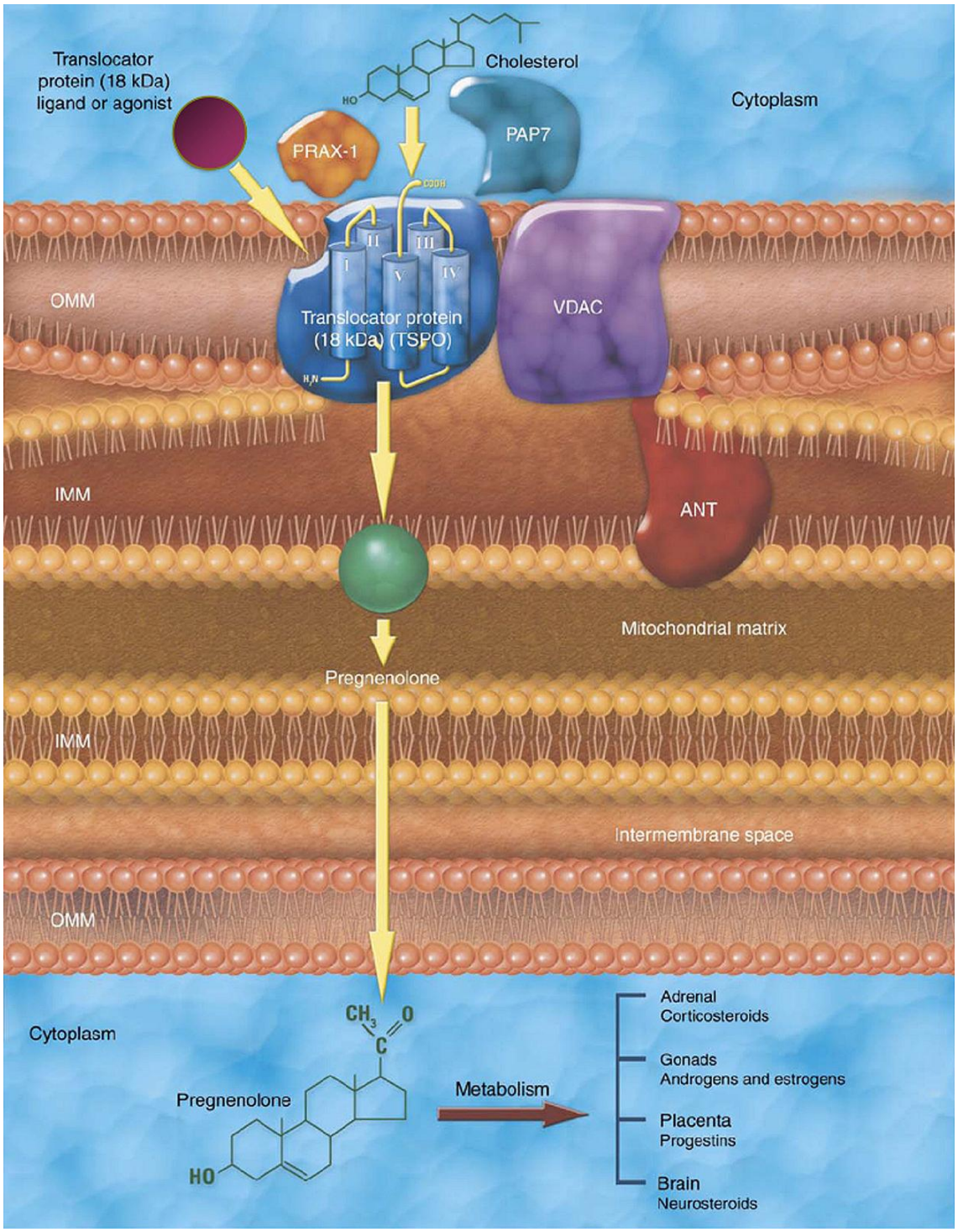

Figure 1. The mithocondrial protein complex (Taken from Papadopoulos et al., 2006).

As previously reported, clinical investigations have revealed that PBR basal expression is up-regulated in a number of human pathologies, including a variety of tumors. Furthermore, significantly enhanced PBR expression has been observed in neurodegenerative diseases (Huntington's and Alzheimer diseases and Multiple sclerosis), as well as in various forms of brain injury and inflammation (Chen MK and

Guilarte RT, 2008). All these findings have stimulated the development of new ligands targeting TSPO as powerful tools to image and measure the expression level of this protein in both humans and animals (Fookes C J et al., 2008, Briard E et al, 2008, Dollè F et al, 2009, Taliani S et al., 2010).

Fluorescent ligands represent a safer faster and less-expensive alternative to radioligands in probing the ligand-receptor complex. Fluorescent agents with high specificity and attractive spettroscopic properties are therefore needed in the field of biomedical research.

Experimental section

Novel irreversible fluorescent probes targeting the 18kDa translocator protein: biological characterization

In this field, Taliani et al. have recently developed novel highly potent and selective fluorescent probes targeting TSPO with the general formula II, designed as derivatives of the highly potent N,N-dialkyl-2-phenylindol-3-ylglyoxylamide ligands I, (Primofiore G et al., 2004, Da Settimo F et al., 2008) featuring the fluorescent moiety linked to the N-alkyl chain (see Figure 2) (Taliani S et al., 2007). For these compounds, the researchers selected the well-known 7-nitrobenz-2-oxa-1,3-diazol-4-yl (NBD) group as the fluorophore, because its small size does not generally affect affinity of the parent ligand (Taliani S et al., 2007).

Tissue experimental procedures using a labelled ligand often cause the alteration of the chemical equilibrium and the subsequent loss of the bound fluorescent ligand. To overcome this problem, some high affinity ligands which bind covalently to the receptor protein have been developed (Taliani S et al., 2007).

In this chapter the biological characterization of a series of 2-phenylindol-3-ylglyoxylamides, and the test of their validity as new TSPO probes is reported. All of these compounds are characterized by the presence of a chemoreactive isothiocyanate group, able to bind the receptor protein irreversibly and covalently (compounds **7-8**, Figure 2). Moreover, compound **18** (Figure 2) featuring the NBD-fluorescent moiety was synthesized to develop an irreversible fluorescent probe. The presence of these two devices (a chemoreactive group and a fluorescent chromophore) on a single molecule may offer a multiplicity of advantages, both in protein purification/characterization, and in protein cell visualization/density determination.

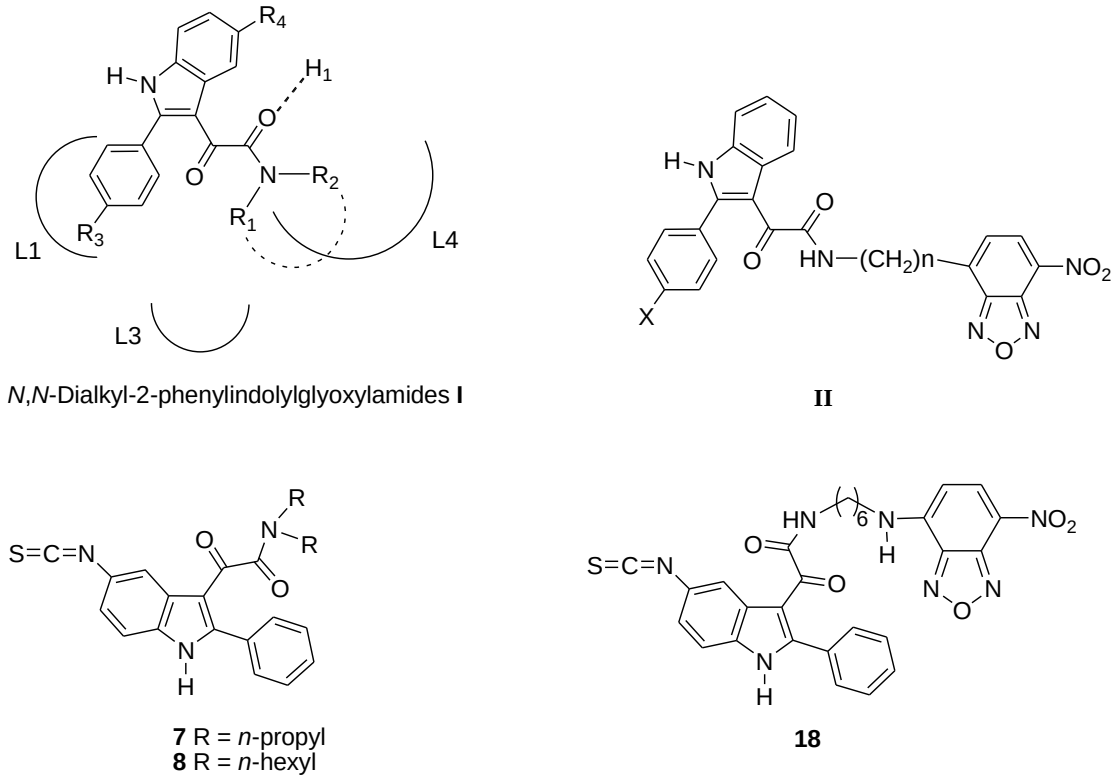

N,*N*-Dialkyl-2-phenylindolylglyoxylamides **I**

II

7 R = *n*-propyl
8 R = *n*-hexyl

18

Figure 2. Structures of Known (I and II) and Novel (**7, 8**, and **18**) TSPO Ligands

Materials and methods

Materials

[3H]Ro 5-4864 (s.a. 70.0 Ci/mmol) was purchased from Perkin-Elmer Life Sciences. Ro 5-4864 powder was obtained from Sigma-Aldrich.

Compounds **7**, **8** and **18** were synthesized in the laboratory of Professor Da Settimo at the University of Pisa.

Cell culture

The human GBM cell line U87MG was obtained from the National Institute for Cancer Research (ICLC) of Genoa. The U87MG cell ($1x10^6$) were seeded onto 10 cm plates and cultured in RPMI medium supplemented with 10% fetal bovine serum (FBS), 2 mM L-glutamine, 100 U/ml penicillin, 100 mg/ml streptomycin, and 1% non-essential amino acids, at 37°C in humidified atmosphere composed of 5% CO2 and 95% O2. After 24 h the medium was replaced by 2ml of serum-free RPMI 1640 containing 2mM

L-glutamine, 100 U/ml penicillin, 100mg/ml streptomycin and 1% of non-essential amino acids.

[3H]Ro 5-4864 binding to Rat Kidney Mitochondrial Membranes: reversible binding

The binding studies were carried out essentially as previously described (Taliani S et al., 2007, Selleri, S et al., 2005).

Time course of binding of the new ligands to the TSPO receptor: irreversible binding

The binding studies were carried on essentially as previously described (Martini C et al., 1987). Briefly, rat kidney membranes were incubated with each compound (concentration range: 1 nM - 1 µM) for different times (0, 10, 30, 60, 90 and 180 min), in binding assay buffer. Incubations were stopped by the addition of 1 ml of ice-cold 50 mM Tris/HCl buffer (pH 7.4), and then the samples were centrifuged for 15 min at 13,000 x g at 4 °C. Pellets were washed twice with cold binding buffer. Then, samples were processed for determination of protein content. [3H]Ro 5-4864 binding assays were performed in a final volume of 500 µl of binding assay buffer containing membranes (65 µg of protein/tube), as mentioned above.

Fluorescent labelling of human glioma cells

U87MG cells were cultured in 96-well plates ($4x10^4$ cells/well) in RPMI 1640 complete medium. After 24 h, the cells were incubated with different concentrations of compound **18** (100 nM, 250 nM and 500 nM) in cell culture medium, for 20 and 90 minutes, under 5% CO2 at 37 °C. In parallel, some samples were incubated with Ro 5-4864 10 µM prior to add compound **18**. To remove the excess of unbound compound, the cells were washed four times with cell medium with cysteine, a molecule able to react with the isothiocyanate group. After washing, PBS was added to the cells and the fluorescence intensity (Ex:485 nm; Em: 535 nm) from each sample was measured by Victor Wallac 2 (Perkin Elmer, Boston, USA). All data are presented as means ± SEM, derived from at least three independent experiments done in duplicate.

Data Analyses

Data were analysed by use of the GraphPad Prism software (GraphPad Software, version 4.0; San Diego, CA). Statistical analyses were performed by one-way ANOVA (with post hoc Bonferroni test).

Results

As a first step, the equilibrium binding parameters (IC50 and Ki values) of the test compounds were derived by competition experiments against [3H]Ro 5-4864 in rat kidney membranes. Ro 5-4864 was used as the reference standard, showing a Ki value of 23 nM. The curves of [3H]Ro 5-4864 displacement by the irreversible ligands **7** and **8**, and by the fluorescent ligand **18** are shown in Figure 3. Binding data for the three ligands **7**, **8**, and **18** are listed in Table 1: all compounds showed affinity values in the nanomolar range, comparable to that of the reference standard Ro 5-4864 (Ki from 37.6 nM to 49.5 nM).

a)

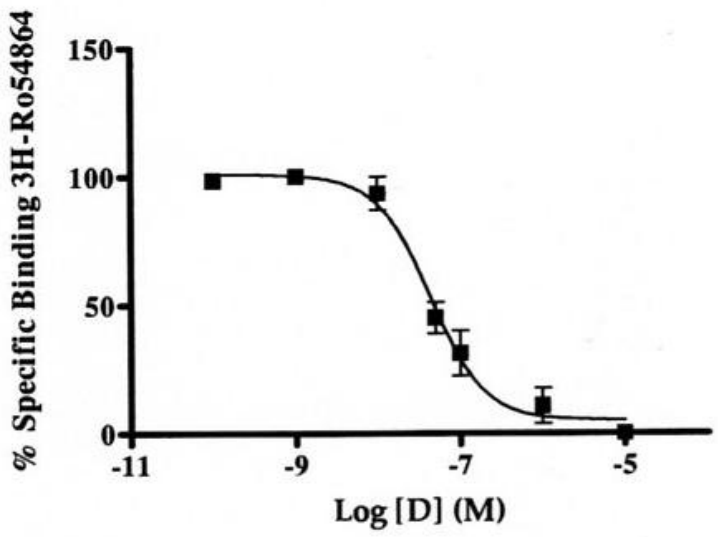

b)

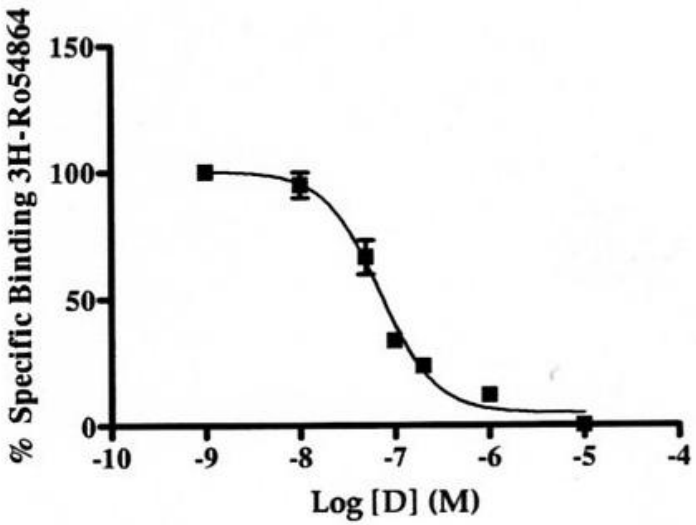

c)

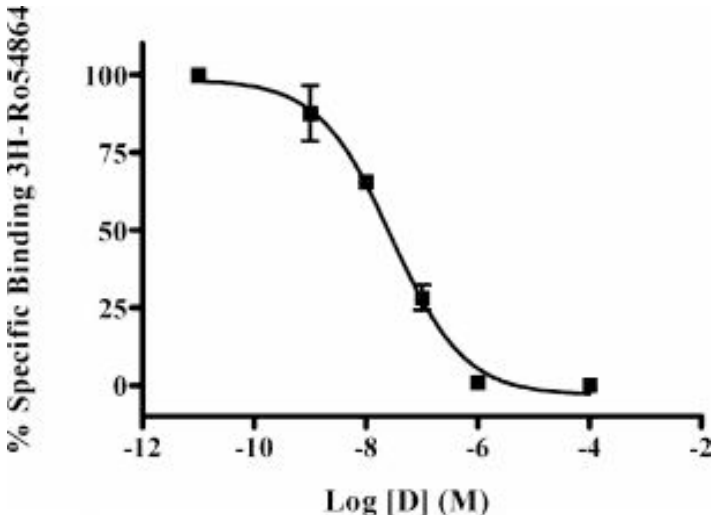

Figure 3. Displacement of [^{3}H]Ro 5-4864 by compound **7 (a)**, **8 (b)**, and **18 (c)** in rat kidney mitochondria membranes. Bound radioactivity is expressed as a percentage of specific binding in the presence of competitor molecule. Points represent the mean values ± SEM of triplicate determinations pooled from three independent experiments.

Compound	IC_{50} (nM)	K_i (nM)
7	45.6±0.4	37.9±0.4
8	59.7±0.6	49.5±0.5
18	42.2±0.4	37.6±0.4
Ro 5-4864	-	23±3.1

Table 1. Values of IC_{50} and K_i for compounds **7**, **8**, and **18** obtained from three independent equilibrium binding assays. The IC_{50} values were converted to an absolute inhibition constant K_i, using the Cheng-Prusoff equation (Cheng Y and Prusoff WH, 1973). Data are shown as values ± SEM.

In order to investigate the potential covalent binding of compounds **7**, **8**, and **18** to TSPO, the samples derived from competition radiobinding assays were diluted more then ten times with fresh buffer at the end of the incubation time: data did not markedly change with respect to those obtained in the undiluted samples (data not shown). This observation indicates that the TSPO-ligand interaction is irreversible, and it immediately disqualifies the application of the Cheng-Prusoff equation (Cheng Y and Prusoff WH, 1973) in binding parameter analysis.

With the aim of evaluating the rate order of the binding reaction, a kinetic analysis method was developed, as reported in literature (Liu-Chen LY et al., 1975, Taliani S et al., 2007). Results showed that mitochondrial membrane pre-treatment with newly synthesized TSPO ligands inhibited the [3H]Ro 5-4864 binding to TSPO. This inhibition was time- and ligand concentration-dependent, as showed in Figure 4, where B is binding after pre-treatment of membranes with different concentrations of TSPO ligands for several times, and B0 is control binding. When the B and B0 ratio was plotted on a logarithmic scale versus incubation times, the decrease in the ln B/B0 values appeared to be linearly related to the pre-incubation time. Therefore, inactivation proceeded according to apparent first-order kinetics.

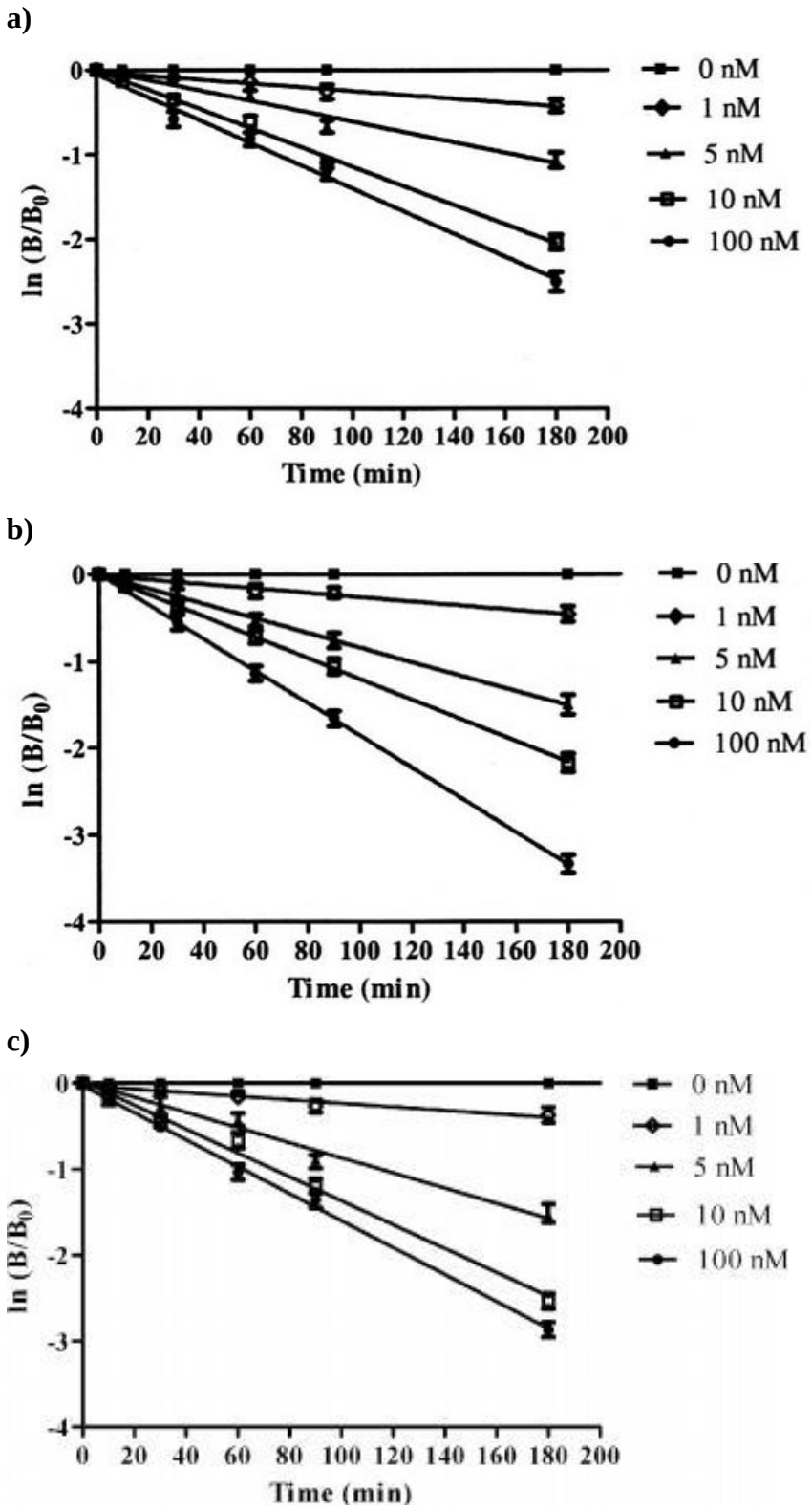

Figure 4. Time course of compounds **7 (a), 8 (b)** and **18 (c)** binding to receptor. The semi logarithmic representation of the decrease in [^{3}H]Ro 5-4864 binding to TSPO by pre-treatment (0, 10, 30, 60, 90 and 180 min) with various concentrations of compound **18** is shown. Points represent the mean values ± SEM of duplicate determinations pooled from three independent experiments.

The apparent first-order rate constant (Kobs) was defined by equation 1:

$$\ln \frac{B}{B_0} = -K_{obs} \times t \qquad \text{[eq. 1]}$$

Thus, a mathematical analysis was conducted to calculate the dissociation constant (Kd) of the reversible receptor-ligand complex, and the pseudo first-order rate constant (K2) for the irreversible interaction between the receptor and the irreversible ligand, as previously reported by Liu-Chen and colleagues (Liu-Chen LY et al., 1975). The mathematical equation describing the process is shown below (eq. 2):

$$\frac{1}{K_{obs}} = \frac{K_d}{K_2} \cdot \frac{1}{[D]} + \frac{1}{K_2} \qquad \text{[eq. 2]}$$

Kobs is the observed first-order rate constant for irreversible binding, and it is derived from the slope of the different straight lines shown in Figure 4. The plotting of 1/Kobs versus 1/[D] (where D is the ligand concentration) gave a straight line that intercepted the ordinate and abscissa axes at 1/K2 and -1/Kd, respectively. The slope of the line was the ratio Kd/K2 (Figure 5). K2 and Kd values of each compound are listed in Table 2. Interestingly, all the Kd values are in the nanomolar range (Kd from 3.17 to 8.31 nM), confirming an effective interaction with the receptor.

a)

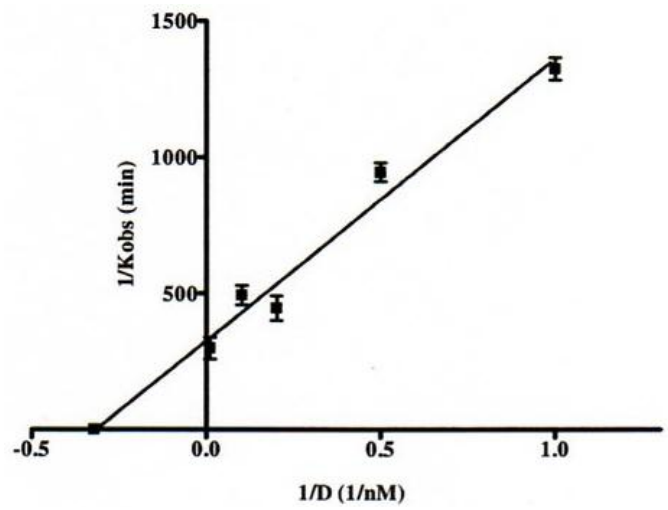

b)

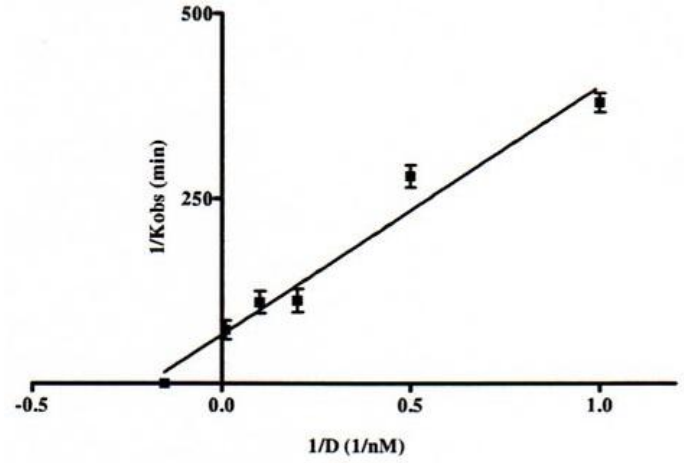

c)

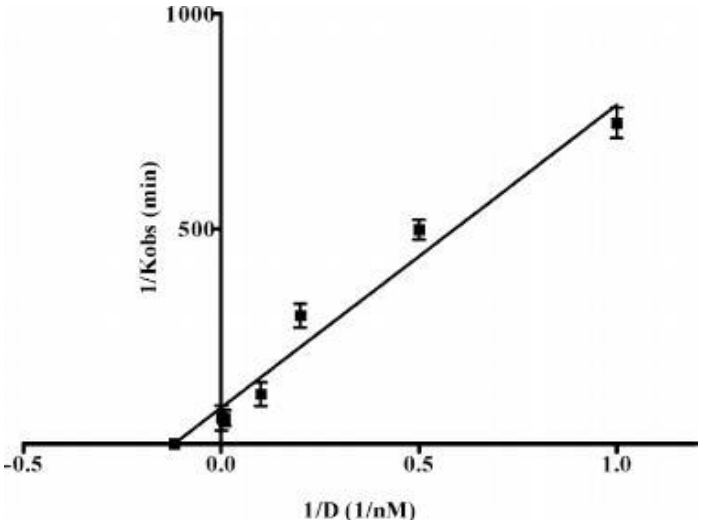

Figure 5. Calculation of K_2 and K_d for ligand **7 (a), 8 (b) and 18 (c).** On the basis of data obtained by three different experiments carried out in duplicate, the values were calculated in accordance with equation 2. Data are shown as mean values ± SEM.

Compound	K_2 (nM)	K_d (nM)
7	0.003±0.001	3.17±0.31
8	0.015±0.002	5.07 ±0.61
18	0.012±0.002	8.31±0.89

Table 2. Values of K_2 and K_d for the irreversible binding of compounds **7**, **8**, and **18** to TSPO. Data, obtained from 3 independent kinetic assays, are shown as values ± SEM.

To estimate the ability of compound **18** to permeate cell membranes, a number of its physicochemical properties were calculated and reported in Table 3. Values obtained were consistent with an adequate distribution of **18** into the cell.

compd	ClogP[a]	ASA[b] (Å)	PSA[c] (Å)	*N*[d]	bond count	rb[e]	MW[f](Da)
18	4.485	847.530	170.945	67	46	13	583.620

[a] Calculated *n*-octanol/water partition coefficient. [b] Total Solvent Accessible Surface Area. [c] Polar Surface Area. [d] Number of atoms. [e] Number of rotatable bonds. [f] Molecular weight.

Table 3. Physicochemical predicted properties of compound **18**.

The ability of the probe to specifically and irreversibly label TSPO was evaluated in live cells of human glioma, using fluorescence spectroscopy. For this purpose, U87MG glioma cells were incubated with different concentrations of **18** (100, 250 and 500 nM) after pre-treatment with buffer (control) or with 10 µM Ro 5-4864. Incubation was performed at 90 min, a time in which the irreversible bound is formed (see equations 2 and 3), and at a shorter time (20 min). As expected, at the shortest time the detected values of fluorescence intensity were smaller than the mean values obtained after 90 min (Figure 6, panel A and B, respectively). Interestingly, at 20 min time incubation, Ro 5-4864 was able to displace compound **18** in a similar extent for all the concentrations assayed, demonstrating the specificity of ligand **18**-TSPO binding.

Conversely, in the experiments performed at the longest time, Ro 5-4864 showed to be unable to displace **18**, demonstrating the irreversibility of the bond.

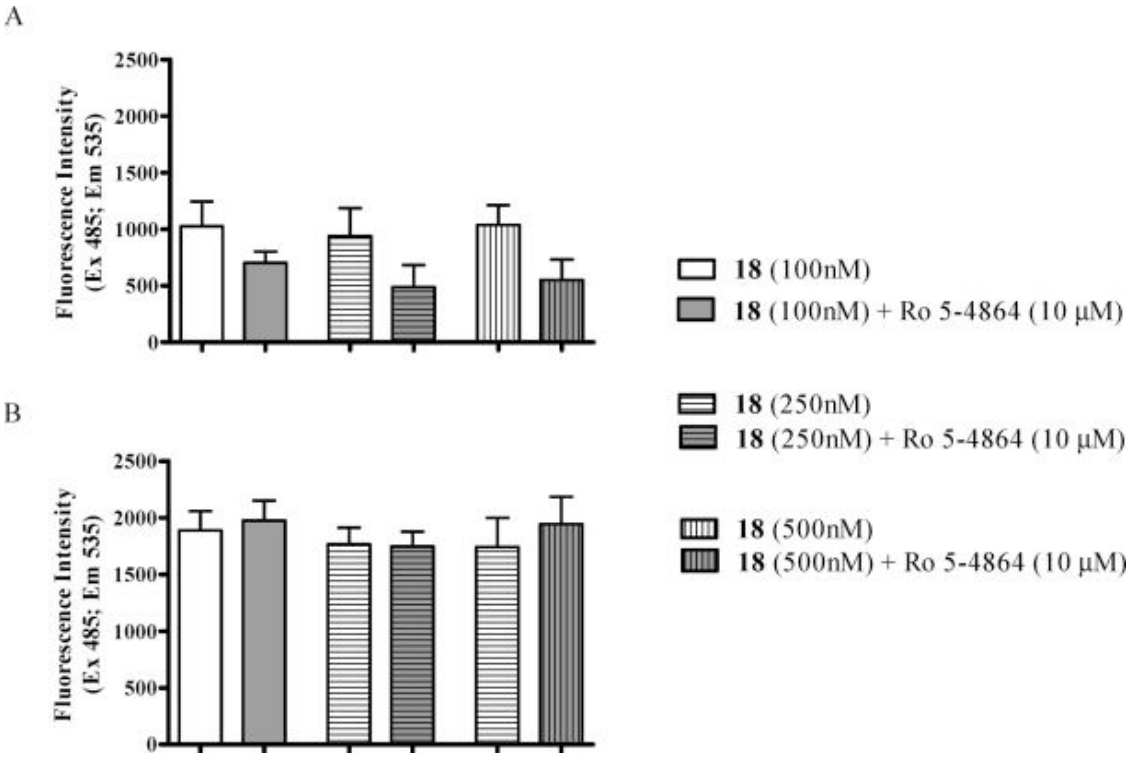

Figure 6. Human glioma cell staining with the irreversible fluorescent TSPO ligand **18**. The cells were incubated with compound **18** for 20 min (A) and 90 min (B), in the absence or presence of 10 µM Ro 5-4864 (grey bars). Data were obtained from 3 independent assays and are shown as mean values of Fluorescence Intensity ± SEM.

Conclusion

In conclusion, we biologically characterized novel irreversible TSPO ligands featuring the 2-phenylindol-3-ylglyoxylamide scaffold. The binding of these compounds to the receptor was investigated in detail, characterizing both order rate and kinetic constants. Experimental data showed that all the new derivatives effectively bind the receptor by means of an irreversible covalent interaction. Fluorescence spectroscopy experiments performed on derivative **18**, featuring an NBD fluorophore group, revealed its ability to specifically and irreversibly label TSPO in live U87MG glioma cells. All these novel irreversible TSPO ligands represent useful tools in the investigation of the physiological role of TSPO and in the detection of its expression levels.

In particular, the fluorescent probe **18** may be employed as diagnostic marker to evaluate the TSPO expression in peripheral cells, post-mortem and biopsy tissues, from patients affected by diseases in which the TSPO density is altered. Actually, irreversible probes offer the advantage of a lasting detection in visualization techniques that generally require multiple washes to remove the non-specific signal, steps in which reversible probes may be lost.

Complementary investigations using irreversible and reversible fluorescent TSPO ligands, in *in vitro* and *in vivo* studies, respectively, may offer a useful platform for the development of new diagnostic approaches in many CNS diseases such as neuroinflammation and neurodegeneration.

Chapter 3: Neurodegenerative diseases

Nrf2-ARE pathway: implications in Amyotrophic lateral sclerosis

Oxidative damage seems to play a major role in the pathogenesis of chronic motor neuron death in ALS based on the following lines of evidence: i) markers of oxidative damage of proteins, lipids, and DNA are elevated in brain and spinal cord in both mutant superoxide dismutase 1 (SOD1) ALS-mouse models (Gurney ME et al., 1994) and in human familial and sporadic ALS (Aguirre N et al., 2005, Beal MF et al. 1997, Ferrante RJ et al. 1997, Perluigi M et al., 2005), and ii) a large number of antioxidant compounds have been shown to be neuroprotective in ALS mouse models.

A major transcriptional modulator of the cellular antioxidant response is the transcription nuclear factor erythroid 2-related factor 2, NRf2. After activation and translocation to the nucleus, NRf2 binds to the ARE, a regulatory enhancer region within gene promoters, thus regulating the expression of more than 200 genes involved in the cellular antioxidant and anti-inflammatory defense. Among these are the classical phase 2 detoxification enzymes such as NAD(P)H quinone oxidoreductase and glutathione, enzymes that are necessary for glutathione biosynthesis, extracellular superoxide dismutase, glutamate-6-phosphatedehydrogenase, heat shock proteins, and ferritin (Figure 1). Furthermore, pro-inflammatory and anti-inflammatory enzymes such as cyclooxygenase 2, inducible nitric oxide synthase, and heme oxygenase-1 are also regulated in this manner (van Muiswinkel FL et al. 2005, Shih AY et al., 2005).

In addition to its role in inducing ARE-dependent gene transcription, Nrf2 also has direct cytoprotective effects via the inhibition of Fas-triggered apoptotic pathways (Kotlo KU et al., 2003).

Neuronal and astroglial cells from Nrf2 knockout mice are more vulnerable to oxidative stress than wild-type cells *in vitro*, and overexpression of Nrf2 increases resistance against oxidative and excitotoxic stimuli (Shih AY et al., 2005, Kraft AD et al., 2004, Lee JM et al., 2003).

The translocation of Nrf2 to the nucleus is inhibited by the actin-bound cytoskeletal zinc metalloprotein Kelch-like ECH-associated protein1 (Keap1), which interacts with Nrf2 and leads to its sequestration and subsequent degradation by the ubiquitin-proteasome system. Decreased Keap- Nrf2 binding (via oxidation of sulfhydryl groups or phosphorylation) results in intranuclear shuttling of Nrf2 and subsequent

transcription of ARE-driven genes (van Muiswinkel FL et al. 2005). Therefore, Keap1 and Nrf2 constitute a mechanism by which cells can sense damage caused by free oxygen radicals (Itoh K et al., 1999) (see Figure 2).

Recent evidence has emerged that Nrf2–ARE signaling may be dysregulated in mSOD1 models of ALS, and in the CNS of patients with ALS.

Multiple studies have shown that oxidative stress interacts with, and potentially exacerbates, other pathophysiological processes that contribute to motor neuron injury, including excitotoxicity, mitochondrial impairment, protein aggregation, ER stress, and alterations in signaling from astrocytes and microglia. Thus, effective alleviation of oxidative stress could potentially ameliorate multiple facets of the pathobiology of motor neuron degeneration. A meta-analysis of therapeutic interventions tested in mSOD1 mice up to 2007 concluded that antioxidant therapies were the most effective class of drug at improving survival (Benatar M, 2007). Antioxidants have not yet shown benefit in patients with ALS, although the reported trials have often been of suboptimal design (Orrell R et al., 2007).

On these bases, is evident the need for molecules able to activate the Nrf2-ARE pathway and exert an antioxidant activity in ALS therapy.

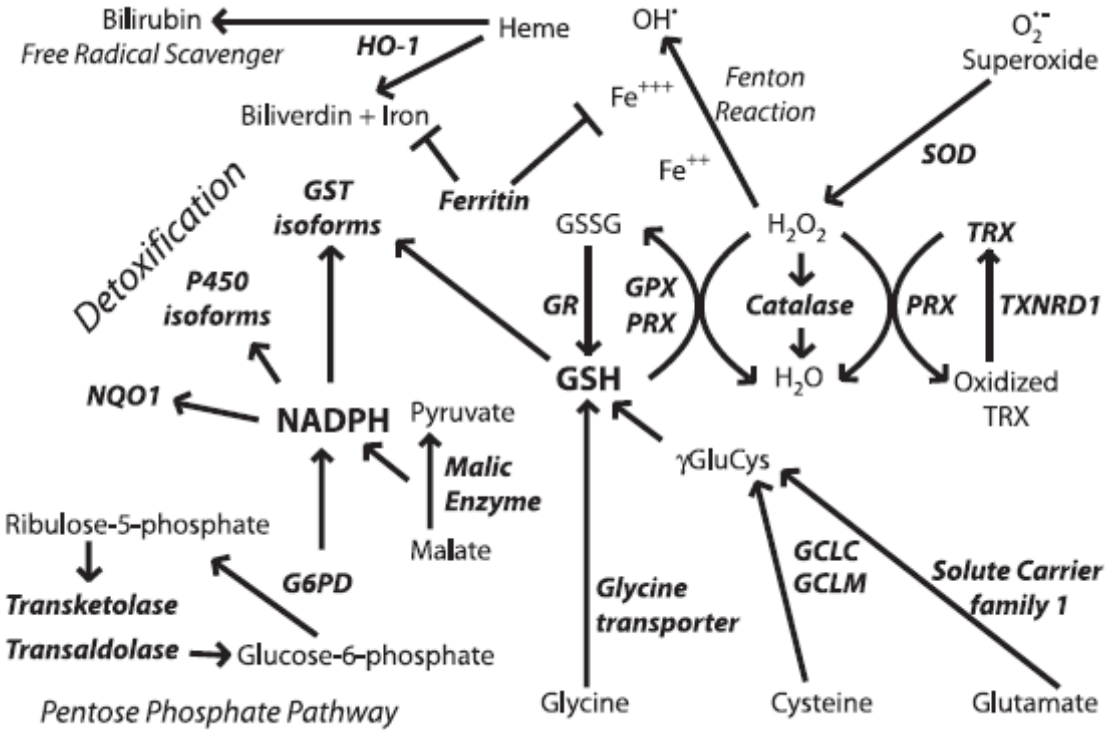

Figure. 1. Coordinated upregulation of cytoprotective genes occurs as a result of Nrf2 activation. Nrf2-dependent genes identified by microarray are listed in bold italics. These genes function together in the production and utilization of glutathione. Genes involved in cellular uptake of glutathione-constituent amino acids glycine and glutamate are increased. Additionally, the rate-limiting step of glutathione synthesis is the formation of the -glutamyl cysteine moiety by -glutamyl cysteine ligase. Transcription of both subunits of this enzyme is induced. Moreover, enzymes responsible for glutathione utilization, reduction, and conjugation are all represented in microarray data. Similarly, production and use of the common detoxification enzyme cofactor NADPH is stimulated. The pentose phosphate pathway is a common cellular mechanism whose two main functions are the production of reduction equivalents in the form of NADPH and the production of ribulose-5-phosphate for nucleotide and nucleic acid synthesis. In the case of Nrf2 activation, the pathway is focused on NADPH production, as the fructose-5-phosphate molecules are recycled back to glucose-6-phosphate by transaldolase and transketolase. NADPH also may be synthesized by malic enzyme oxidation of malate to pyruvate. NADPH is the major cofactor used in cellular reductions and is used especially frequently by detoxification enzymes like NQO1, P450s, and GSTs. Furthermore, Nrf2-dependent genes function together to detoxify superoxide, and meanwhile to prevent Fenton chemistry on the SOD-produced intermediate H2O2. This occurs by two methods. First, ferretin sequesters free iron by binding it in the ferric form. Second, catalase, thioredoxin, and peroxiredoxins reduce H2O2 to water. Thus, Nrf2-driven genes reduce superoxide to water and prevent production of hydroxyl radicals.

[Modified from Lee JM et al., 2003].

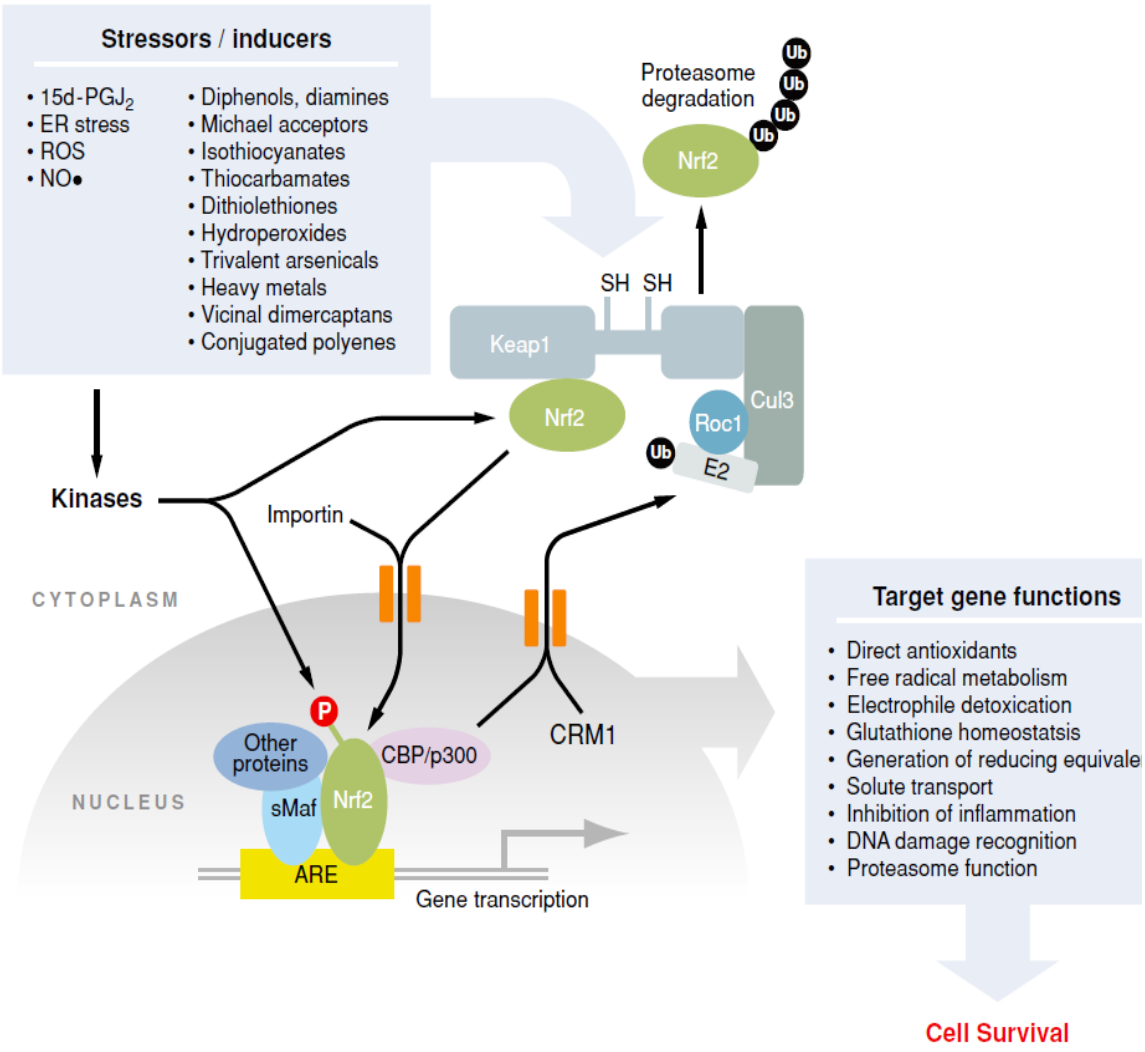

Figure 2. General scheme for the induction of gene expression through the Keap-Nrf2-ARE signaling pathway. Small molecules of endogenous and exogenous origin lead to activation of Nrf2-regulated genes. These agents disrupt the association of Nrf2 with Keap1,leading to diminished rates of proteolysis of Nrf2 and enhanced nuclear accumulation. Phosphorylation of Nrf2 by a series of kinases also affects its fate and distribution. Interaction of Nrf2 with other transcription factors and proteins of the transcriptional complexallows for transactivation of ARE-responsive genes. Induction of these genes, wich include prototypic coniugating and antioxidative genes, results in an adaptive response that enhances te resistance of cells to environmental stresses mediated electrophiles and free radicals.

[Modified from Ferraiuolo L et al., 2011]

Experimental section

Nrf2-ARE pathway as an attractive target for neuroprotection in ALS: identification of small molecule activators of Nrf2-mediated transcription in two libraries of drugs

Mounting evidence suggests that ALS is not simply an event that occurs within neurons, distinct from influence by surrounding cells. This concept may be best illustrated in the context of the familial form of ALS, in which several groups have found major astrocyte and microglial involvement in disease progression. Researchers studying this disease have found that expression of the mutated allele in astrocytes alone is sufficient to cause motor neuron degeneration *in vitro* (Nagai M et al., 2007, Vargas MR et al., 2006). Furthermore, knocking down expression of the mutated allele in astrocytes leads to diminished microglial activation and overall disease progression (Yamanaka K et al., 2008). The mechanism by which astrocyte dysfunction leads to neural degeneration in ALS was explored by Barbieto (Barbieto LH et al., 2004). Several potential routes exist by which reactive astrocytes may potentiate neurodegeneration, including downregulation of glutamate transporters, release of reactive nitrogen species, or active release of proapoptotic proteins such as Fas-ligand or NGF. Thus, targeting non-neuronal cells may be a valuable option for therapeutic intervention, not only to prevent toxicity mediated by glia, but also to stimulate glial protective responses. Interestingly this hypothesis has been extended and tested in cell culture by using the ALS model with Nrf2 as a protective agent. The therapeutic potential of Nrf2 was explored in a model of ALS in isolated astrocytes from mice overexpressing the gene coding for superoxide dismutase-1 that was mutated from glycine to alanine at position 93 (G93A-SOD). Wild-type motor neurons were plated on top of the astrocytes. It was previously found that this co-culture scheme leads to motor neuron apoptosis that is not observed when the astrocytes were derived from wild-type mice (Vargas MR et al., 2006). The investigators coupled this knowledge to the observation that astrocyte-induced apoptosis in similar systems could be mediated by NGF and nitric oxide (Pehar M et al., 2004) and hypothesized that decreasing reactive nitrogen species could rescue the motor neurons. Follow-up experiments showed that activation of Nrf2 in the G93A-SOD–containing astrocytes was able to prevent apoptotic signaling (Vargas MR et al., 2006).

Based on this data, the multifaceted response of Nrf2 makes it an attractive target for prevention of neurodegeneration in ALS, and its activation in astrocytes may rescue motor neurons from death.

For these reasons, during the period I spent at the SITraN in United Kingdom, I screened two libraries of small molecules on different reporter cell lines in order to identify activators of Nrf2-mediated transcription. The cell lines I used were CHO cells and C6 cells, both cell lines were efficiently used in a previous library screening conducted in the SITraN laboratories. The two libraries I screened were from two different commercial sources, Tocris and Prestwick libraries, and each of them was composed of almost 1000 molecules.

Most of the molecules from Prestwick are already used in human therapy and are employed in different pathologies, but their activity on Nrf2-ARE pathway is unknown. Moreover, many molecules in this library have known human safety data as they are that did not make it to clinic. This can be simply because they were no better than other drugs on the market rather than negative reasons.

Tocris library is designed to identify pathways, as it has inhibitors and activators of known pathways. As for molecules from Prestwick library, also the activity of Tocris molecules on Nrf2-ARE pathway is unknown.

Materials and Methods

Cell Culture

Chinese Hamster Ovary (CHO) and C6 (rat) astrocyte cell lines were routinely maintained in DMEM supplemented with 10% FCS and penicillin/streptomicyn. The ARE-TK-GFP and the TK-GFP reporter constructs were a kind gift of the laboratory of cancer research of the University of Wisconsin. The TK-EGFP reporter construct consists of a 123bp thymidine kinase promoter inserted in the multiple cloning site of pEGFP and the ARE-TK-EGFP also contains 4 repeats of a 41bp GST ARE motif 3' to the TK promoter. These plasmids were transfected into CHO and C6 cell lines and after selection in 0.5 mg/ml G418 they were expanded and selected for basal expression using fluorescence activated cell sorting (BD, FACSAria). These mixed populations of stable transfectants with basal eGFP expression were used in subsequent assays and designated 4xARE-TK-GFP for the ARE containing line and TK-GFP for the control cell line.

Andrographolide EC 10, EC 50 and EC 90 determination

Andrographolide is a diterpen lactone and the principal active component in extracts of the herb Andrographis paniculata, which is widely used in Indian herbal medicine as an anti-infective, anti-inflammatory and hepatoprotective agent. From a previous library screening conducted in the SITraN laboratories, andrographolide was identified as an activator of the Nrf2-ARE pathway in CHO and C6 cells. For these reason andrographolide was used as positive control that represented our current best and its EC10, EC50 and EC90 on CHO and C6 transfected cell lines was determined.

ARE reporter assay-library screening validation

In order to screen the two libraries of 2000 small molecules the TK-GFP CHO ARE reporter cell line and the TK-GFP C6 ARE reporter cell line were subjected to a Z' score assay in a 384 well plate using different methods of seeding and treating ("z' score determination based on "Assay Validation", Eli Lilly and Company and the National Institutes of Health Chemical Genomics Center). In brief, 15,000 cells/well were seeded in a 384 well plate and after 24 hours alternate wells were incubated with andrographolide at different concentrations corresponding to its EC90, EC50 and EC10 respectively. GFP fluorescence (ARE induction) was then measured at Ex485/Em530 using a fusion plate reader (Packard Bioscience). The Z' score was calculated as follows:

$$Z' = \frac{\left(\mathrm{AVG}_{max} - 3\,\mathrm{SD}_{max}/\sqrt{n}\right) - \left(\mathrm{AVG}_{min} + 3\,\mathrm{SD}_{min}/\sqrt{n}\right)}{\mathrm{AVG}_{max} - \mathrm{AVG}_{min}}$$

Acceptable Z' scores were >= 0.4

The Z' score assay was performed for both the CHO and C6 transfected cell lines.

Library screening

For the library screening, CHO and C6 transfected cell lines were plated at a density of 15000 cells for each well in a 384 multiwell in normal DMEM containing 10% FBS on day -1 and on day 0, media was replaced and cells were incubated for 24 hours with drug (1 compound/well). The cell seeding was performed using the cell dispenser Matrix Control Mate, (Thermo Scientific). After the seeding, drugs were delivered to the assay using the Echo® Liquid Handling System (Labcyte Inc., USA). Echo® 550 was able to dispense the compounds directly from the 96 well of the library through the use of acoustic energy to transfer liquids. Sound waves ejected precisely-sized droplets from the source liquid into the 384 well plate suspended above the source. The Echo liquid handling platform used no tips, pin tools, or nozzles, so there was no contact between the instrument and the liquid. The Drop transfer volume for Echo® is 2.5 nL and the volume transfer range is 2.5 to 10,000 nL (source-plate specific), moreover its transfer accuracy is <10% of the deviation from target volume. Echo® 550 offered many advantages in respect to hand pipetting, indeed we could deliver tiny volumes, maximize the use of the library and limit contaminations of our cells.

GFP fluorescence (ARE induction, Ex 485nm/Em 530) were then measured. The TK- GFP CHO ARE cell line was tested twice in a single point assay at 10µM, and once at 500nM.

The control TK-GFP CHO cell line was screened once at 10µM and once at 500nM to eliminate false positives.

ARE reporter assay-determination of EC 50

Reporter assays were run as for the library screen with a concentration curve raging from 0.001-100uM in triplicate in normal DMEM for 24 hours. Non linear regression was used to fit sigmoid dose-response curve on a semi-Log plot to calculate the EC50 using Graph Phad Prism (Graph Pad Software). The reporter assay was performed

similarly in CHO an C6 cell lines stabily transfected with 4xARE-TK-GFP and TK-GFP constructs.

Results

Andrographolide EC 10, EC 50 and EC 90 determination

From a previous library screening conducted in the SITraN laboratories, andrographolide was identified as an activator of the Nrf2-ARE pathway in CHO and C6 cells. For this reason, in this study andrographolide was used as positive control that represented our current best and its EC10, EC50 and EC90 on CHO an C6 cell lines stably transfected with 4xARE-TK-GFP was determined.

As reported in Figure 1, andrographolide showed similar activity on both C6 and CHO cell lines (C6 EC50=1.8±0.2µM; CHO EC50=1.4±0.15µM).

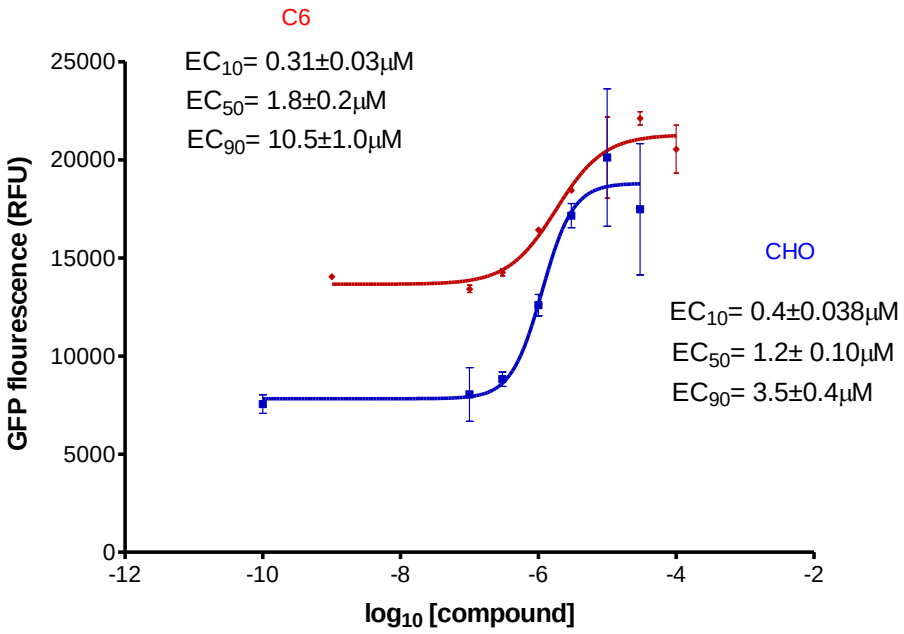

Figure 1. Data obtained by three different experiments carried out in duplicate. Data are shown as mean values ± SEM.

ARE reporter assay-library screening validation

The Z' score assay was performed in order to determine working conditions of confidence and reproducibility necessary to perform the drug screening. Although we set the assay up with a known activator with a dose response already determined, using a single dose assay we had a good chance of identifying a positive response.

The drug screen logistically had to be done at a single dose, therefore it was unlikely that the hits would have been at optimal dose, so we simply needed to know at a dose that we could identify any activation, not simply good activation. Even more, we did not consider any difference between hits until we did the secondary assays of dose response, however big or little the response in the primary screen, they were simply above or below the threshold set by us.

The Z' score determination was run using different combined methods, as reported in table 1 and 2. The best Z' score determined for the CHO cells was equal to 0.773; the best Z' score determined for the C6 cells was 0.300. Both these Z' scores were obtained using a cell dispenser for the seeding and the Echo® Liquid Handling System for the treatments.

CHOcells	Seeding	Teatments	Z score
1st	By hand	By hand	2,153
2nd	Cell dispenser	Plate mate	0,681
3rd	Cell dispenser	Echo	0,473

Table 1.

C6 cells	Seeding	Treatments	Z score
1st	By hand	By hand	0,077
2nd	Cell dispenser	Plate mate	0,490
3rd	Cell dispenser	Echo	0,300

Table 2.

Library screening and reporter assay validation

In order to screen the two libraries of compounds, Nrf-2-ARE reporter cell lines were generated in Chinese hamster ovary (CHO), the libraries were screened twice with compounds at 10 µM and once at 500nM, in both the reporter and control cell lines.

For the 10 µM, we used a single dose assay and we identified every positive response, baring in mind it could be well out of its ideal range.

A good concentration for a drug is usually in the nanomolar range; this can limits the side effects and avoid the aspecific binding to other receptors or molecules.

Our screening was performed at a higher concentration than nanomolar concentration, but as previously explained, the drug screen logistically had to be done at a single dose, therefore it was unlikely that the hits would have been at optimal dose, so we simply needed to know at a dose that we could identify any Nrf2-ARE pathway activation, not simply good activation.

The approach we used in this work was the "fast track" approach, whereas in a normal clinical trial it's necessary to optimize leads by chemical modification. Obviously, we wouldn't be adverse to optimization, but it is more expensive and requires more time.

As a second step, we repeated the screening also at 500 nM in order to see if we had missed some very good hits that might show toxicity at 10 µM. Using this method we found the compound 14P for the Prestwick library and that we had missed in the previous screening at 10 µM. Moreover, using the results from the 500 nM screening, for the Tocris library we could reduce the number of compounds to test and so that of assays (i.e. dose-response curves) to perform because of time constraints.

In the end, a total of 14 compounds (1P-14P) from the Prestwick library and 21 compounds (1T-21T) from the Tocris library were identified as hits (positive response in both the 10 µM screenings and/or in the 500nM screening, no false positive response in the control cell line and no evidence of toxicity).

The selected compounds (hits) from both the libraries were assessed in full concentration response curves in the same assay.

In Figure 2 the dose-response curves for the 14 hits from the Prestwick library are reported. As shown in Figure 2, compounds 3, 11, 9 and 12 didn't fit the curve, so they were excluded from the next screening.

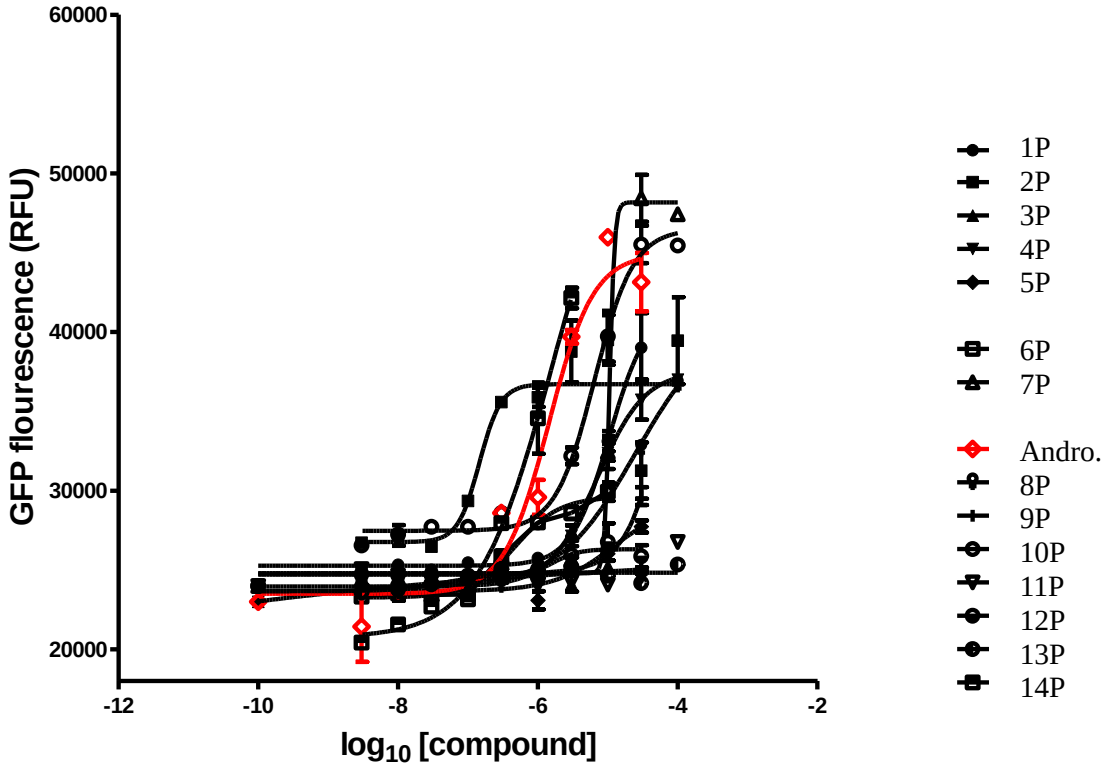

Figure 2. Dose-response curves on CHO cells for the 14 hits from the Prestwick library. Data obtained by three different experiments carried out in triplicate. Data are shown as mean values ± SEM.

Seven of the twenty-one hits identified from the Tocris library screening showed background fluorescence (due to compound autofluorescence) on control cells when tested at higher concentrations (>10 µM), so they were excluded from the next screening.

In Figure 3 the dose-response curves for the 14 hits remaining from the Tocris library are reported.

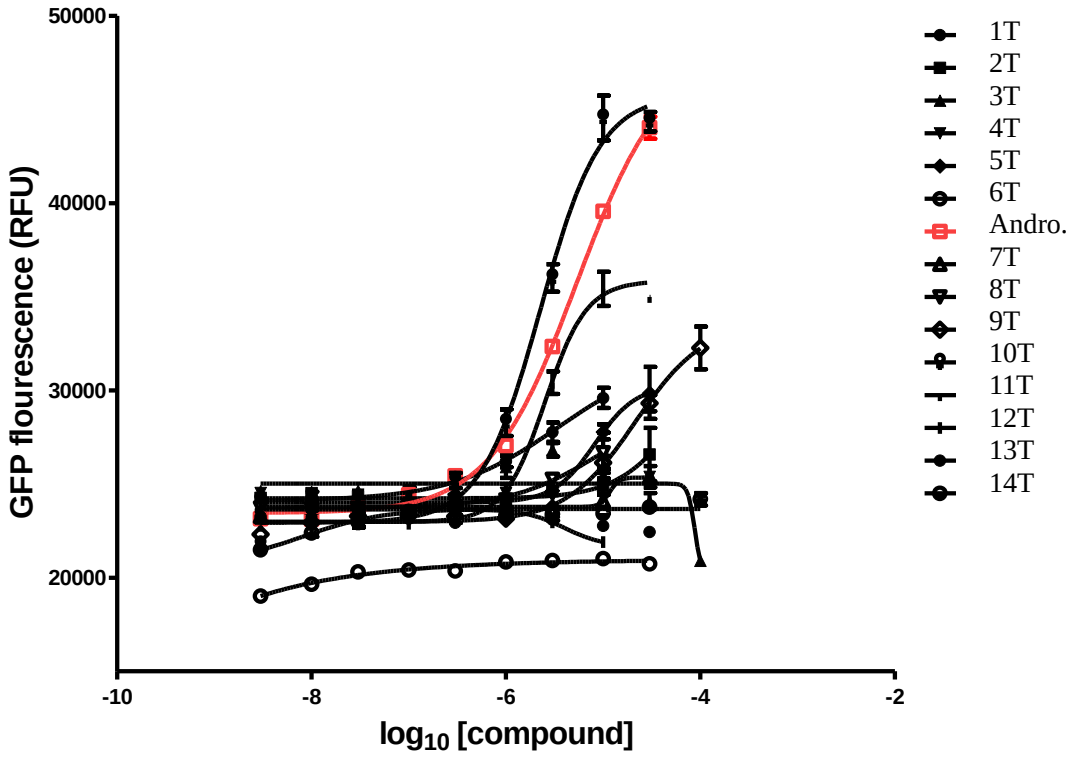

Figure 3. Dose-response curves for the 14 hits remaining from the Tocris library; seven of the twenty-one hits identified from the Tocris library screening were excluded from the next screening because they showed background fluorescence when tested at high concentrations. Data obtained by three different experiments carried out in triplicate. Data are shown as mean values ± SEM.

In order to determine whether the selected hits were able to induce activation of the Nrf2-ARE pathway also in cells that correlate directly with the ALS diseases, the best hit molecules were screened in C6 astrocytic cells stably transfected with the Nrf2-ARE construct.

Ten Prestwick library molecules identified as hits from the previous screening (dose-response curve on CHO cells) were selected and tested for the dose-response curve on C6 cells. The ten selected molecules were those that fitted the curve or that showed a good dose-response activity on CHO cells. As reported in Figure 4, the molecules that showed the best activity on Nrf2-ARE pathway in C6 cells were the compound 2P (EC50=209.4±30 nM) and the compound 14P (EC50=412.1±40 nM). Indeed, both these molecules were able to induce the activation of the Nrf2-ARE pathway at a 10x times lower concentration than the reference compound andrographolide (EC50=1.8±0.2µM).

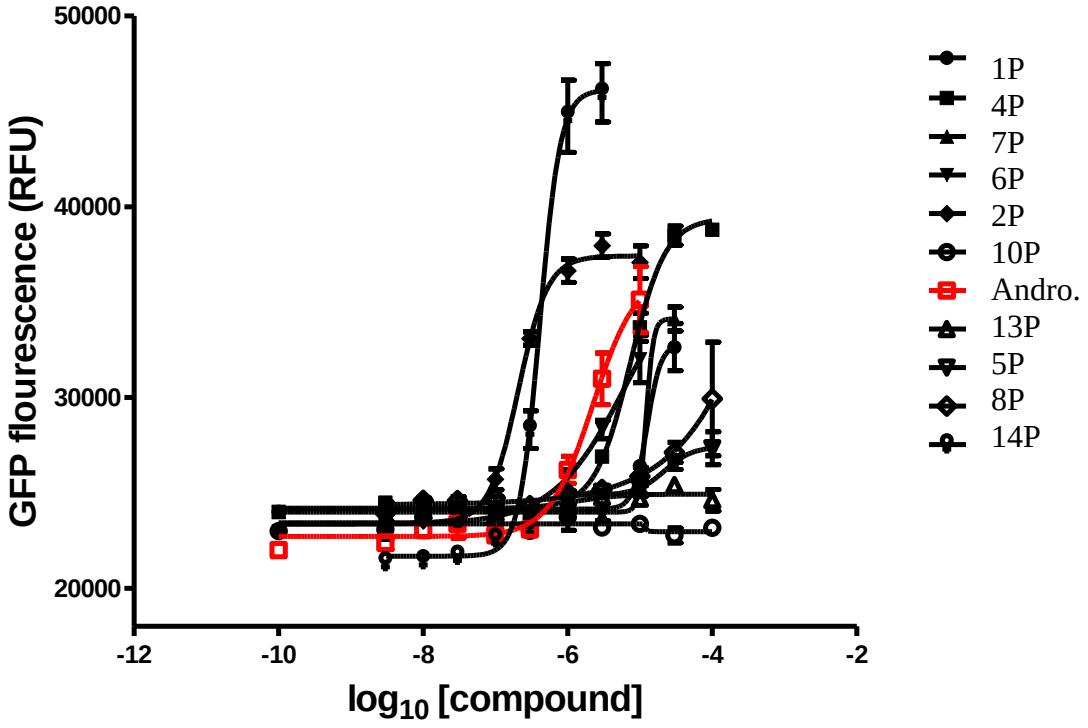

Figure 4. Dose-response curve on C6 cells of ten Prestwick library hits selected from the previous screening on CHO cells. Data obtained by three different experiments carried out in triplicate. Data are shown as mean values ± SEM.

Moreover, seven hits from the previous screening on CHO cells of the Tocris library were selected following the same criteria used for the Prestwick library. These molecules were tested on C6 cells and a dose-response curve was determined.

As shown in Figure 5, the molecules 1T, 5T, 2T and 11T showed a good activity on Nrf2-ARE pathway in C6 cells and their EC50 values were 4.4±0.4 µM, 4.4±0.45 µM, 5.8±0.5 µM, 5.2±0.5 µM respectively. Unfortunately no one of them showed higher activity than andrographolide, but their EC50 values are still quite good and comparable with that of andrographolide itself.

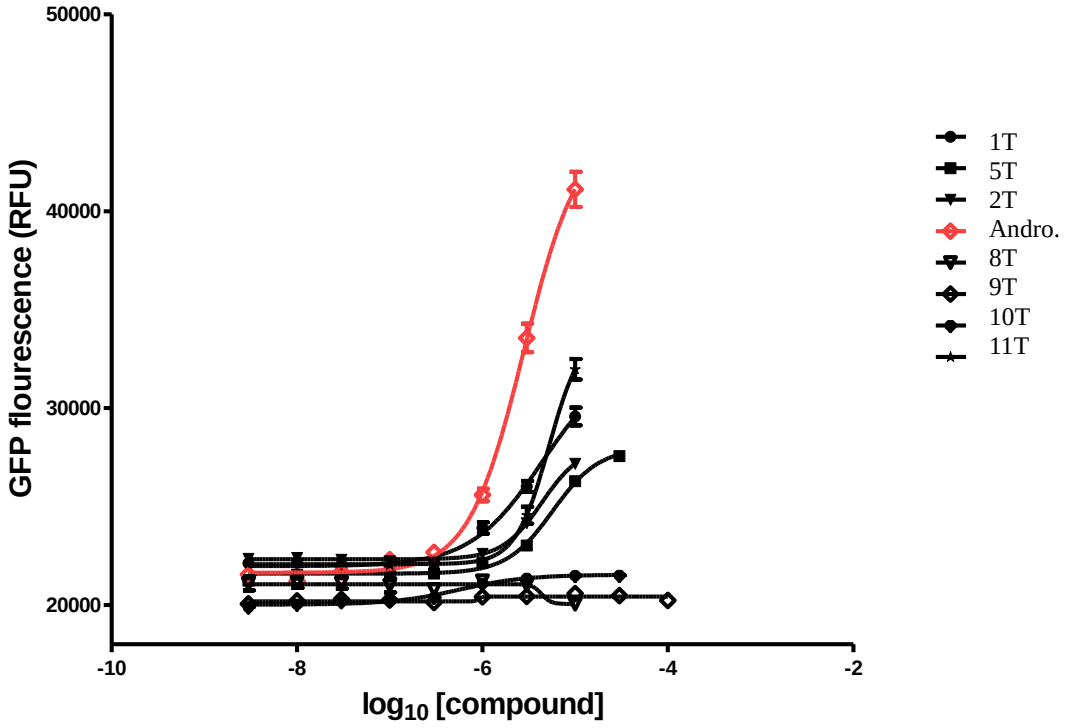

Figure 5. Dose-response curve on C6 cells of seven Tocris library hits selected from the previous screening on CHO cells. Data obtained by three different experiments carried out in triplicate. Data are shown as mean values ± SEM.

Discussion

Pathogenic mechanisms underlying ALS are not fully understood. Evidence from model systems, and from ALS patients, provides strong evidence for a role of oxidative stress in disease phatogenesis (Barber SC et al. 2006).

Oxidative stress has significant crosstalk with other potential mechanisms of neuronal injury, including mitochondrial dysfunction, excitotoxicity, protein aggregation etc. More importantly it can feed into these mechanisms or be enhanced by them.

Despite the central role, therapeutic targeting of oxidative stress in ALS has failed to translate into clinical benefit for patients. This may be due in part to the lack of sufficiently potent anti-oxidants able to penetrate the CNS (Barber SC et al. 2006). An alternative novel approach to limiting neurodegenerative disease is to promote activation of the transcription factor Nrf2.

The key objective of this program of work was to identify molecules that could be fast-tracked for clinical testing in ALS, having been used previously in humans, as those of the Prestwick library or designed to identify new pathways, as those of the Tocris library.

With this data, some interesting molecules from both the libraries were identified, as shown by their EC50 concentration values determined on activation of Nrf2-ARE pathway in C6 cells.

Two molecules were selected from the Prestwick library, and four molecules were selected from the Tocris library.

In particular the molecules 2P and 14P were able to induce the activation of the Nrf2-ARE pathway at a 10x times lower concentration than the reference compound andrographolide (EC50=1.8±0.2µM).

Because fast track was used we cannot optimize the hits further chemically, or else these would need further safety trials. Indeed, modification of a known safe molecule needs re-testing (i.e. pre-clinical and clinical trials) as we have a new molecule. On the other hand, this consideration gives us the possibility to have already useful information about their activity and safety in humans. We could affirm that, using the fast track approach, we are able to save on the costly human trials for safety, but we possibly could be sub-optimal on compounds potency. The fast track approach is a good approach to proof of target, but then it often requires investments to find a better hit of the pathways identified.

The compound 2P, for example is used in alcohol abuse and recent *in vitro* studies on breast cancer cell lines evidenced its good anticancer activity. The compound 2P has no significant side effects; meanwhile the compound 14P can cause nausea, loss of appetite and stomach cramps. The compound 14P is used as antirheumatic and its effects on other pathologies or pathways were not been investigated before.

Such as the Prestwick compounds, also the Tocris molecules were well known to act on pathways and receptors different from Nrf2, such as the valinoid receptor, the µ-receptor of morphine or the 5HT release, but not on the Nrf2-ARE pathway. It's important to highlight that, differently from the Prestwick hits already used in therapy, the Tocris ones primarily tell us about Nrf2-pathway activation and understanding novel pathways that could be a therapeutic target in neurodegenerative diseases.

Further investigations, as *in silico* assays, are necessary in order to determine chemical and physical characteristics (LogP, PSA etc) of some of the selected molecules. Moreover, to confirm that these "lead inducers" are able to activate the Nrf2-ARE

pathway, quantitative RT-PCR for Nrf2 target genes, as NADPH quinine oxidoreductase 1 (NQO1) are necessary in C6 cells.

Another interesting aspect to investigate is the ability of these molecules to activate the Nrf2-ARE pathway on human cells. Unfortunately, due to time constrain, I couldn't test the hit molecules from both libraries on a human astrocytic cell line (1321N1), but experiments conducted on this cell line could give important information on the molecules activity in a human cell type.

NOTE:

In order to do not preclude the possibility of a patent on some of these molecules, I couldn't show the names and the molecular structures of the compounds tested in this thesis.

Chapter 4: Glioblastoma multiforme I

Matrix Metalloproteinases

The Matrix Metalloproteinases (MMPs) family consists of more than 25 structurally related, zinc-dependent endopeptidases that are secreted in the zymogen, or inactive, form. So far, 23 human MMPs have been identified and divided into subgroups based on their structure and substrate specificity: collagenases, gelatinases, stromelysins, matrilysins and membrane-type MMPs (MT-MMPs). In the active form they are capable of degrading various components of the extracellular matrix (ECM) (Nagase H and Woessner JF Jr, 1999, Vihinen P and Kähäri, VM 2002). The proteolytic degradation of the ECM, the alteration of the cell-cell and cell-ECM interactions, and the migration of cancer cells through the basement membrane are the main problems in tumour progression (Cauwe B et al., 2007, Heino J, 1996; Konstantinopoulos PA et al., 2008, Plate KH et al., 1994, Tonn JC et al., 1999). Moreover, some MMPs have been demonstrated to be upregulated in many tumours and have become attractive targets for anti-tumour drug development (Brown PD and Giavazzi R, 1995, Lein M et al., 2000, Rabbani SA et al., 2000). Among the members of the MMP family, the gelatinases, MMP-2 (gelatinase A) and MMP-9 (gelatinase B), are thought to play a key role in degradation of type IV collagen and gelatin, the two major components of ECM. Increased expression of MMP-2 and MMP-9 is reported in many human tumors, including ovarian, breast and prostate tumors, and melanoma (Roomi MW et al., 2003).

Elevated levels of MMP-2 and MMP-9 have also been found in human glioblastoma tissue samples, compared with low-grade brain tumors and normal brain tissue (Rao JS, 2003).

In particular, MMP-2 is highly expressed in gliomas and both mRNA and protein levels increase along with tumor progression and grade (Kargiotis O et al., 2008). It has been shown that MMP-2 is localized in both tumor and vasculature cells, thus indicating multiple roles for this enzyme in tumor progression, including angiogenesis (Forsyth PA et al., 1999). MMP-2 expression is also known to be associated with tumor invasion and metastasis (Komatsu K et al., 2004).

On these bases, the two gelatinases MMP-2 and MMP-9 can be considered one of the prime factors in glioma invasiveness, and their expression correlates with the progression and the degree of malignancy of gliomas (Forsyth PA et al., 1999, Kim SY

et al., 2008). Unfortunately, in the past, the clinical development of MMP inhibitors (MMPIs) has been very problematic, because these drugs, often with a broad spectrum of activity, produced dose-limiting musculoskeletal toxicities (Whitaker M et al., 1999). Indeed, it is important to emphasize that not all MMPs contribute to tumour progression. Recently, it has been demonstrated that some MMPs are involved in innate immunity and host defence against cancer, others inhibit tumour growth and malignant transformation, and others exert antiangiogenic effects (Konstantinopoulos PA et al., 2008). In particular, inhibition of MMP-1 and MMP-14 has been hypothesized to be the cause of the muskoloskeletal syndrome (MSS) observed clinically with broad spectrum inhibitors, while MMP-8 (López-Otín C et al., 2009) and MMP-3 (Overall CM et al., 2006) were demonstrated to have anti-tumor properties and their inhibition may be counterproductive.

Hence, both the side effects and the poor outcome due to wide inhibition of MMPs could be avoided by the use of selective MMP-2 and MMP-9 inhibitors.

Experimental section

Matrix Metalloproteinases inhibitors

The inhibition of MMP activity represents a promising non-cytotoxic approach to glioma treatment. Almost all MMPIs are based on a chelating moiety interacting with the catalytic zinc ion and a hydrophobic portion protruding into the hydrophobic S1' subsite, which is a deep pocket situated in proximity to the catalytic zinc ion. These compounds behave as competitive inhibitors since the zinc-binding group (ZBG) binding mode can mimic one of the transition states occurring during the substrate hydrolysis (Nuti E et al., 2009).

Widely utilized ZBGs include: hydroxamic acids, carboxylic acids, pyrones (Puerta DT et al., 2005) and pyrimidinetriones. The most used of these is the hydroxamate group since it has excellent chelating properties (Nuti E et al., 2009, Flipo M et al., 2009)

Unfortunately, clinical trials with MMPIs in cancer patients conducted over the past years failed to show a significant therapeutic response, mostly because the majority of patients enrolled had advanced metastatic disease (Coussens LM et al., 2002). Moreover, most of these clinical trials were carried out using broad-spectrum MMPIs, such as marimastat 1 (BB2516) (Beckett RP et al., 1996), prinomastat 2 (AG3340) (Sorbera LA 2000) and CGS27023A (Levitt NC et al., 2001) **3** (Figure 1), and thus produced undesired side effects.

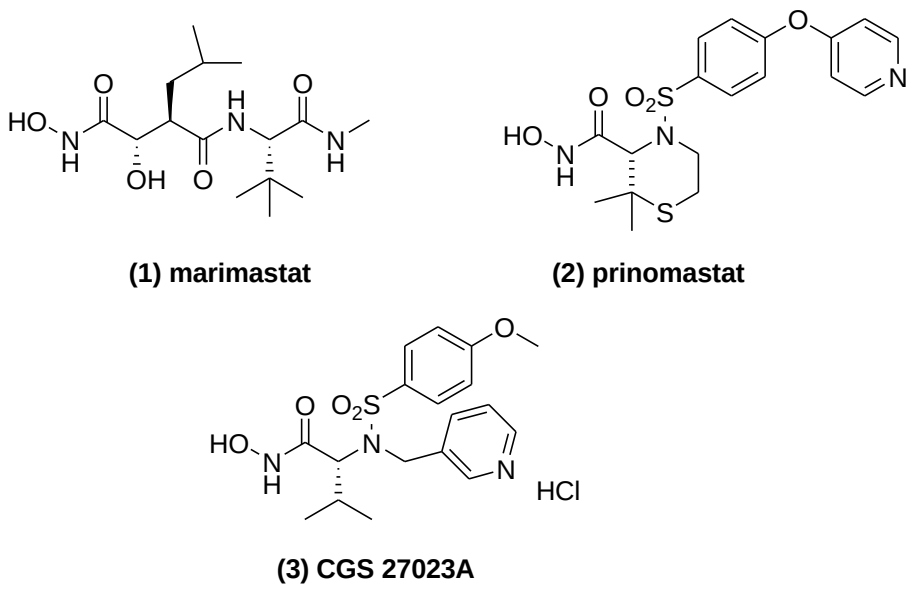

Figure 1. Broad spectrum MMP inhibitors used in clinical trials for cancer.

In vitro studies focusing on marimastat demonstrated significant inhibition of invasion in glioma cell lines, suggesting that MMPIs may have a role in the treatment of gliomas (Tonn JC et al., 1999). Unfortunately, *in vivo* marimastat did not improve survival in patients with glioblastoma following surgery and radiotherapy if used as single agent (Levin VA et al., 2006). Furthermore, the use of broad spectrum MMPIs in clinical trials has been greatly limited by muskoloskeletal side effects, which imply a reduction of the dose, and consequently also a reduction of beneficial effects

On the basis of these considerations, the aim of this work was to identify new compounds that could selectively inhibit gelatinases without significantly affect other MMPs and that can be potentially useful as antiglioma agents.

In this chapter, the biological characterization of new MMP-inhibitors is reported. In the first part of this chapter (section 4.1), the attention has been directed towards a new class of MMP-2 inhibitors belonging to the recently identified family of *N*-O-isopropyl sulfonamide hydroxamates (Nuti E et al.,2009; Rossello A et al., 2004, 2005), which have shown potent inhibition of MMP-2 activity in *in vitro* test tube assays, and have been demonstrated to inhibit the invasiveness of the fibrosarcoma cell line HT1080 (Rossello A et al., 2004). Two of these MMP inhibitors *N*-*O*-isopropyl sulfonamido-based hydroxamates (compound 1 and 2) were tested at nanomolar concentrations to investigate their potential efficacy in inhibiting the invasiveness and the proliferation of the human glioma cell line, U87MG. As a first step, the two

compounds at nanomolar concentrations were assayed on their ability to inhibit MMP-2 cleavage of gelatin. Moreover, the MMP-2 expression was assessed following MMP inhibitor cell treatments. In order to help the development of multitarget therapies against GBM, the combined treatment of the U87MG glioma cells with the MMP inhibitors and the conventional chemotherapeutic drug TMZ was evaluated.

In the second part of this chapter (section 4.2) has been described the biological evaluation of a new series of 4-butylphenyl(ethynylthiophene)sulfonamido-based hydroxamates, **4-7**, synthesized in the laboratory of Prof. Rossello at the University of Pisa. Previous studies on carboxylate MMP inhibitors (Tamura Y et al., 1998, Kiyama R et al., 1999) had shown that the presence of an elongated hydrophobic substituent in P1' like 4-butylphenylethynylthiophene could ensure a good activity toward gelatinases, sparing other enzymes like MMP-1, -3 and -7. In fact, gelatinases have a deep S1' pocket while MMP-1 and MMP-7 present a shallow pocket in the catalytic site. For this reason, Rossello and his collaborators chose to maintain this type of substituent in the sulfonamido moiety and to change the ZBG in an effort to improve the selectivity also over other deep-pocket MMPs, such as MMP-8 and -3. In fact, as previously shown (Rossello A et al., 2005) selectivity of action against some deep-pocket MMPs can also be dependent on the nature of the ZBGs, that have different chelating geometries and different pKa.

Moreover, starting from the simple, un-substituted secondary sulfonamide **4**, derivatives **5a-d** bearing various (R) aryl-alkyl chains in position α of the hydroxamate were synthesized by Rossello and his collaborators according to the hypothesis that the selectivity profile could be also affected by the presence and structure of the α-chain (P1 group), as previously observed by Hanessian et al. (2001). The scaffold was further stiffened up by introducing α-chains fused with the sulfonamido moiety, thus affording cyclic compounds **6** and **7** (Figure 2).

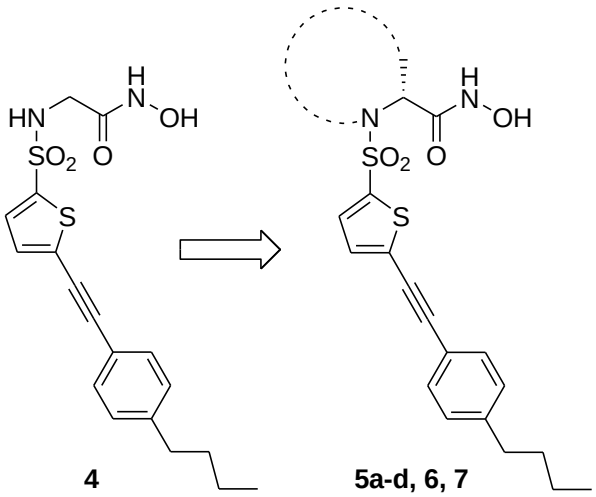

Figure 2. Evolution of the new 4-butylphenylethynyl-thiophene derivatives scaffold.

In this section the effects of these substitutions on MMP-2 and MMP-9 activity and selectivity have been described. First, the reported compounds were examined *in vitro* by fluorometric assay on isolated enzymes. The compounds **5a-d, 6, 7** were then tested for their ability to inhibit *in vitro* invasion of U87MG glioma cells through matrigel and to inhibit cell growth.

4.1 Inhibition of metalloproteinases derived from tumours: new insights in the treatment of human Glioblastoma

Matherials and Methods

MMP inhibitors: “in tube” activity

The *N*-*O*-isopropyl sulfonamido-based hydroxamates MMP inhibitors, compounds 1, 2 and the standard MMP inhibitor belonging to the classical tertiary sulfonamido-based hydroxamates family (CGS_27023A) were synthesised as reported by Rossello et al. (2004) and Mc Pherson et al., (1997), respectively. All compounds were solubilized in dimethyl sulfoxide (DMSO). The ability of compounds to inhibit activity of human recombinant MMP enzymes on synthetic peptide substrates was performed as previously described (Rossello et al., 2004, Rossello et al., 2005) and reported as compound concentration able to inhibit the 50% of enzyme activity.

U87MG cell line culture

U87MG cells: see chapter 3.

MMP inhibitors: cell derived MMP-2 activity tested on natural substrate

In order to evaluate the inhibition of MMP-2 activity exerted by compounds 1, 2 or CGS_27023A, the serum-free medium from cells was collected, centrifuged to r move the cell debris and the supernatant was incubated with IC50 dose compounds 1, 2 or CGS_27023A for 3h. Gelatin zymography was performed as previously described by Wang et al., (2005) and Lim et al., (2009) with minor modification. Briefly, 2 μg of protein from each sample were mixed with the 5X-sample buffer (50mM Tris–HCl, 2% SDS, 0.1% bromophenol blue, 15% glycerol) and electrophoresed on 10% denaturing sodium dodecyl sulfate (SDS) polyacrylamide gels containing 1 mg/ml of gelatin. After electrophoresis, the gel was washed twice for 30 min in 2.5% Triton X-100 and incubated for 19 h at 20°C in 50mM Tris HCl (pH 7.5), 10mM CaCl2, 150mM NaCl and Briji 35 0.05%. The gel was stained with Coomassie Brilliant Blue R-250 (0.25% Coomassie Brilliant Blue R-250, 50% methanol, 10% acetic acid in H2O) and then

destained (30% methanol, 10% acetic acid in H2O). The MMP-2 activity was discernible by clear bands of gelatin digestion on a blue background and was quantified by using a densitometric image analysis software (ImageJ, National Institutes of Health, Bethesda, Maryland, USA).

MMP inhibitors: effect on cell derived MMP-2 expression

In order to evaluate MMP-2 expression, the 24 h treated and untreated adherent cells were lysed and used to evaluate MMP-2 mRNA levels by the means of real-time polymerase chain reaction (real-time PCR). Moreover, the serum-free medium from treated and untreated cells was collected and employed to detect MMP-2 protein level by the means of enzymelinked immunosorbent assay (ELISA). The relative quantification of MMP-2 gene expression was evaluated as previously described (Papi A et al., 2007). In brief, total RNA was isolated using Rneasy® Mini Kit and reverse transcribed in cDNA with Quantitect® reverse transcriptase. Real-time PCR was performed by using Brilliant® II SYBR® Green. The MMP-2 mRNA levels for each sample were normalised against β-glucuronidase (GUSB) mRNA levels, and relative expression was calculated by using Ct value. The primer sequences were:

MMP-2 forward, 5'-CTGAAGGACACACTAAAGAAGATG-3';
MMP-2 reverse, 5'-GGAAGGCACGAGCAAAGG-3';
GUSB forward, 5'-TGGTATAAGAAGTATCAGAAGCC-3';
GUSB reverse, 5'-GTATCTCTCTCGCAAAAGGAAC-3'.

The MMP-2 protein levels was determined in duplicate using the RayBio® Human MMP-2 ELISA kit designed to measure its pro and active forms, according to the manufacturer's instructions. Specimens were incubated with an enzyme substrate and 3,3',5,5'- tetramethylbenzidine for the development of colour, that was analyzed using an ELISA plate reader (Wallac Victor 2, 1420 Multilabel Counter, Perkin-Elmer) at 450 nm. The peroxidase activity was proportionate to the amount of antigen in the specimens, determined according to a standard curve. The minimum detectable dose of MMP-2 was less than 3.5 ng/ml. The intraassay and inter-assay CV were <10% and <12%, respectively.

MMP inhibitors: effect on cell proliferation

Cell proliferation was estimated by the colorimetric MTS conversion assay (Cell Titer 96® Aqueous One Solution Cell Proliferation Assay, Promega), as previously reported (Chelli B et al., 2004). Cells were seeded at 10,000 cells/cm2 in completed medium at 37°C and 5% CO2. After overnight, the cells were incubated for 24 h with DMSO (control sample) or with test compounds, MTS reagent was added, and the absorbance of individual wells was measured with a microplate reader (Wallac Victor 2, 1420 Multilabel Counter, Perkin-Elmer).

Each compound concentration was tested in duplicate, and the experiments were repeated at least three times.

MMP inhibitors: effect on cell viability in the absence and in the presence of TMZ

Cell viability was measured by the Trypan Blue exclusion assay, as previously reported (Ruan S et al., 1999). This assay was performed on U87MG cells treated with the tested compounds for 24 h (short-term treatment) and for several days (long-term treatment). Previously, in order to allow the adhesion of cells to the plates, the cells were seeded at 10,000 cells/cm2 (24 h short-term treatment) or at 3,000 cells/cm2 (several days long-term treatment) in complete medium at 37°C and 5% CO2 for 24 h.

Short-term treatment: the culture medium was replaced, the cells were incubated with DMSO (control sample) or with compounds 1, 2 or CGS_27023A and collected after 24 h. *Long-term treatment:* the culture medium was replaced, the cells were incubated with TMZ (50 µM or 100 µM) or DMSO (control sample) for several days (until to 16 days). On day 7, 1 ml of fresh complete medium was added with or without the compounds 1, 2 or CGS_27023A. The cells were collected at various times (1, 3, 7, 9, 13, 16 days). The collected cells were stained with Trypan Blue dye (0.4% solution in 0.9% NaCl), and counted in a haemocytometer chamber (Burker counting chamber).

MMP inhibitors: effect on cell invasiveness in the absence and in the presence of TMZ

The chemotaxis and Matrigel invasiveness of U87MG cells were evaluated as previously described (Albini and Benelli, 2007). Matrigel basement membrane matrix (BD Biosciences), and 24 Transwell® (6.5 mm diameter 8.0 μm pore size polycarbonate filters, Costar, Corning, NY) were utilised. Several concentrations of Matrigel were tested to ascertain the best "invasive index". In an optimal test, the number of invasive cells should be about 50% of the number of cells that migrated by chemotaxis alone. The best experimental conditions to evaluate the invasiveness of cells were the following: the surface of the transwell was coated with Matrigel (25 μl of a solution of 0.32 mg/ml for each well) at room temperature overnight to form a genuine reconstituted basement membrane. The U87MG cells were suspended in serum free medium (60,000/400 μl) and added to the upper compartment of the transwell in the absence and in the presence of the compounds 1, 2 or CGS_27023A, while 200 μl of RPMI containing 10% foetal bovine serum was added to the lower compartment. The cells were allowed to invade through the matrices at 37 °C for 24 h. The number of invading cells was quantified by counting the cells on the lower surface of the transwell membrane after fixing with p-formaldehyde and staining with crystal violet. Nonmigrating cells on the upper surface were removed with a cotton bud. Pictures of randomly picked light microscope fields were taken (5 fields for each filter), and cells were counted using ImageJ (ImageJ Software, version 1.41o; USA). This method was also employed to evaluate cell invasiveness after TMZ treatments with or without MMP compounds. Each drug concentration was tested in duplicate, and the experiments were repeated at least three times.

Data Analyses

Statistical analyses were performed by one-way ANOVA (with post hoc Newman-Keuls test) by using the GraphPad Prism computer program (GraphPad Software, version 4.0; San Diego, CA). P value < 0.05 was considered statistically significant. All data are presented as the mean ± S.E.M., derived from at least three independent experiments done in duplicate.

Results

The *N*-isopropoxy-biphenylsulfonamide hydroxamic acids 1 and 2 (Figure 3) were employed in cell treatment experiments.

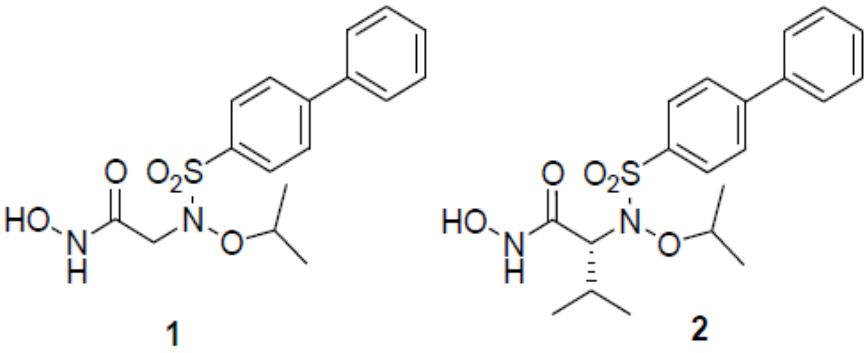

Figure 3. Structures of the MMP inhibitor compounds 1 and 2 used in this study.

In test tube assays, nanomolar concentrations of compounds 1 and 2 resulted to selectively inhibit the activity of the human recombinant matrix metalloproteinases, MMP-2, MMP-9 and MMP-12.

	IC_{50} (nM)		
	1	**2**	**CGS_27023A**
MMP-1	12000±1000	490±76	56±6
MMP-2	12±2	1.0±0.2	25±4
MMP-3	5900±340	50±2	16±1.8
MMP-9	200±40	6.7±1.6	4.8±1.3
MMP-12	18±0.7	0.20±0.05	-
MMP-14	2300±170	9.8±0.2	23±1.6
TACE	130000±12000	14000±1000	160±9

Table 1. Inhibitory activity of compounds **1**, **2** and **CGS_27023A** on human recombinant MMPs measured by a fluorometric assay as reported by Rossello et al., (2004 and 2005) and Knight et al., (1992). Assays were run in triplicate. The final values given here are the mean ±SD of three independent experiments.

The ability of the compounds to affect MMP-2 activity at such concentrations (12 nM compound 1, 1 nM compound 2 and 25 nM CGS_27023A) prompted us to investigate their ability to affect glioma cell parameters, such as viability, proliferation and invasiveness. As first step, the ability of compounds to affect MMP-2 derived from cells was assayed on gelatin natural substrate.

MMP inhibitors: cell derived MMP-2 activity tested on natural substrate

The serum-free medium from U87MG cells was collected, centrifuged, aliquoted and incubated without or with the compounds 1, 2, or CGS_27023A for 3 h; then the aliquots were subjected to zymography, as described in the method section. A decrease in gelatinolytic activity of MMP-2 was observed after treatment with the compound 1, 2 or CGS_27023A (Figure 4).

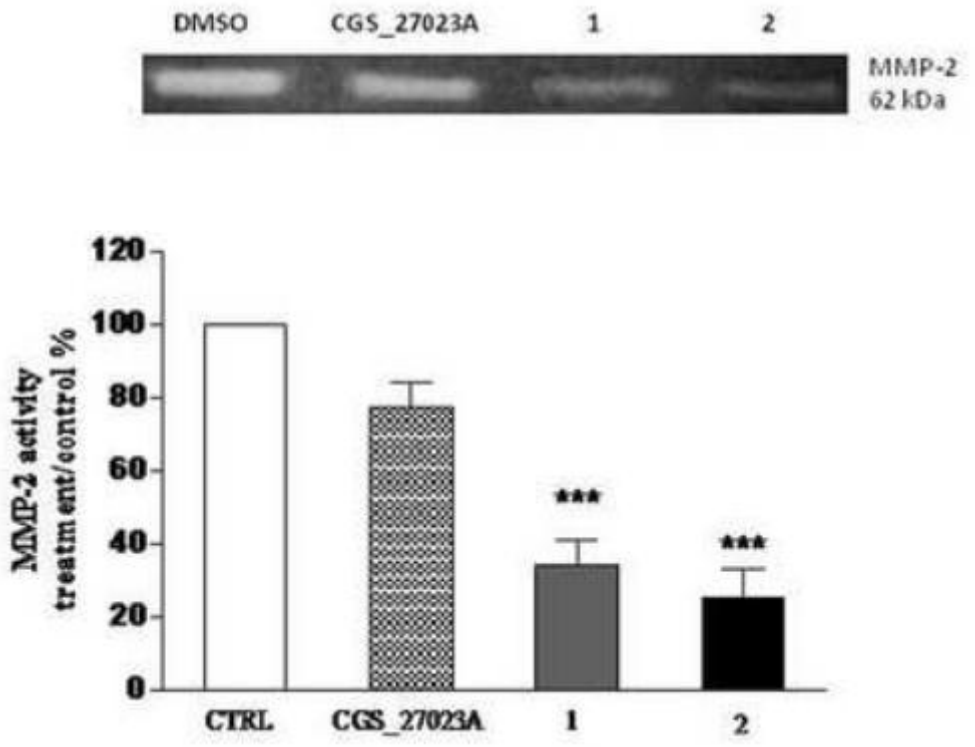

Figure 4. Effect of MMP inhibitor compounds 1, 2 and CGS_27023A on cell derived MMP-2 activity: zymogram analysis of gelatinolytic activity. Following treatment with the compounds (12 nM compound 1, 1 nM compound 2 and 25 nM CGS_27023A), as described in experimental section the proteins were separated with 10% SDS-PAGE containing gelatin (1 mg/mL). The unstained bands corresponded to the areas of gelatin digestion (a typical result from a single experiment is shown). Band intensity was quantified by a densitometric image analysis software (ImageJ, National Institutes of Health, Bethesda, MD, USA), and data (bottom) are expressed as the percentage of treated samples with respect to untreated samples. Each bar represents the mean±SEM of three independent experiments; *** *P*_0.0001.

MMP inhibitors: effect on cell proliferation

The synthetic compounds did not affect cell survival at MMP inhibitor nanomolar concentrations, as shown in Figure 5.

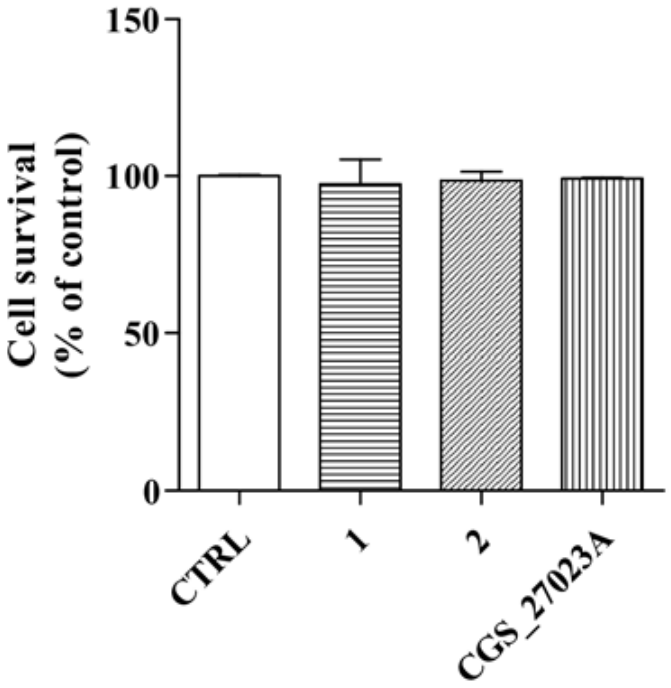

Figure 5. Inhibition of the viability of U87MG glioma cells by MMP inhibitors. U87MG cells were treated with MMP inhibitors 1, 2 and CGS_27023A for 24 h. After incubation, cell viability was measured by the MTS conversion assay as described in the Materials and methods section. Results are expressed as a percentage of the MTS activity observed after treatment with the compounds (12 nM compound 1, 1 nM compound 2 and 25 nM CGS_27023A), compared to untreated control cells (100%), and shown as the mean±SEM. Data are obtained from at least three separate experiments done in duplicate.

Specifically, the MTS activities of the cells treated with MMP inhibitors compared to control cells treated with the vehicle, DMSO, were 97.4%, 98.6% and 99.2% for compounds 1, 2 and CGS_27023A, respectively. The Trypan Blue dye-exclusion assay gave similar results (data not shown).

MMP inhibitors: effect on cell invasiveness

As shown in Figure 6, the U87MG cells treated with the synthetic MMP inhibitors showed a marked reduction in glioma cell invasion through the Matrigel membrane. In particular, the cells treated with compounds 1, 2 or CGS_27023A exhibited a significant reduction in invasion, equal to 50%, 48%, and 31% ($p<0.001$), respectively (Figure 6b).

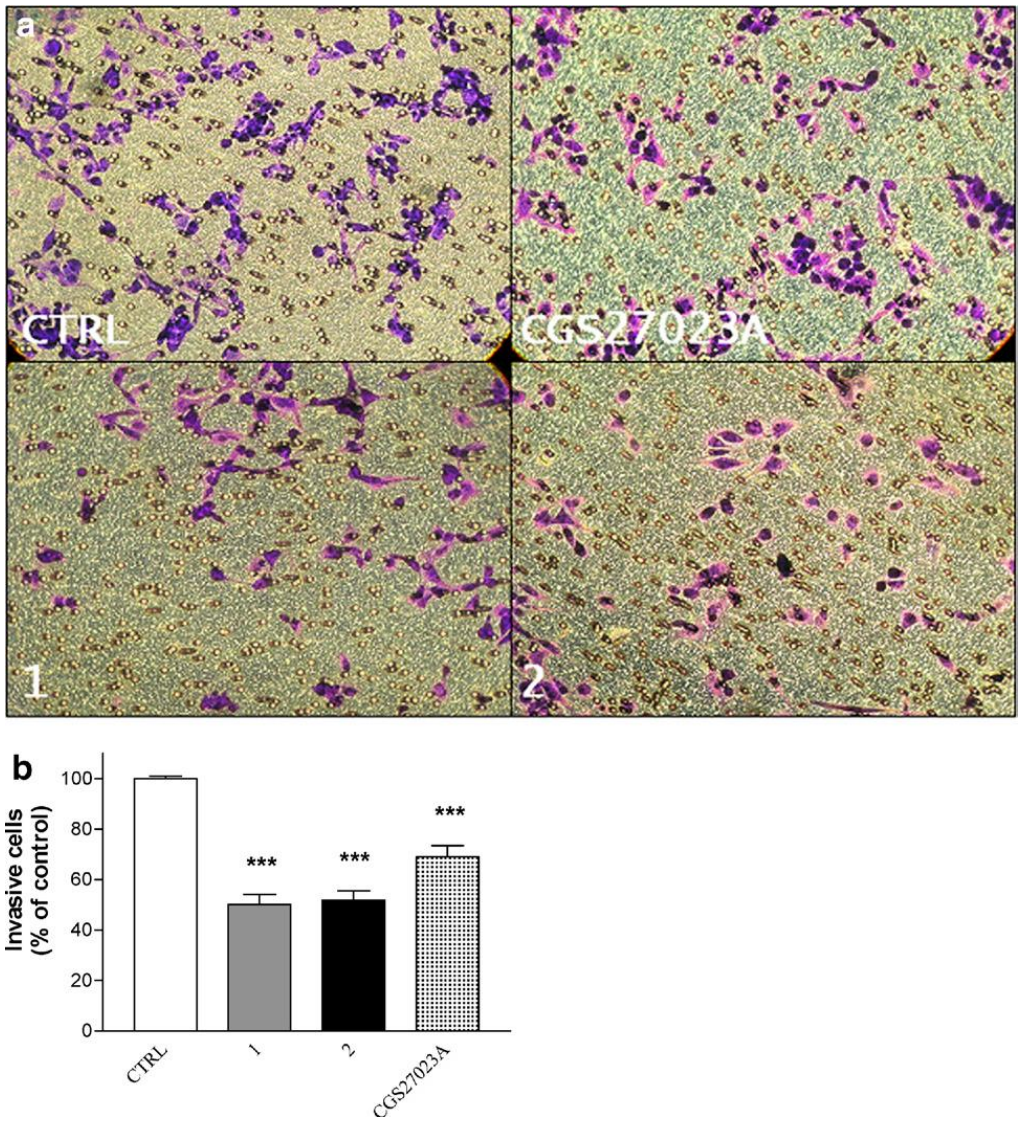

Figure 6. Compounds 1 and 2 affect U87MG cell invasiveness. (a) Cell invasion was analysed using the Matrigel basement membrane transwell system as described in Materials and Methods. Cell migration was quantified by counting the number of cells that migrated into the lower surface of the transwell membrane. Images in the Figure panels show cells that migrated to the lower surface of the transwell membrane. The magnification was 200x. The migration of untreated cells is shown in the panel marked CTRL. The migration of the cells treated with compound 1, compound 2 or the standard, CGS_27023A is shown in panels labelled 1, 2 and CGS_27023A, respectively. (b) Treatment of cells with compound 1 (12nM) or 2 (1nM) for 24 h significantly reduced the invasiveness of glioma cells by 50% and 48%, respectively. In the figure, significant reduction of cell invasiveness (31%) is also shown for treatment with the standard compound, CGS_27023A (25nM). The results are expressed as the mean value of the percentage of invasive cells observed after treatment compared to untreated control cells. *** Statistically significant result ($P<0.01$).

MMP inhibitors: effect on MMP-2 expression

To determine whether the 24 h MMP inhibitor cell treatments were accompanied by an effect on MMP-2 expression, we analysed MMP-2 mRNA and protein levels by real-time PCR and ELISA, respectively. MMP-2 mRNA was reduced by 52%, 71% and 25% with respect to the control following cell treatments with compounds 1, 2 and CGS_27023, respectively (Figure 7a). The MMP-2 protein level in the serum-free medium from untreated U87MG cells was 10.4 ng/ml (at which 100% was attributed). The treatment for 24 h with compound 1, or CGS_27023A resulted in a 47%, and 16% decrease of MMP-2 protein level (Figure 7b). The MMP-2 expression levels were not detectable (<3.5 ng/ml) following treatment with compound 2.

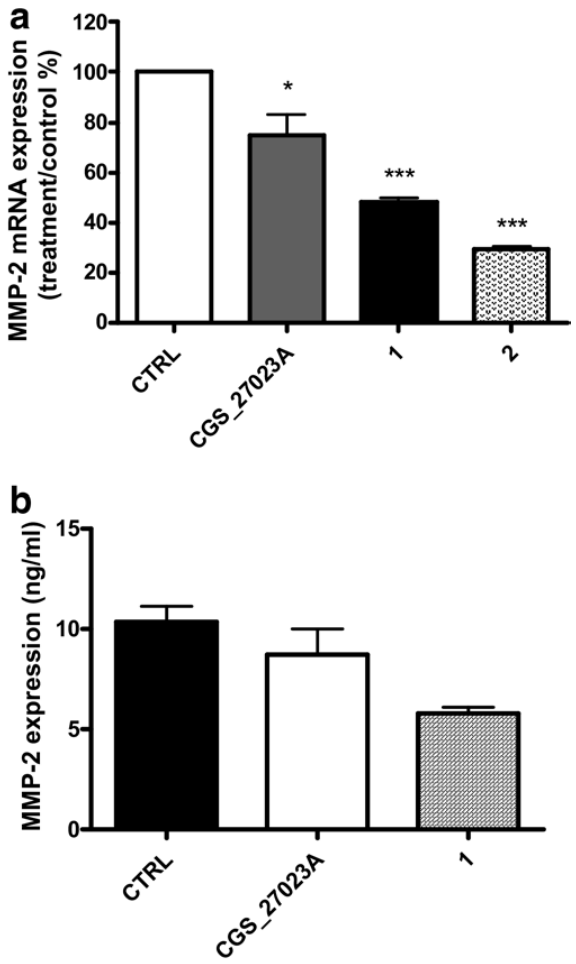

Figure 7. MMP inhibitors: effect on MMP-2 expression. The MMP-2 mRNA and protein levels were determined following 24 h cell exposure to CGS_27023A (25nM), compounds 1 (12nM) or 2 (1nM) by the means of real-time PCR and ELISA, respectively. (a) Quantitative real-time PCR was performed in triplicate, and repeated twice. Results±SEM are expressed as the percentage of control; * $P<0.05$; *** $P<0.0001$. (b) ELISA was performed in duplicate, and repeated twice. Results_SEM are expressed as the percentage of control. MMP-2 protein level was reduced by 47% and 16% after treatment with the compound 1 and CGS_27023A, respectively. MMP-2 protein level after treatment with compound 2 was not detectable (<3.5 ng/mL).

MMP inhibitors: effect on cell viability in the presence of TMZ

First, we established the growth curves for untreated cells using two different growth conditions to optimize the cell culturing for treatments longer than 48 h. In the first experimental condition, to investigate the fate of glioma cells from 0 to 16 days, we seeded the U87MG cells in 1 ml of 10 % FBS medium and assessed the number of viable U87MG cells at various times using the trypan blue dye-exclusion method. In the second experimental condition, we added 1 ml of fresh complete medium on the 7th day after cell seeding. In the experiment carried out without addition of fresh medium, the number of viable cells increased until the 8th day, after which the viable cell number

significantly decreased. In the samples to which fresh medium had been added on the 7th day, the cells showed transient growth arrest for one day, after which they proliferated until the 13th day and then lost viability. To assess proliferating cells, we chose to carry out the subsequent experiments with the addition of 1 ml of fresh complete medium on the 7th day of culture. The U87MG cells were incubated in the presence of DMSO or of two different TMZ concentrations (50 or 100 μM) and counted at different times after the treatment (from the 1st to the 13th day), using the trypan blue exclusion method. The data, shown in Figure 8, demonstrated that the TMZ treatments markedly reduced the number of human glioma cells, both at 50 μM and 100μM TMZ.

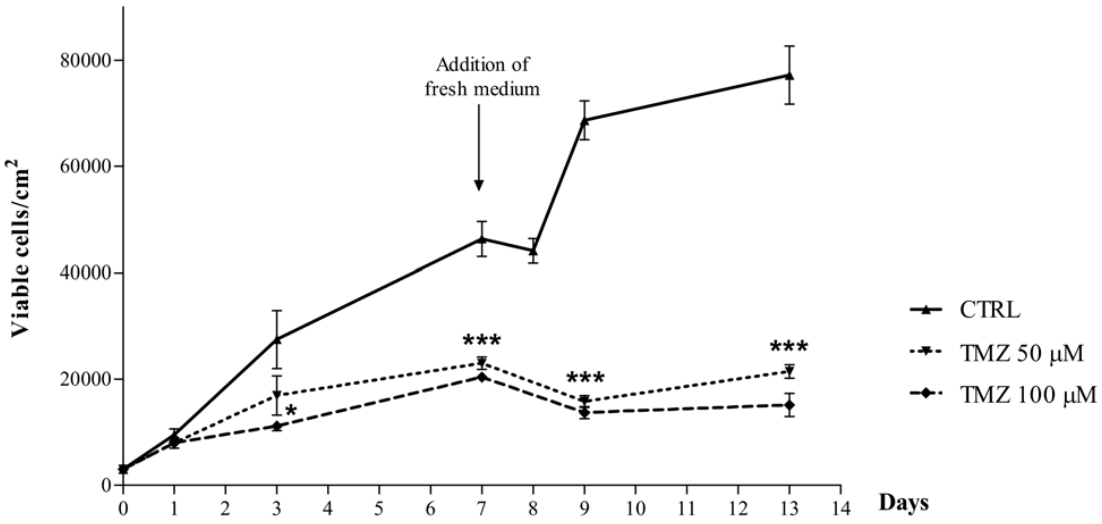

Figure 8. Proliferation curve of U87MG cells treated with TMZ. Glioma cells were treated with 50 or 100 μM TMZ or with DMSO (control cells) and cultivated for 13 days. At various times, cells were collected and counted by using the Trypan Blue assay. Results are expressed as the number of viable cells per cm2 of surface. Data were obtained from at least three separate experiments done in duplicate (* $P<0.05$; *** $P<0.0001$).

At the shortest time (1 day), TMZ did not affect cell viability; however, after three days, TMZ at 100 μM caused a significant reduction in viable cell number ($P<0.05$). The reduction in cell growth increased during longer treatments with TMZ ($P<0.0001$). Comparable results were observed for treatment with TMZ at 50 μM.

We also evaluated cell death for each treatment and incubation time. After short incubation times, the difference between control cells and treated cells was less than 10%, as verified by counting cells taking up trypan blue. After prolonged incubation times, the number of dead control cells did not exceed 20% of the total number of cells.

As we expected, when cells were treated with TMZ, the number of dead cells increased in a time dependent manner, ranging up to 40-50% of total cells on the 13th day (data not shown). Next, we examined the effect of treating cells with TMZ and compound 1 or seventh day, we added 1 ml of fresh medium containing compound 1 or CGS_27023A to the TMZ-treated cells. The co-treated cells were collected at different times and counted using the trypan blue exclusion assay. The data for compound 1 or CGS_27023A co-treatments are shown in Figure 9.

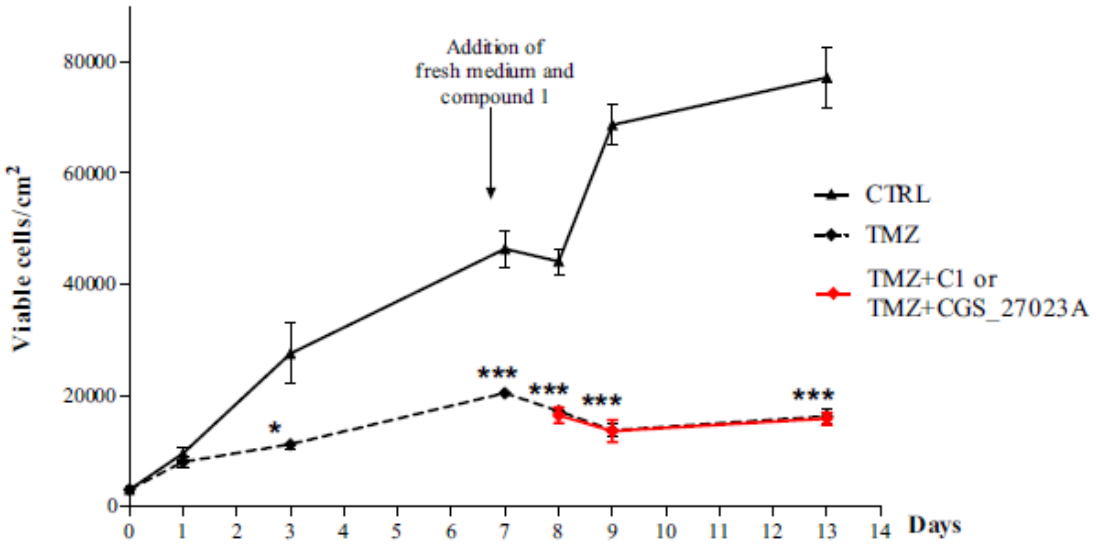

Figure 9. MMP inhibitors: effect on cell viability in the presence of TMZ. U87MG cells were treated with 50 or 100 µM TMZ and cultivated for 13 days. On the seventh day, 1 ml of fresh medium containing compound 1 or CGS_27023A to the TMZ-treated cells was added. At various times, cells were collected and counted by using the Trypan Blue exclusion assay. Results are expressed as the number of viable cells per cm2 of surface. Data were obtained from at least three separate experiments done in duplicate (* $P<0.05$; *** $P<0.0001$).

The cell growth curves established with the TMZ alone treatment and with the combination of TMZ and the MMP inhibitor 1 or CGS_27023A did not show any differences in cell proliferation. Both the cell treatments completely inhibited cell growth compared to the control (P<0.0001). As evidenced in the experiment with TMZ alone, in the cells co-treated with TMZ and MMP inhibitors, the percentage of blue cells increased in a time-dependent manner, up to 50-60% of the total cell number at the 13th day of treatment (Figure 9). The same experiments were repeated using compound 2, and the results were comparable to those obtained for compound 1 (data not shown).

MMP inhibitors: effect on cell invasiveness in the presence of TMZ

We studied whether the TMZ-MMP inhibitor co-treatment was able to suppress the invasive capacity of the U87MG cells. The results, shown in Figure 10, demonstrated that the co-treatment inhibited the number of cells invading through the Matrigel compared to the control.

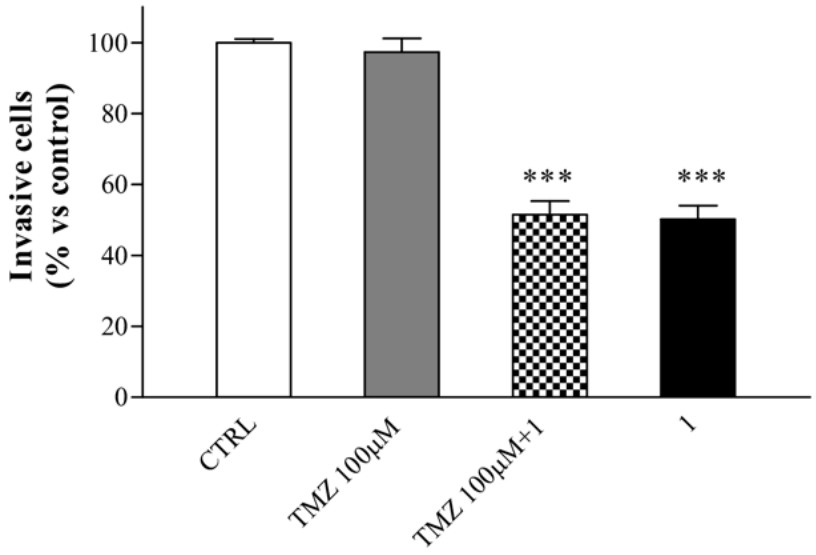

Figure 10. Glioma cell invasion through the reconstituted Matrigel basement membrane. U87MG cells were treated with TMZ or TMZ and compound 1 or compound 1 alone (12nM). The invasion assay was carried out as described in the Materials and methods section. Results are expressed as a percentage of invasive cells observed after treatment compared to untreated control cells (100%) and shown as the mean±SEM. Data are obtained from at least three separate experiments done in duplicate (*** P<0.001).

Quantification indicated that in TMZ-treated cells, invasion was similar to that in control cells. In contrast, the cells co-treated with TMZ and the MMP inhibitor 1 showed a marked reduction in glioma cell invasion to 50% of the control (P<0.001).

The combination of TMZ and MMP inhibitor 1 evidenced the same effect obtained with inhibitor alone. The same experiments were repeated using compound 2, and the results were comparable to those obtained for compound 1 (data not shown).

Discussion

In the present chapter section I reported the investigation of the potential anticancer activity of MMP inhibitor N-O-isopropyl sulfonamidobased hydroxamates (compounds 1 and 2), on the human glioblastoma cell line. Compounds 1 and 2 were chosen because they resulted, at nanomolar concentrations, potent inhibitors of MMP-2 activity against the synthetic peptidic substrate (IC50=12 nM for compound 1, IC50=1.0 nM for compound 2). Zymography analysis demonstrated that each compound was also effective, at nanomolar concentration, to inhibit the activity of cell derived MMP-2 tested on the natural substrate, gelatin. Moreover, the results demonstrated that IC50 nanomolar concentrations of compounds 1 and 2 can affect cell parameters, such as invasiveness, without affecting viability and proliferation. The low active concentration of compounds should spare the inhibition of both protective MMPs (anti-cancer) and those MMPs involved in other cell processes, probably resulting in reduced toxicity compared to broad-spectrum MMP inhibitors, such as CGS_27023A. Indeed, in order to obtain a more specific action with fewer side effects, the recent strategy is to use MMP inhibitors at very low-dosage. Compound 1 has been employed at a very low dose (4.5 pmol) in mouse experiments to investigate the role of MMP-2 and MMP-9 in neuropathic pain development (Kawasaki Y et al., 2008). In a previous study, compound 1 has been demonstrated to affect the invasive activity of the fibrosarcoma cell line, HT1080 (Rossello A et al., 2004). Treatment of U87MG glioma cells with compounds 1 or 2 for 24 h evidenced their ability to inhibit cell invasiveness without affecting viability, demonstrating their activity on different types of cancer. Compounds 1 and 2 were used at nanomolar concentrations, corresponding to their IC50 values for MMP-2, even though we cannot exclude that the observed inhibitory effects on invasiveness may be partly mediated by inhibition of MMP-9 and MMP-12. Indeed, MMP-9 and MMP-12 have been demonstrated to play a cooperative tumour-promoting effect, together with MMP-2, in GBM (Forsyth PA et al., 1999, Wang M et al., 2003). Thus, the inhibition of all these proteases could contribute to the arrest of cell invasiveness.

On the other hand, we found that the tested compounds inhibited MMP-2 expression at both the mRNA and protein levels. Our results are consistent with those of other researchers who have found a reduction of MMP-2 expression levels following treatment of tumoral cells with other MMP inhibitors (Lee SK et al., 2007). Further

studies are required to clarify the molecular mechanisms underlying the MMP-2 expression decrease in our experimental conditions.

Appropriate combinations of MMP inhibitors with other chemotherapeutic agents may prove to be a very effective anti-cancer strategy. The combination of MT, a broad spectrum MMP inhibitor, with cytotoxic compounds, such as TMZ, has shown interesting results deserving further studies to minimize the side effects associated with the use of MMP inhibitors (Levin VA et al., 2006).

In line with this strategy, the U87MG cell parameters were investigated after treatments with TMZ alone and in combination with compounds 1 or 2. The treatment of U87MG cells with TMZ markedly reduced the number of viable cells. These data are in line with previous studies reporting that TMZ induces G2-M arrest in human U87MG glioma cells, and this is the most prominent effect of TMZ in gliomas (Hirose Y et al., 2001). Compounds 1 or 2 did not affect the anti-proliferative activity of TMZ. Indeed, these co-treatments evidenced a significant reduction in the number of proliferating cells compared to that obtained in the control cells. On the other hand, the potent inhibitory effect of compounds 1 and 2 on invasiveness of glioblastoma cells was also observed during co-treatments with TMZ, suggesting that TMZ did not inhibit the anti-invasive property of these compounds.

In conclusion, taken together, these data suggest that this combination of drugs may have good therapeutic potential for the treatment of brain tumours. The ability of glioma cells to proliferate quickly and to infiltrate the surrounding brain tissues, escaping current therapeutic modalities, could be minimized using the combined treatment. These co-treatments could block the growth of the tumour by means of an alkylating agent, such as TMZ, and could stop the invasiveness through MMP-2 inhibitors. Moreover, the ability of MMP inhibitors 1 and 2 to act at nanomolar concentrations paves the way in developing efficacious clinical glioblastoma combined therapies without the side effects typically associated with broad spectrum MMP inhibitors.

4.2 Biological Evaluation in U87MG Glioma Cells of (Ethynylthiophene)Sulfonamido-Based Hydroxamates as Matrix Metalloproteinase Inhibitors

Material and Methods

U87MG cell culture

U87MG cells: see chapter 3

MMP inhibition assays

Recombinant human MMP-14 catalytic domain was a kind gift of Prof. Gillian Murphy (Department of Oncology, University of Cambridge, UK). Pro-MMP-1, pro-MMP-2, pro-MMP-3, pro-MMP-8, and pro-MMP-9 were purchased from Calbiochem.

Proenzymes were activated immediately prior to use with *p*-aminophenylmercuric acetate (APMA 2 mM for 1 h at 37 °C for MMP-2 and MMP-8, APMA 2 mM for 2 h at 37 °C for MMP-1, 1 mM for 1 h at 37 °C for MMP-9). Pro-MMP-3 was activated with trypsin 5 µg/mL for 30 min at 37 °C followed by soybean trypsin inhibitor 62 µg/mL. For assay measurements, the inhibitor stock solutions (10 mM in DMSO) were further diluted, at 7 different concentrations for each MMP in the fluorometric assay buffer (FAB: Tris 50 mM, pH = 7.5, NaCl 150 mM, $CaCl_2$ 10 mM, Brij 35 0.05% and DMSO 1%). Activated enzyme (final concentration 0.5 nM for MMP-2, 1.3 nM for MMP-9, 1.5 nM for MMP-8, 5.0 nM for MMP-3, 1.0 nM for MMP-14cd, 2.0 nM for MMP-1) and inhibitor solutions were incubated in the assay buffer for 2 h at 25 °C. After the addition of the fluorogenic substrate Mca-Arg-Pro-Lys-Pro-Val-Glu-Nva-Trp-Arg-Lys(Dnp)-NH_2 (Sigma) for MMP-3 and Mca-Lys-Pro-Leu-Gly-Leu-Dap(Dnp)-Ala-Arg-NH_2 (Bachem) for all the other enzymes in DMSO (final concentration 2 µM), the hydrolysis was monitored every 15 s for 15 min, recording the increase in fluorescence (λ_{ex} = 325 nm, λ_{em} = 395 nm) with a Molecular Devices SpectraMax Gemini XS plate reader. The assays were performed in duplicate in a total volume of 200 µL per well in 96-well microtiter plates (Corning black, NBS). The MMP inhibition activity was expressed in relative fluorescent units (RFU). Percent of inhibition was calculated from control reactions without the inhibitor. IC_{50} was

determined using the formula: $V_i/V_o = 1/(1 + [I]/ IC_{50})$, where V_i is the initial velocity of substrate cleavage in the presence of the inhibitor at concentration [I] and V_o is the initial velocity in the absence of the inhibitor. Results were analyzed using SoftMax Pro software and GraFit software.

Cell treatment

U87MG cells were seeded at 30,000 cells/cm^2 in serum-free medium and incubated in the absence (control) or presence of the MMP inhibitors for 24 h. The MMP inhibitors were tested at a single concentration (5 nM). Compound 5a was tested also at 1, 5, 25, 125 nM concentrations to verify the dose-dependency of cell invasiveness inhibition. The vehicle (DMSO) in which the compounds were dissolved never exceeded 1% of the final volume of culture medium.

Trypan Blue exclusion assay

Cell viability in serum-free medium after drug treatments was measured by the Trypan Blue exclusion assay, as reported in the precedent section.

Matrigel invasion assay of U87MG glioma cells

This method was employed to evaluate cell invasiveness after treatments with MMP inhibitors, as reported in the precedent section

Statistical analyses

The nonlinear multipurpose curve-fitting program Graph-Pad Prism was used for data analysis and graphic presentations. All data are presented as the mean ± SEM derived from at least three independent experiments done in duplicate. $p<0.0001$ was considered statistically significant.

Results and discussion

MMPs inhibition

The newly synthesized hydroxamates **4-7** were tested *in vitro* for their ability to inhibit human recombinant MMP-1, MMP-2, MMP-3, MMP-8, MMP-9, and MMP-14 by a fluorometric assay, which used a fluorogenic peptide as the substrate. The broad spectrum inhibitor **3** was taken as reference compound (Table 2).

Table 2. *In vitro*[a] activity (IC_{50} nM values) of 4-butylethynylthiophene derivatives **4**, **5a-d**, **6**, **7** and the reference compound **3**.

Compd	R	MMP-1	MMP-2	MMP-3	MMP-8	MMP-9	MMP-14
4	H	13000	1.5	46	200	79	700
5a	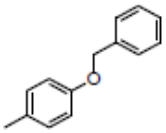	4800	2.3	180	490	63	2100
5b	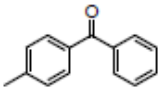	37000	4.0	84	440	50	6600
5c	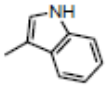	2300	6.0	93	280	77	1700
5d	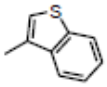	56000	17	320	1700	650	23000
6		21000	2.5	38	500	21	1600
7		6700	1.3	11	30	4.3	112
3		56	25	16	7.7	4.8	23

[a]Enzymatic data are mean values for three independent experiments performed in duplicate. SD were generally within ±10%.

As can be seen from data in Table 2, the introduction of various (*R*) aryl-alkyl chains in position α of the hydroxamate did not substantially affect activity toward MMP-2 with respect to the un-substituted derivative **4**. In fact, all α-substituted compounds displayed nanomolar inhibitory activity for MMP-2 (IC_{50} values between 1.3 and 17 nM) comparable to compound **4** activity (IC_{50} = 1.5 nM). As expected, these data confirmed that the activity for MMP-2 was principally determined by the P1' group, a 4-butylphenylethynylthiophene substituent, which is the same for all compounds. On the contrary, the selectivity profile was greatly affected by the presence

of the α-chain (P1 group) and by its structure. The cyclic derivatives **6** and **7**, bearing a thiazolidine and a tetrahydroisoquinoline ring respectively, were poorly selective over the anti-target MMPs. In particular, the tetrahydroisoquinoline derivative **7** was the least selective of the series, having nanomolar activity toward all tested enzymes, except MMP-1. Among the non-cyclic inhibitors, the benzyloxy benzyl derivative **5a** was the most active on both MMP-2 and MMP-9 (IC_{50} = 2.3 nM and 63 nM, respectively), showing the highest selectivity over MMP-1, -3, -8 and -14. This compound exhibited a 2000-fold selectivity for MMP-2 over MMP-1, a 1000-fold selectivity over MMP-14, a 200-fold selectivity over MMP-8 and a 80-fold selectivity over MMP-3. These very good selectivity data are probably due to the presence of a more bulky α-chain compared to the other derivatives. The benzothienyl derivative **5d** resulted the weakest inhibitor of MMPs, on all tested enzymes.

Matrigel invasion assay and viability assay on human U87MG glioma cells.

Firstly, the ability of the newly synthesized gelatinases inhibitors **4-7** and the reference compound **3** to inhibit invasion through Matrigel was evaluated using U87MG cells. In addition, potential cytotoxicity of these compounds was determined on parallel cultures using the trypan blue exclusion method. The data, shown in Table 3, indicate that drug treatments only slightly reduced the cell survival of glioma cells ($p>0.05$) after a 24 h incubation of the cells at a 5 nM concentration of the inhibitors. Furthermore, MMPI-treated U87MG cells with a 5 nM inhibitor dose showed a marked reduction ($p<0.0001$) in invasion through Matrigel after 24 h, as shown in Table 3. Invasion data were normalized by subtracting the percentage of dead cells at the end of the assay, which did not exceed an average of ~15% among the different compounds.

Table 3. *In vitro* cellular activity in U87MG cell line of synthesized compounds **4-7** and the reference compound **3.**

Compd	% of death cells	inhibition %[a] of cell invasiveness
DMSO	10.0±1.04	0.00
4	11.5±0.20	39.5±1.55
5a	12.3±0.44	42.6±0.97
5b	9.38±2.77	27.5±1.66
5c	6.80±1.24	48.4±2.80
5d	14.4±0.07	34.0±1.45
6	17.8±1.28	16.0±0.60
7	13.6±4.15	35.9±1.45
3	10.8±1.81	28.3±0.40

[a] Percent inhibition observed at 5 nM concentration of the tested compounds, normalized to cell death. Invasion data were normalized by subtracting the percentage of dead cells at the end of the assay, which did not exceed an average of ~15% among the different compounds.

Taken together, these results identify a new series of MMPIs with potent anti-invasive activity at nanomolar concentrations without cytotoxicity in cultured glioma cells. Furthermore, all compounds, except the cyclic derivative **6**, were more active than the broad spectrum inhibitor **3**. In particular, as shown in Figure 11A, compounds **5c** and **5a** displayed the highest inhibitory activity of cell invasiveness (48 and 43% at 5 nM, respectively). As shown in Figure 11B, a dose-dependent cell invasiveness inhibition was observed following treatment with 1, 5, 25, 125 nM concentrations of compound **5a** (IC_{50} = 12 nM).

From these data, it appears evident that probably MMP-2 is not the only enzyme responsible for the invasion process in glioma cells. In fact, according to inhibition data on isolated enzymes (Table 2), all these compounds have similar activity on MMP-2 but they show different ability to inhibit invasion (from 16 to 48% inhibition). However, selectivity for MMP-2 and MMP-9 seems to be fundamental to achieve activity on glioma cells, because compound **5a** was the one with the best selectivity profile on MMP-2 and MMP-9.

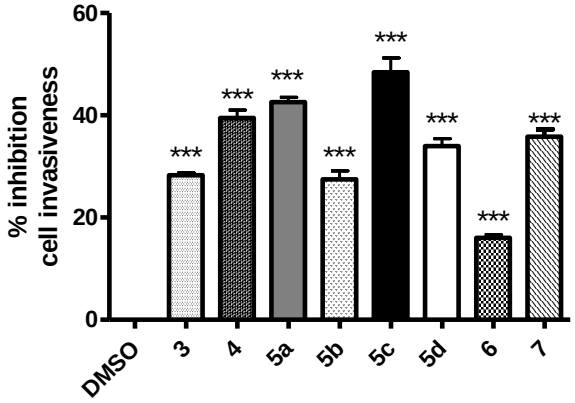

11A.

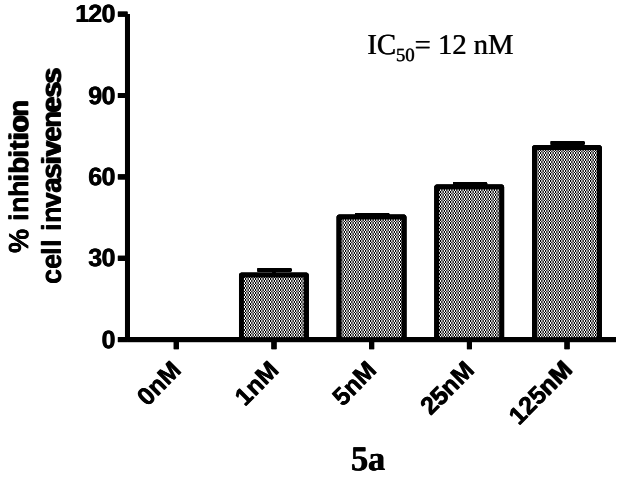

11B.

Figure 11. Effect of MMPIs on U87MG cell invasiveness. (A) Treatment of cells with compounds **4-7** and the reference compound **3** (5 nM) for 24 h reduced the invasiveness of glioma cells. (B) Dose-dependent cell invasiveness inhibition following treatment with compound **5a** for 24 h. The IC_{50} value represents the compound concentration producing a 50% decrease in tumor cells invasiveness. The results are expressed as the mean value of the inhibition percentage of invasive cells observed after treatment compared to untreated control cells.*** = statistically significant result (p<0.0001).

The migration of cells treated with compounds **5a**, **5c** or the reference compound **3** is shown in Figure 12.

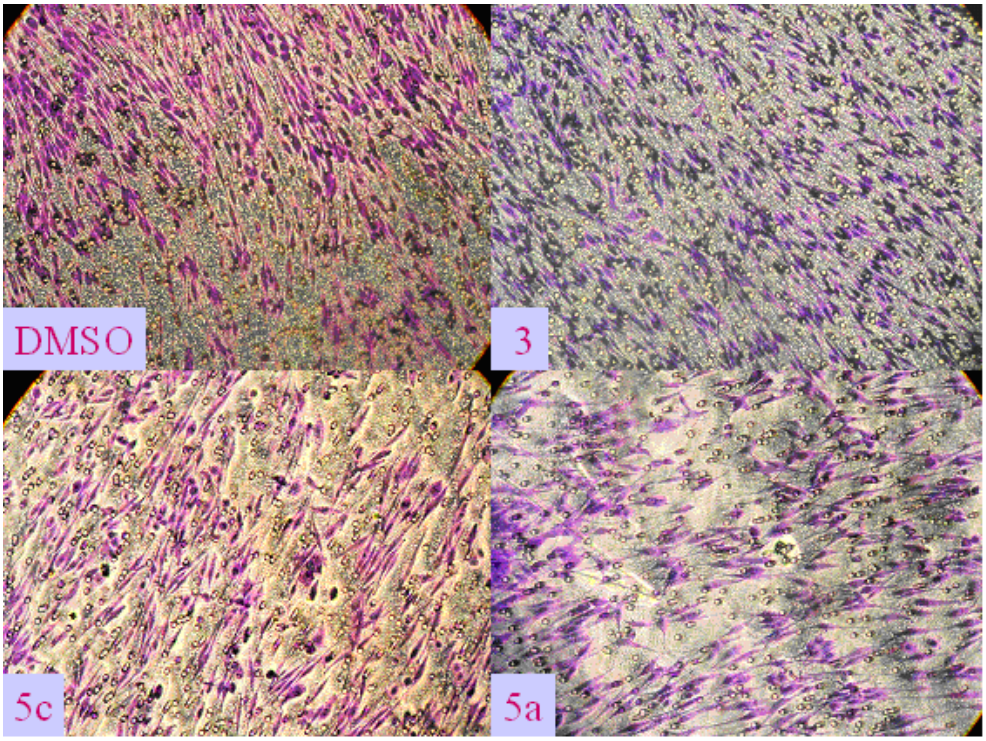

Figure 12. Cell invasion was analysed using the Matrigel basement membrane transwell system as described in Experimental Section. Images in the figure panels show cells that migrated to the lower surface of the transwell membrane. The magnification was 200x. The migration of untreated cells is shown in the panel marked DMSO. The migration of cells treated with compounds **5a**, **5c** or the reference compound **3** is shown in other panels.

Conclusion

In this chapter section, a small series of new 4-butylphenyl(ethynylthiophene)sulfonamido-based hydroxamate inhibitors for MMP-2, selective over MMP-1 and MMP-14, was tested for their ability to inhibit glioma cell invasion in vitro. Among these compounds, a very promising derivative was identified (**5a**) with nanomolar activity for MMP-2 and MMP-9 and good selectivity over the anti-target MMP-8 and MMP-3, by fluorometric assay on isolated enzymes. To assess the new hydroxamates activity in cells, Matrigel invasion assay and viability assay on human U87MG glioma cells were performed. No toxicity was detected for these compounds at the nM concentration used, and **5a** was found to inhibit by 43% glioma invasiveness at 5 nM (IC50 = 12 nM). Finally, this compound has been shown to possess a nanomolar inhibitory activity against MMP-25, a recently discovered target involved in glioma progression (data not shown, see Nuti E et al., 2011). After the

disappointing clinical results of broad spectrum MMP inhibitors in cancer therapy of the last years, this preliminary study, together with the results reported in the previous section of this chapter (section 4.1), has the aim to reopen the search for more selective MMPIs with anti-invasive activity to be used also in combination with cytotoxic compounds, as TMZ (Gabelloni P et al, 2010). The use of more specific and efficacious inhibitors should allow to reduce the doses necessary to have therapeutic efficacy without the side effects typically associated with broad spectrum MMP inhibitors.

Chapter 5: Glioblastoma multiforme II

p53 reactivation by the new small-molecule ISA27 MDM2 inhibitor is highly effective in inducing apoptosis of U87MG human glioblastoma multiforme cells.

The dysregulation of intracellular mechanisms mediated by p53, the main cellular gatekeeper, plays a crucial role in the high resistance of GBMs to DNA-damaging therapy (Ohgaki H and Kleihues P, 2009).

It is indeed a transcription factor that acts as a tumor suppressor and mediator of cell cycle and has been called "the guardian of the genome", referring to his role in the preservation of stability by preventing mutations. In normal circumstances, following DNA damage, the activation of the p53 pathway results in cell cycle arrest to allow DNA repair, and if the DNA lesion is too extensive, p53 induces apoptotic cell death (Vousden KH and Lu X, 2002).

In GBM, p53 function is frequently impaired, and cells became resistant to apoptosis induced by genotoxic damage. In a small percentage of cases, the gene encoding p53 is mutated, rendering the p53 protein inactive (Ohgaki H and Kleihues P, 2009, Vousden KH and Lu X, 2002, Cerami E et al., 2010). In the majority of cases, p53 retains its wild-type status, but its function is effectively inhibited by the Murin-Double-Minute-2 (MDM2) oncoprotein, the primary cellular inhibitor of p53 (Cerami E et al., 2010, He J et al., 1994).

The MDM2 protein tightly controls p53 activity through an autoregulatory feedback loop; p53 activates MDM2 expression, which in turn represses p53 by three mechanisms. First, the MDM2 protein binds p53 at its transactivation domain and blocks its ability to activate transcription. Second, MDM2 exports p53 out of the nucleus. Third, MDM2 promotes the proteosome-mediated degradation of p53 through its E3 ubiquitin ligase activity (Freedman DA et al., 1999, Juven-Gershon T and Oren M, 1999, Wu X et al., 1993). In GBMs, genetic alterations that cause MDM2 overexpression and excessive nuclear accumulation have been reported (Ohgaki H and Kleihues P, 2009, Cerami E et al., 2010, Halatsch ME et al., 2006) and documented in approximately 15% of GBMs.

The loss of the locus containing the gene for PTEN (a protein that counteracts excessive MDM2 nuclear accumulation) has been found in up to 80% of GBMs.

All of these data suggest that the restoration of p53 function is an appealing approach to treating GBMs. Several distinct approaches have been pursued to restore p53 function as a new cancer therapeutic strategy (Chène P, 2003, L.T. Vassilev LT et al., 2004, Wiman KG, 2006).

Three recent studies, using unique genetic models, have demonstrated that p53 restoration universally leads to a rapid and robust regression of established sarcomas, lymphomas and liver tumors (Xue W et al., 2007, Ventura A et al., 2007).

Experimental section

p53-MDM2 inhibitors

One attractive pharmacological approach to p53 reactivation is to use a small molecule to block the MDM2-p53 interaction. The discovery of the Nutlins provided the important proof of concept for this approach, as they have been shown to bind to MDM2, block the MDM2-p53 interaction, activate p53 and induce apoptotic cell death in several tumor models. Interestingly, these drugs have been reported to induce cancer cell apoptosis even without the concomitant application of DNA-damaging agents. Nutlin-3 has recently entered phase I clinical trials with patients suffering from advanced solid cancers or hematologic malignancies.

To the best of our knowledge, little is known about the efficacy of MDM2 inhibitors in human GBMs, although a study of the effect of Nutlin-3 on GBM cells was published while this thesis was written. We investigated whether a novel small-molecule MDM2 inhibitor, named ISA27, affected the growth of the U87MG human GBM cell line and compared its efficacy with that of Nutlin-3. We chose U87MG cells because they express wild-type p53 and are PTEN-null (Kondo S et al., 1995).

We showed that ISA27 activated the p53 pathway in U87MG cells and elicited a dose- and time dependent inhibition of cell growth by the induction of permanent cell cycle arrest and apoptosis. Compared to Nutlin-3, ISA27 was effective at a lower dose and caused a faster antiproliferative response.

Materials and Methods

U87MG cell line culture and preparation of circulating cell samples

- U87MG cells: see chapter 3.

- Blood samples were drawn into test tubes containing Li-Heparin and then processed for mononuclear cell preparation according to the method of Boyum (Boyum A, 1969). The final cell pellet was re-suspended in complete RPMI 1690 media supplemented with 15% FBS, 2 mM L-glutamine, 100 units/ml penicillin and 100 mg/ml streptomycin. To evaluate cell populations, random cell samples (n=7) were employed for flow cytometric analysis.

Cell treatment with MDM2 inhibitors

For U87MG cell treatment, the cells were seeded at 5,000 cells/cm2. After 24 h, the culture medium was replaced with fresh medium with ISA27 (Gomez-Monterrey I et al., 2010) or Nutlin-3 for the indicated incubation times. DMSO was added to control cells (<1% v/v). For short-term treatment (24 h), U87MG cells were incubated with increasing concentrations of the MDM2 inhibitors (from 5 nM to 15 µM). For long term treatment (up to 5 days), U87MG cells and lymphomonocytes were incubated with 2.5 µM ISA27 or 10 µM Nutlin-3.

Cell survival/growth analysis

The effects of MDM2 inhibitor treatment on U87MG cell survival/growth were estimated by MTS conversion (Chelli B et al., 2004) and Trypan blue exclusion assays (Ruan S et al., 1999). The MTS assay was used to establish the MDM2 inhibitor concentration that inhibited 50% (IC50 value) of the cell survival/growth after 24 h of treatment and was performed according to the manufacturer's instructions. Sigmoidal dose-response curves were generated using Graph Pad Prism 4 software (GraphPad Software Inc., San Diego, CA), from which the IC50 values were derived. Trypan blue dye exclusion was used to examine the long-term effects of MDM2 inhibitor treatment on U87MG cell and lymphomonocyte viability at the indicated times.

Analysis of the complex p53-MDM2 levels

The complex p53-MDM2 levels in U87MG cells were determined using the Assay Design® p53-MDM2 Immunoset. Cell lysates (3.2 µg of protein) were added to multi-well plates that were previously coated with p53 antibody and incubated for 1 h. After 4 washings, MDM2 antibody was added to each well and then incubated with a colorimetric enzyme substrate and analyzed at 450 nm. The p53-MDM2 complex amount was determined according to a standard curve. The percentage of the complex in samples from MDM2 inhibitor treated-cells was calculated with respect to untreated cells, at which 100% was attributed.

Relative mRNA quantification of target p53 genes

The relative mRNA quantification of target p53 genes in untreated and MDM2 inhibitortreated cells was performed by real-time polymerase chain reaction (real-time PCR) as described in the chapter 4. The primer sequences used were:

MDM2 forward, 5'-TCTAGGAGATTTGTTTGGCGT-3';
MDM2 reverse, 5'-TCACAGATGTACCTGAGTCC-3;
p21 forward, 5'-AAGACCATGTGGACCTGTCACTGT-3';
p21 reverse, 5'-GAAGATCAGCCGGCGTTTG-3';
PUMA forward, 5'-TCCTCAGCCCTCGCTCTCGC-3';
PUMA reverse, 5'-CCGATGCTGAGTCCATCAGG-3';
ß-actin forward, 5'-GCACTCTTCCAGCCTTCCTTCC-3';
ß-actin reverse, 5'-CGTGTGGATCGGCGGCTC-3'.

Cell cycle analysis

Cell cycle analysis was performed by flow cytometric analysis (FACScalibur flow cytometer, Becton Dickinson, USA) (Chelli B et al., 2004, Chelli B et al., 2005).

The percentage of PI-stained untreated and MDM2 inhibitor-treated cells was estimated in each cell cycle phase using the ModFit LT software program.

Cellular senescence assays

The senescence marker SA-β-Gal was detected as previously described (Dimri GP et al., 1995), and cells were then washed in PBS (1X) and photographed at 100X magnification. Images of random light microscopic fields were captured (5 fields per

well), and cells were counted using ImageJ (ImageJ Software, version 1.41o; USA). The average cell size was assessed using the Scepter 2.0 handheld automated cell counter (Millipore, Billerica, MA, USA).

Analysis of apoptotic parameters

Mitochondrial membrane potential ($\Delta\Psi$m). Changes in..m were assessed using the fluorescent dye JC-1 as previously described (Chelli B et al., 2004, Chelli B et al., 2005), and fluorescence was analyzed by FACS. As a positive control, a cell pellet was incubated with the uncoupling agent CCCP (50 µM).

Cytosolic Cytochrome c release from mitochondria. The cytosol fraction from untreated and MDM2 inhibitor-treated cells was obtained using the mitochondrial fractionation Active Motif ® Kit according to the manufacturer's instructions. The cytosolic protein content was determined as previously described (Dimri GP et al., 1995), and the cytochrome c content was determined using the Platinum Human Cytochrome c ELISA. The minimum detectable dose of cytochrome c was 0.05 ng/mL.

DNA fragmentation analysis. DNA fragmentation was estimated by evaluating the DNA PI staining using FACS. The percentage of apoptotic cells was estimated as previously described (Chelli B et al., 2004, Chelli B et al., 2005). The percentage of cells in the sub-G0 fraction was determined using the ModFit LT software program.

Statistical analyses

The nonlinear multipurpose curve-fitting program Graph-Pad Prism was used for data analysis and graphic presentations. All data are presented as the mean ± SEM. Statistical analysis was performed by one-way analysis of variance (ANOVA) with Bonferroni's corrected t-test for post-hoc pair-wise comparisons. $P < 0.05$ was considered statistically significant.

Results

Lower dose of ISA27 restores p53 function and inhibits U87MG cell growth/survival than that of Nutlin-3

GBM cells were treated with the small molecule ISA27 (see Figure 1 for chemical structure) because it efficiently dissociated the reconstituted human MDM2-p53 complex (Gomez-Monterrey I et al., 2010). To evaluate ISA27 efficacy, parallel experiments were performed using Nutlin-3, the standard MDM2 inhibitor (Vassilev LT et al., 2004). The GBM cell model was the U87MG human GBM cell line because it expresses wild-type p53 and overexpresses MDM2 (Kond S et al., 1995, Zhao P et al., 1998).

To examine the effects of ISA27 on U87MG cell growth/survival and compare its efficacy with that of the standard Nutlin-3, the concentration at which each small-molecule inhibitor inhibited 50% of cell growth (IC50 value) after 24 h of treatment was estimated. Both small molecules had a dose-dependent inhibitory effect on cell growth/survival. The IC50 values were 2.5±0.4 μM for ISA27 and 10±2.1 μM for Nutlin-3, indicating that ISA27 is a more potent cell growth/survival inhibitor than Nutlin-3. These IC50 inhibitor concentrations were then used in the following experiments.

Next, we evaluated whether ISA27 was able to disrupt the intracellular MDM2-p53 interaction with the same efficiency as reported in a cell-free system (Gomez-Monterrey I et al., 2010). The ISA27-treated cells showed a statistically significant reduction in MDM2-p53 complex formation compared to control cells ($t=5.48$, $p<0.01$) (Figure 1A). Comparable results were obtained with Nutlin-3 ($t= 6.16$, $p<0.01$) (Figure 1A).

MDM2 inhibition should stabilize p53 and induce the expression of p53 target genes. Thus, we examined the effect of ISA27 on the mRNA levels of the two p53 target genes MDM2 and p21. Short-term ISA27 treatment led to a statistically significant increase in MDM2 and p21 mRNA. Specifically, ISA27 caused a 4.3- and 4.5-fold induction of MDM2 and p21 mRNA, respectively (for MDM2: $t=3.87$, $p<0.01$; for p21: $t=8.26$, $p<0.001$) (Figure 1B). These results suggest that the low MDM2-p53 complex formation in ISA27-treated U87MG cells leads to an elevation in the MDM2 and p21 mRNA levels in a manner that is consistent with activation of the p53 pathway. The standard Nutlin-3 caused a 2.3- and 4.3-fold induction of MDM2 and p21 mRNA,

respectively (for MDM2: t=3.43, p<0.05; for p21: t=7.79, p<0.001) (Figure 1B). One of the main cellular consequences of p53 activation in proliferating cells is cell cycle arrest at the G1/G2 phases, and the cyclin-dependent kinase inhibitor p21 plays a major role in this arrest. Cell cycle analysis by cytofluorimetric DNA content analysis revealed an increase in the G1 fraction and a nearly complete depletion of S-phase cells after ISA27 or Nutlin-3 short-term treatment (Figure 1C).

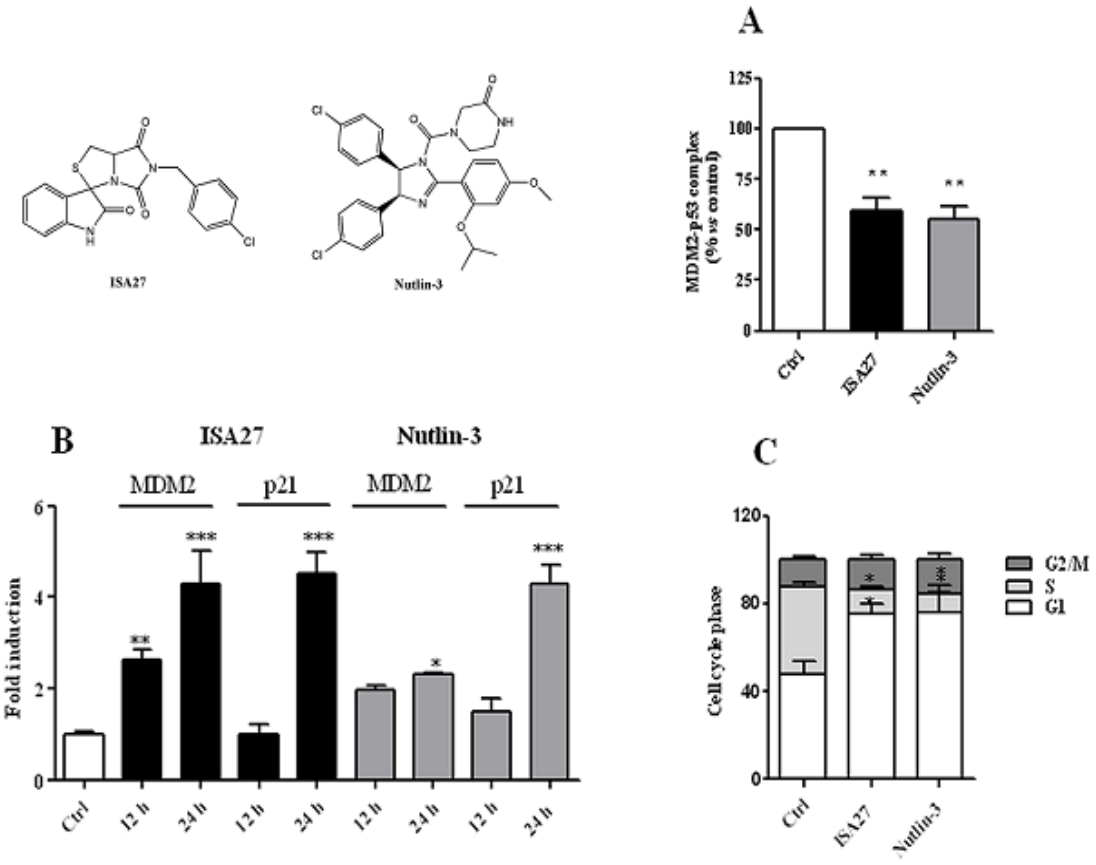

Figure 1. ISA27 restores p53 function in U87MG cells. **1A)** ***ISA27 reduces MDM2-p53 complex formation***: A significant reduction in MDM2-p53 complex formation was shown following short-term treatment with ISA27 or Nutlin-3. **1B)** ***ISA27 induces p53 target gene expression*****:** Real-time PCR analyses showed a statistically significant increase in MDM2 and p21 mRNA levels following short-term ISA27 or Nutlin-3 treatment. **1C)** ***ISA27 induces cell cycle arrest***: cell cycle analysis revealed a statistically significant increase in the G1 fraction and a nearly complete depletion of the S-phase in short-term-treated cells.

Long-term ISA27 treatment leads to the complete inhibition of U87MG GBM cell growth but not that of normal lymphomonocytes

U87MG cells were exposed to ISA27 for 5 days and then viable and dead cells were counted at indicated time points. A substantial decrease in cell survival was observed after one day of treatment and progressed at each subsequent time point, until

almost all viable cells were depleted after 5 days (Figure 2A). When the time-course curves of ISA27 and Nutlin-3 were compared, the data showed that ISA27 was able to reduce U87MG cell viability faster than Nutlin-3 (Figure 2A). We also examined the effect of ISA27 on the viability of normal human lymphomonocytes. Flow cytometry was performed to evaluate cell populations isolated from blood samples of healthy individuals. As shown in the scatter cytogram in Figure 2B, the two cell populations were clearly visible (G2= 74.0% lymphocytes; G3= 14.2% monocytes). As shown in Figure 2C, ISA27-treated lymphomonocytes were still viable by 48 h, suggesting that ISA27 is selective for cancer versus normal cells. Nutlin-3 showed a similar lack of cytotoxicity in this normal peripheral cell model (Figure 2C).

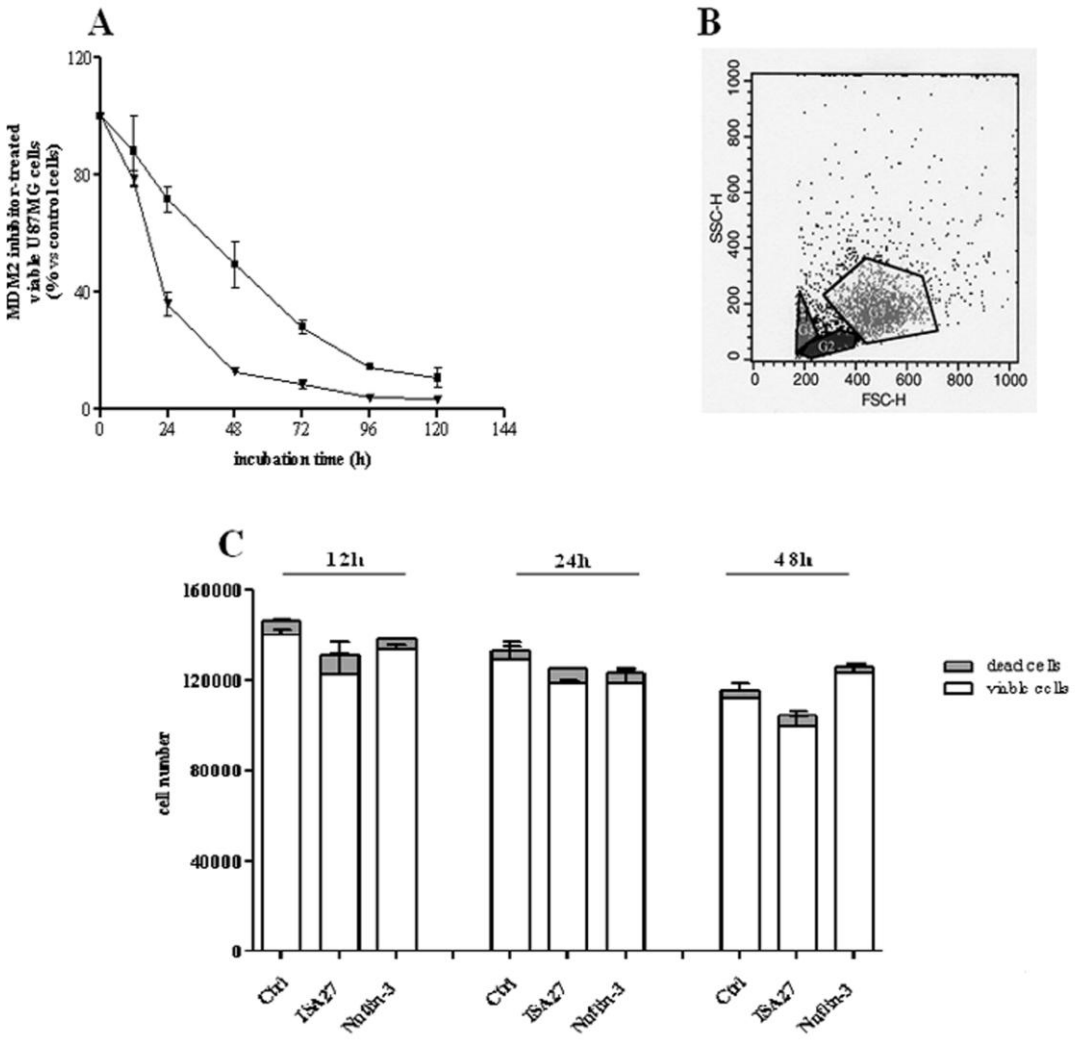

Figure 2. Long-term ISA27 treatment of U87MG cells and human lymphomonocytes. **2A)** ***Time-response curve of U87MG cell viability:*** The percentage of ISA27- (▼) or Nutlin-3- (■) treated viable cells was calculated with respect to untreated viable cells at the indicated incubation times. **2B)** ***Scatter cytogram analysis of cell populations from blood:*** Scatter cytogram analysis showing cell separation by size and granularity (G2=lymphocytes; G3=monocytes). One representative experiment is presented. **2C)** ***Time-response of human lymphomonocyte viability following ISA27 treatment:*** No significant differences were observed between MDM2 inhibitor-treated and control viable or dead cells at each incubation time.

Long-term ISA27 treatment leads to permanent cell cycle arrest and apoptosis in U87MG human GBM cells

We first analyzed cell cycle profiling and p21 mRNA levels after long-term ISA27 treatment. ISA27 treatment of U87MG cells for 24 h effectively arrested cell-cycle progression, depleted the S-phase population compartment ($t=5.67$, $p<0.05$) and increased the G0/G1-phase population ($t=5.25$, $p<0.05$), and treatment for 72 h depleted

the S-phase population and increased the G2-phase population ($t=7.69$, $p<0.01$) (Figure 3A). A persistent induction of p21 mRNA was observed, suggesting that the major transcription target of activated p53 was involved in the cell cycle arrest (Figure 3B). Nutlin-3 arrested cell-cycle progression in U87MG cells 24 and 72 h after treatment, depleting the S-phase compartment and increasing the G0/G1-phase compartment (Figure 3A).

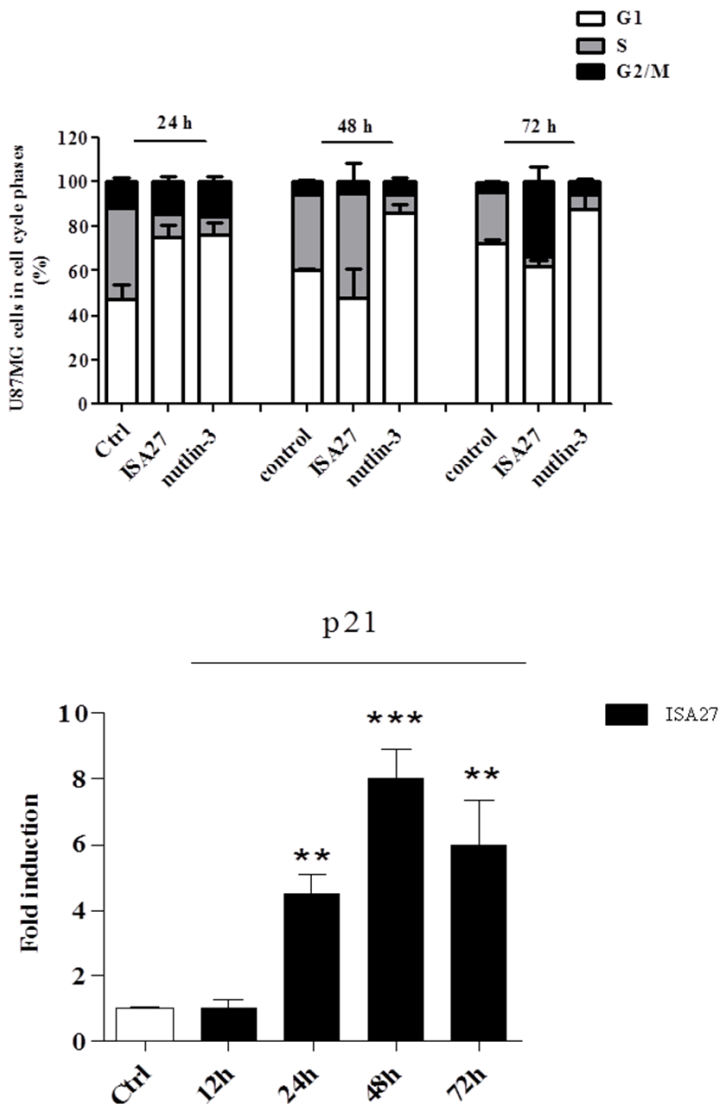

Figure 3. Long-term ISA27 treatment induces cell cycle arrest and persistent p21 mRNA increase in U87MG cells. 3A) ***Flow cytometric cell cycle profiling*****:** the figure shows the percentage of untreated and MDM2 inhibitor-treated U87MG cells in G1, S and G2/M phases. **3B)** ***p21 mRNA evaluation*****:** ISA27 caused a statistically significant increase in p21 mRNA at 24, 48 and 72 h**.**

To elucidate whether ISA27 induced permanent cell cycle arrest (cellular senescence) or reversible cell cycle arrest in U87MG cells, the ability of these cells to resume proliferation after ISA27 treatment was evaluated. The cells were incubated with ISA27 for 4 days, washed to remove the drug and then incubated for an additional 4 days in fresh culture medium. After removal of the drug, U87MG cells barely resumed proliferation. We then evaluated whether ISA27 induced a morphological change in U87MG cells (i.e., large and flat cells), which is compatible with senescence, and whether the widely used senescence marker SA-β-Gal could be detected in ISA27-treated cells. The ISA27-treated cells acquired an enlarged and flat morphology as

revealed by measuring the mean cell diameter (12.36±1.56 .µm and 13.59±1.74 .µm for control and ISA27- treated cells, respectively). The onset of cellular senescence was rapid; indeed, a high number of U87MG cells were positive for SA-β-Gal after 1 day of treatment. Figure 4A shows representative images of SA-β-Gal detection in ISA27-treated and control cells. As shown in Figure 4B, ISA27 significantly enhanced the number of SA-β-Gal-expressing cells after 24 h ($t=4.04$, $p<0.01$). Nutlin-3 caused an increase in the number of SA-β-Gal expressing cells also at both 24 ($t=4.41$, $p<0.01$) and 72 h ($t=5.34$, $p<0.001$).

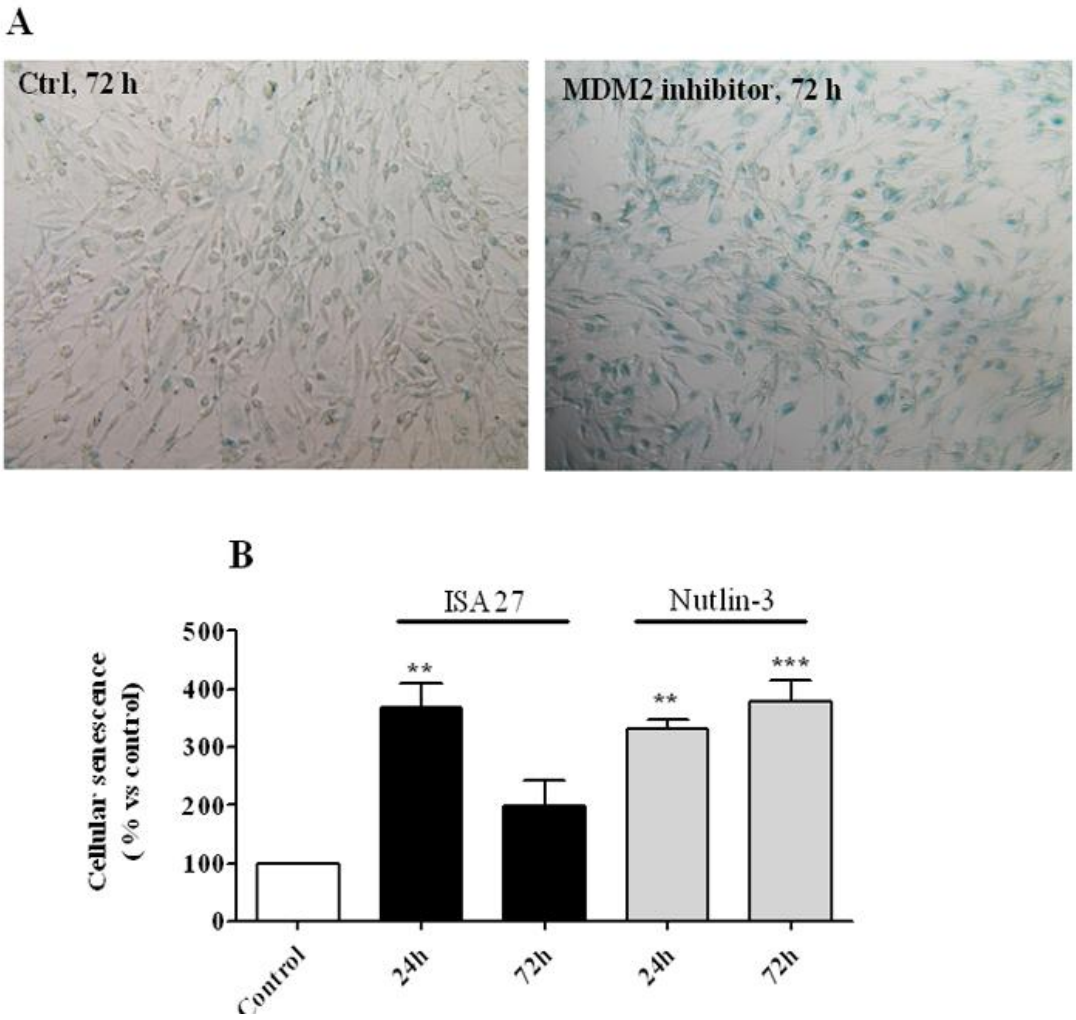

Figure 4. **ISA27 induces U87MG cell senescence.4A)** ***Representative images of SA-β-Gal-expressing cells:*** The panel shows the SA-β-Gal-expressing MDM2 inhibitor-treated and untreated cells at 72 h. **4B)** ***Percentage of SA-β-Gal-expressing cells:*** The number of SA-β-Gal-expressing cells was expressed with respect to total cells in each sample (untreated cells, ISA27- and Nutlin-3-treated cells). The percentage of SA-β-Gal-expressing cells for MDM2 inhibitor-treated samples was then calculated with respect to untreated cells, at which 100% value was attributed.

To investigate whether ISA27 induced apoptosis, the following parameters were evaluated: dissipation of mitochondrial potential ($\Delta\Psi$m), cytosolic cythocrome c content, PUMA mRNA levels and DNA fragmentation.

A decrease in $\Delta\Psi$m was indicated by a reduction in orange JC-1 aggregate fluorescence (recorded by the FL 2 channel) accompanied by a concomitant increase in green JC-1 monomer fluorescence (recorded by the FL 1 channel). Representative examples of the cytometric analysis are given in Figure 5A. The majority of untreated cells (99%) showed high fluorescence emission in both channels and were found in the

upper right (UR) quadrant of the plot. The remaining (1%) of the untreated cells showed low fluorescence emission in FL2, therefore plotting in the lower right (LR) quadrant. For ISA27 treatment, an increase was seen in the percentage of the cells plotting in the LR quadrant, consistent with $\Delta\Psi$m dissipation. In particular, significant changes in $\Delta\Psi$m were observed after treatment at 24 and 48 h (8.5% and 31%, respectively; $p<0.05$), as shown in Figure 5B.

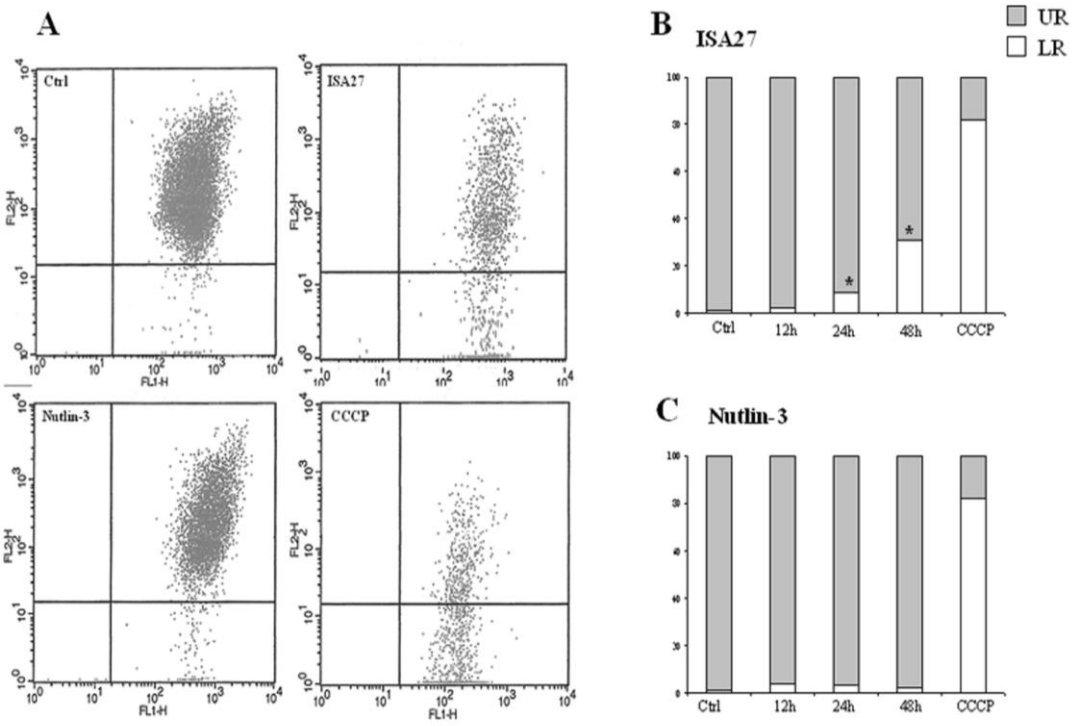

Figure 5. ISA27 induces dissipation of the mitochondrial membrane potential. 5A) ***Representative dot-blots of untreated and MDM2 inhibitor-treated cells:*** After ISA27 treatment, mitochondrial depolarization is visible by a decrease and increase of fluorescence in the FL-2 and FL-1 channels, respectively. After Nutlin-3 treatment, mitochondrial depolarization is not visible; CCCP is the positive control. **5B and C)** ***Time-course analyses of $\Delta\Psi$m dissipation:*** Histograms show the mean values of cell percentages either in the UR (polarized mitochondria) or LR (depolarized mitochondria) quadrant of the $\Delta\Psi$m analysis plots derived from three independent experiments.

Real time RT-PCR analysis showed that ISA27 led to a statistically significant PUMA mRNA level increase at 24 and 48 h compared to the control (Figure 6A).

Figure 6B shows that ISA27-treated cells exibited a 25% increase in cytochrome c in the cytosolic fraction compared to the control. DNA-specific PI staining showed that treatment with ISA27 caused a significant increase in the percentage of cells with hypodiploid DNA content, a clear sign of apoptosis, as shown

in the frequency histograms from a representative flow cytometric experiment (Figure 6C). In particular, the quantity of apoptotic cells (sub-G0 cells) observed after exposure of U87MG cells to ISA27 for 72 h increased to 17.7±1.27% ($p<0.001$), while that of the control was 0.43±0.05%. Nutlin-3 did not give statistically significant results after the indicated incubation times for these apoptotic parameters (Figure 6B and 6C), with the exception of increased PUMA mRNA levels after treatment for 72 h (Figure 6A).

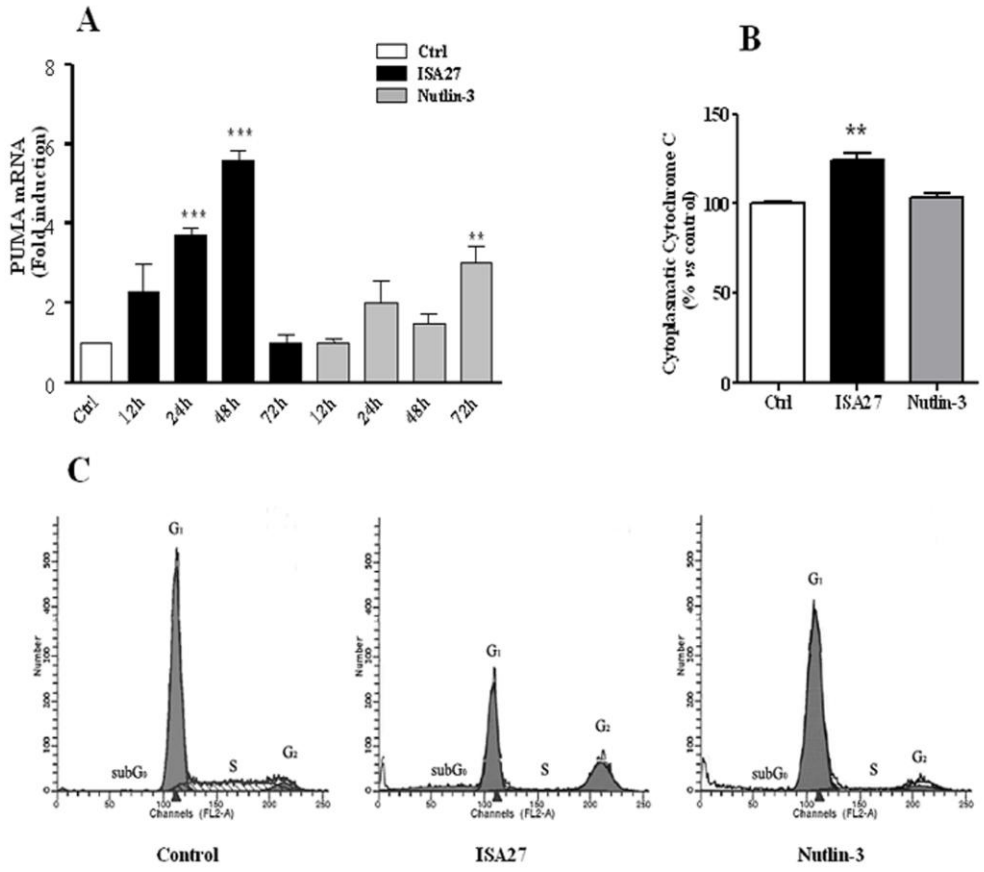

Figure 6. ISA27 induces an increase in PUMA mRNA levels, mitochondrial cytochrome c release, and DNA fragmentation. 6A) ***PUMA mRNA relative quantification:*** ISA27 induced a statistically significant increase in PUMA mRNA levels at 24 and 48 h. Nutlin-3 caused a statistically significant increase at 72 h. **6B)** ***Cytosolic cytochrome c content evaluation*****:** ISA27-treated cells showed a 25% increase in cytochrome c in the cytosolic fraction. Nutlin-3-treated cells did not give statistically significant results. **6C)** ***DNA content evaluation***: Frequency histograms from a representative experiment are shown. ISA27-treated cells showed a significant increase in the percentage of nuclei with hypodiploid DNA content at 72 h compared with control cells. In contrast, Nutlin-3 did not induce significant nuclear DNA fragmentation.

Discussion

The direct and specific activation of the p53 pathway without inducing collateral DNA damage offers a tantalizing answer to the shortcomings of current therapeutic regimens and seems to be a reasonable approach for GBM therapy in view of the infrequent occurrence of p53 gene mutations (Cerami E et al., 2010, He J et al., 1994).

The cumulative evidence of aberrantly increased activity of the primary p53 inhibitor MDM2 in GBMs (Ohgaki H et al., 2009, Cerami E et al., 2010, Halatsch ME et al., 2006) incited us to examine the effects of targeted inhibition of the MDM2-p53 interaction by the spiro-oxindole analog ISA27, a recently introduced MDM2 small molecule inhibitor (Gomez-Monterrey I et al., 2010). Little is known about the effects of MDM2 inhibitors on the *in vitro* growth of GBM cells. Recently, Nutlin-3, the first potent MDM2 small-molecule inhibitor (Vasilev LT et al., 2004), was reported to be effective at inhibiting *in vitro* GBM cell growth (Villalonga-Planells R et al., 2011), suggesting the validity of this experimental approach for the treatment of GBMs.

In this study, we investigated whether ISA27 affected the growth of GBM cells and explored the intracellular effects activated following ISA27 treatment. Moreover, we compared the results with those obtained using Nutlin-3 to evaluate the efficacy of ISA27. The U87MG cell line was chosen as a cell culture model of human GBM because it maintains wild-type p53 (Kondo S et al., 1995, Zaho P et al., 1998). In this cell line, the primary mechanism of p53 inactivation is through high nuclear MDM2 levels caused by a lack of PTEN, a tumor suppressor protein that counteracts MDM2 translocation into the nucleus under normal circumstances (Mayo LD et al., 2002). The lack of PTEN makes this cell line a suitable representative model of GBM, as the loss of the locus containing the gene for PTEN has been found in up to 80% of GBMs (Ohgaki H et al., 2009, Cerami E et al., 2010, Halatsch ME et al., 2006). In addition, U87MG cells exhibit an efficient DNA repair system that has been associated with peculiar aberrant cell proliferation and resistance to conventional DNA-damaging therapy (Pegg AE, 1990, Dhandapani, KM et al., 2007).

This is the first report to demonstrate that ISA27 is a potent inhibitor of U87MG cell growth. Previous studies have shown that ISA27 activates p53, resulting in growth inhibition in HEK-293 transformed human embryonic kidney, M14 human melanoma and U937 human monocyte lymphoma cell lines (Gomez-Monterrey I et al.,

2010). Our results demonstrated that ISA27 blocks the cell cycle and triggers an apoptotic death program in U87MG cells, which are similar to the responses obtained with human M14 melanoma cells.

We observed a dose-dependent antiproliferative effect in U87MG cells following short-term treatments (24 h) with increasing ISA27 concentrations. Moreover, ISA27 inhibited U87MG cell growth at a lower dose than Nutlin-3. The specificity of the antiproliferative effects was demonstrated by the reduction of MDM2-p53 complex formation and the restoration of p53 function in U87MG cells after ISA27 treatment. The reactivation of p53 was suggested by the induction of the transcriptional activation of the primary target p53 genes MDM2 and CDKN1A. The CDKN1A gene encodes the cyclin-dependent kinase inhibitor p21, an essential mediator of p53-induced cell cycle arrest. Exponential U87MG growth was significantly inhibiting following long-term ISA27 treatment. The number of viable cells was substantially reduced after 1 day of ISA27 treatment, and this reduction reached almost total growth inhibition after 5 days. Kinetic analyses of the ISA27-induced intracellular effects showed that the decrease in viable cells was mainly due to a G1 cell cycle block and cellular senescence during the initial phase of ISA27 treatment. However, apoptotic parameters, such as the dissipation of mitochondrial membrane potential, began to appear. Prolonged ISA27 exposure time caused a further decline in viable cells, a G2 cell cycle block and apoptosis of the remaining cells. By analyzing U87MG gene expression and apoptotic parameters in response to ISA27, we identified the upregulation of the PUMA gene, which is involved in mediating the apoptotic response of p53, mitochondrial potential dissipation, cytochrome c release into the cytoplasm and DNA fragmentation, all features consistent with apoptotic cell death.

It is important to note that even long-term treatment of Nutlin-3 effectively inhibited U87MG cell growth. The primary cellular response to Nutlin-3 was the permanent cell cycle arrest that continued until the end of treatment. Only in the final stage of treatment did apoptosis signs begin to appear, as indicated by high levels of PUMA mRNA. This finding is consistent with literature data that reported U87MG apoptosis after Nutlin-3 treatment for 96 h (Villalonga-Planells R et al., 2011). As described above, ISA27 triggered a permanent cell cycle arrest, although this response induced early apoptosis. The comparison between long-term ISA27 and Nutlin-3 treatment indicated that ISA27 stimulates a faster antiproliferative response than Nutlin-3, inducing a more effective reduction in the number of viable cells. This feature of

ISA27 may be beneficial in the treatment of human GBM, considering that this cancer is characterized by rapid cell growth. Cellular responses with different kinetics have been recently shown for ISA27 and another small molecule, 10d, in the M14 human melanoma cell line (Gomez-Monterrey I et al., 2010). Treatment with ISA27 for 24 h induced both cell cycle arrest and apoptosis, while caused cell cycle arrest only.

It is not clear how Nutlin-3 and ISA27 stimulate cellular responses with different kinetics in U87MG cells. ISA27 may induce a faster dissociation of p53 from MDM2 than Nutlin-3, and this more rapid reactivation of p53 function could be favorable for apoptosis induction.

Of significant importance is that the Nutlin-3 and ISA27 are non-toxic in normal cells. Specifically, they did not reduce the viability of a normal human cell model (lymphomonocytes). This result is consistent with those previously obtained by other authors using a number of normal cell models and suggests a selective toxic effect of MDM2 inhibitors on cancer cells. It has been demonstrated that Nutlin-3 is not toxic to peripheral blood mononuclear cells, bone marrow-derived hematopoietic progenitors and bone marrow stromal epithelium cells (Secchiero P et al., 2006, Stühmer T et al., 2005, Kojima K et al., 2005). In *in vivo* studies, Nutlin-3 and other MDM2 inhibitors showed antitumor activity in xenograft models of human cancers without causing visible signs of toxicity in the animals, as assessed by necroscopy analyses and body weight assessment (Vasilev LT et al., 2004, Tovar C et al., 2006, Shangary S et al., 2008).

The precise mechanism of cell death resistance in normal cells remains unclear. Cancer cells express a variety of oncogenes that provide a survival advantage to cancer cells but render them susceptible to oncogene intervention strategies. For example, cancer cells that are sensitive to MDM2 inhibitors show higher expression of the MDM2 oncoprotein than normal cells. Indeed, it was observed that MDM2 overexpression in cancer cells is an indicator of their sensitivity to apoptosis induction by MDM2 inhibitors. Hence, MDM2 overexpression in cancer cells leads to a strong suppression of p53 activity and renders them highly susceptible to p53 reactivation by MDM2 inhibitors. It has also been proposed that different p53 levels in normal and cancer cells can explain the selective activity of the MDM2 inhibitors (Shangary S et al., 2008). It has been shown that although p53 is activated by a specific MDM2 inhibitor in both normal colon fibroblast cells and HCT-116 colon cancer cells, the levels of p53 accumulation differ (Shangary S et al., 2008). Both basal and MDM2

inhibitor-induced p53 levels were appreciably lower in normal cells than in cancer cells. The authors of that study proposed that lower levels of p53 may favor cell cycle arrest, whereas higher levels of p53 lead to both cell cycle arrest and apoptosis induction.

In conclusion, our data show that ISA27 disrupts the MDM2-p53 interaction and unchains the powerful antitumor capacities of p53 in U87MG GBM cells. If confirmed *in vivo*, the use of this MDM2 inhibitor could offer a novel therapy concept for the treatment of GBM patients by inducing tumor growth inhibition and regression.